Endothelial dysfunction during Graft-versus-Host Disease

Inaugural-Dissertation
to obtain the academic degree
Doctor rerum naturalium (Dr. rer. nat.)
submitted to the Department of Biology, Chemistry and Pharmacy
of Freie Universität Berlin

by

Steffen Cordes

from Stadtlohn

2017

The present thesis was prepared from August 2012 until November 2017 at the Medical Department of Hematology, Oncology and Tumor Immunology, Charité University Medicine under the supervision of PD Dr. Olaf Penack.

First Reviewer:	PD Dr. Olaf Penack
Second Reviewer:	Prof. Dr. Rupert Mutzel

Date of defense: 01.02.2018

Für meine Familie

Acknowledgements

Ich möchte die Gelegenheit nutzen, all jenen meinen Dank auszusprechen, die mich während der Zeit in Berlin sowohl innerhalb als auch außerhalb des Labors unterstützt und damit zum erfolgreichen Gelingen meiner Promotion beigetragen haben.

Meinem Doktorvater, PD. Dr. Olaf Penack, möchte ich für die Möglichkeit danken, das spannende Feld der hämatopoetischen Stammzelltransplantation in seiner Arbeitsgruppe erforschen zu dürfen. Durch das hohe Maß an Vertrauen, welches mir entgegengebracht wurde, konnte ich sowohl wissenschaftlich als auch persönlich wachsen. Obwohl das Projekt lange Phasen der Etablierung erforderte und Misserfolge mit sich brachte, hast Du nie Deine Geduld verloren und mich darin unterstützt, das Projekt zu einem erfolgreichen Ende zu bringen. Dafür möchte ich mich ganz speziell bei Dir bedanken.

Nach langer Suche war Herr Prof. Dr. Mutzel bereit, die Begutachtung meiner fortgeschrittenen Promotion anzunehmen. Dafür möchte ich Ihnen meinen Dank aussprechen.

Aus der Welt des Laboralltags, möchte ich mich bei meinen aktuellen und ehemaligen Arbeitskollegen; Martina, Katarina, Sarah, Andrea, Tharsana, Aleix, Jörg und Yu bedanken. Ohne Euch wäre diese Arbeit nicht möglich gewesen. Mein besonderer Dank gilt meinen beiden PhD Kolleginnen, Dr. Katarina und Sarah. Danke für Eure Kompetenz, Kollegialität und Geduld. Ihr hattet immer ein offenes Ohr für mich. Mein Dank gilt auch Jörg und Yu. Ihr habt einige Anstöße für die Richtung dieser Arbeit geliefert. Bei Martina möchte ich mich im besonderen Maße für die tatkräftige Unterstützung bedanken. Dein hoher Einsatz und Deine unermüdliche Bereitschaft haben einen großen Teil zum Gelingen dieser Arbeit beigetragen.

Ich möchte mich auch bei allen Kooperationspartnern für ihre Kompetenz und das Gelingen der Arbeit bedanken. Zeinab und Andreas für die wunderbaren LSFM Bilder und deren Analyse, Johanna für das Mounten der Arterien, Petra für die exzellente Assistenz beim CTEM, Maria für die Färbungen der humanen Biopsien und Dir, Jens, für die Lösungen etlicher Probleme bei den Sort Runden.

Mein Dank gilt auch den Menschen außerhalb des Labors: Meinen Freunden: Jonas, Ismail, Lennart, Anna, Heppe, Adam, Nadine und allen, die ich aus Platzgründen nicht nennen kann. Vielen Dank für Eure Ratschläge und Diskussionsrunden. Meinen Eltern: Vielen Dank, dass Ihr mich immer unterstützt habt und die Promotion so erst ermöglicht habt. Meinen Geschwistern: Christin, Janek und Miklas. Ich bin dankbar mit Euch aufgewachsen zu sein. Durch Euch bin ich der Mensch, der ich heute bin.

Ganz besonders möchte ich mich bei meiner eigenen kleinen Familie bedanken, die die letzten Wochen vor Abgabe nochmal sehr spannend gestaltet haben. Meiner lieben Frau, Magdalena, die mich auf meinem Weg aus Düsseldorf begleitet hat und mir immerzu Motivation und Zuversicht zugesprochen hat. Vielen Dank für Deinen bedingungslosen Rückhalt und Deine Liebe. Meiner lieben kleinen Tochter, Kalina, möchte ich für ihr fröhliches und unkompliziertes Gemüt danken. Du schenkst mir jeden Tag viel Freude und volle Windeln. Ich liebe Euch.

Table of contents

ABSTRACT (ENGLISH VERSION)

Transplantation of donor stem cells, called allogeneic hematopoietic stem cell transplantation (allo-HSCT), is currently the only curative treatment for a variety of hematopoietic diseases, in particular for malignant diseases. Despite the progress made in the past decades in terms of safety, complications by allo-HSCTs lead to high post-treatment mortality rates. The primary complication after allo-HSCT is the "graft-versus-host disease" (GVHD). GVHD is an inflammatory disease affecting liver, intestine and skin. Allo-reactive T lymphocytes are the main mediators of this inflammatory condition. Current therapeutic approaches aim to reduce activation and expansion of effector T lymphocytes, resulting in increased infection rates due to systemic immune suppression by steroids. Approximately 30% of patients develop a progressive GVHD despite immune suppression; this condition is called "steroid refractory GVHD" (srGVHD). Especially in the srGVHD condition, there is an urgent need to find appropriate treatment options. The study of srGVHD, to find targets for successful treatment, is hampered by the lack of mouse models.

Recent studies revealed an increased endothelial damage during GVHD and srGVHD. Up to now, the characterization of endothelium during GVHD is incomplete.

In this thesis, endothelial dysfunction during GVHD has been investigated in human samples by caspase staining. Endothelial dysfunction in murine GVHD was accompanied by a reduced pericyte coverage, an increased leakage and a higher contraction capability of endothelium in GVHD target organs without structural changes. The increase in adhesion, co-stimulatory and antigen-presenting molecules at the surface of endothelial cells indicates an active role of these cells in the pathogenesis of GVHD. Targeting different functions with compounds directed to the endothelium was not successful in ameliorating the course of GVHD. Gene array performed with isolated hepatic endothelial cells revealed metabolomic pathways, which were altered during established GVHD. Additionally, known pathways to induce apoptosis and cellular dysfunction were increased in hepatic endothelial cells during established GVHD. In our murine srGVHD model increased endothelial damage and leakage index in the colon indicated a contribution of endothelial cells to the pathophysiology of srGVHD. The reduced number of hepatic endothelial cells and the reduced expression of adhesion molecules add evidence to a potential role of endothelial dysfunction in srGVHD.

This study highlights the importance of endothelial cells to the GVHD cascade in mice and humans, while therapeutic approaches were not successful to ameliorate murine GVHD. A murine model of srGVHD showed involvement of endothelial cells in this condition. A deeper insight to endothelial cell pathophysiology in established GVHD and srGVHD may help to identify clinical markers for early stages of GVHD and open a new field of therapeutics to ameliorate GVHD while preserving immunity.

ABSTRACT (GERMAN VERSION)

Die Übertragung fremder Stammzellen bei der allogenen Stammzelltransplantation (allo-HSCT) ist die einzige kurative Behandlung für eine Vielzahl von hämatopoetischen und malignen Erkrankungen. Leider kommt es häufig zu schweren Komplikationen mit hoher Mortalität. Die Hauptkomplikation nach allo-HSCT ist die „Graft-versus-host“ Krankheit (GVHD). Die GVHD ist eine entzündliche Erkrankung, die Leber, Darm und Haut betrifft. Allo-reaktive T-Lymphozyten sind hierbei die Hauptmediatoren. Die derzeit verwendeten therapeutischen Ansätze zielen darauf ab, die Aktivierung und Expansion von Effektor-T-Lymphozyten zu reduzieren. Hierbei stellen jedoch erhöhte Infektionsraten - aufgrund systemischer Immunsuppression - ein erhebliches Problem dar. Rund 30% der Patienten entwickeln eine progressive GVHD trotz Immunsuppression mit Steroiden, die „Steroid-refraktäre GVHD“ (srGVHD). Fehlende Mausmodelle behindern die Suche nach geeigneten Therapien der srGVHD.

Aktuelle Studien zeigen erhöhte Endothelschäden sowohl bei der GVHD als auch bei srGVHD Patienten. Bisher ist die endotheliale Schädigung während der fortgeschrittenen GVHD nur unvollständig charakterisiert.

In dieser Arbeit wurde die endotheliale Dysfunktion während der etablierten GVHD in humanen Proben durch Caspase Färbungen beschrieben. Die endotheliale Dysfunktion in der murinen GVHD wurde begleitet von einer reduzierten Pericytendichte, erhöhter Kontration von mesenterischen Aterien, sowie einer erhöhten Durchlässigkeit des Endothels in den GVHD-Zielorganen, ohne zu strukturellen Veränderungen der Mikrogefäße zu führen. Die erhöhte Oberflächenexpression von Adhäsionsmolekülen, co-stimulierenden und antigenpräsentierenden Molekülen auf Endothelzellen, lässt vermuten, dass diesen Zellen eine wichtige Rolle während der GVHD zukommt. Verschiedene therapeutische Ansätze, die endotheliale Funktion zu modulieren, bewirkten keine Abschwächung der GVHD. Hepatische Endothelzellen wiesen eine erhöhte Genexpression von Genen auf, die für metabolische Signalwege codieren. Zusätzlich war die Genexpression von Genen, die bei der Induktion von Apoptose und zellulärer Dysfunktion wichtig sind, während der etablierten GVHD erhöht. Die Verwendung eines srGVHD-Modells zeigte eine erhöhte Endothelschädigung mit erhöhter vaskulärer Permeabilität im Kolon, was auf einen Beitrag von Endothelzellen zur Pathogenese von srGVHD hindeutet. Hinweise auf eine endotheliale Dysfunktion in der srGVDH waren die reduzierte Anzahl von Endothelzellen der Leber und die Reduktion in der Expression von Adhäsionsmolekülen während der srGVHD.

Diese Studie konnte neue Evidenzen für die Bedeutung von Endothelzellen in der murinen und humanen GVHD hervorbringen. Therapeutische Ansätze, den Verlauf der murinen GVHD zu mildern, zeigten keinen Erfolg. Ein murines Modell der srGVHD wies endotheliale Schädigung auf, was eine Beteiligung des Endothels bei der srGVHD vermuten lässt. Weitere Kenntnisse über das Endothel bei der etablierten GVHD und bei der srGVHD könnten es zukünftig ermöglichen, klinische Marker für

den Beginn der GVHD zu ergänzen und die Sensitivität bereits genutzter Marker zu erhöhen. Der Einsatz von Therapeutika, die spezifisch auf das Endothel wirken und den Verlauf der GVHD abmildern, könnten zukünftig das Auftreten von Infektionen und Tumorrezidiven als schwere Nebenwirkung der Immunsupression verringern.

ABBREVIATIONS

ACh	Acetylcholine
Allo	Allogeneic
ANG1	Angiopoietin-1
ANG2	Angiopoietin-2
APC	Antigen-presenting cell
Auto	Autologous
B6	C57BL/6
BALB/c	BALB/cByJRj
B-cell	Bone marrow-derived lymphocyte
BDF	B6D2F1
BM	Bone marrow
BMT	Bone marrow transplantation
BSA	Bovine serum albumin
Caps3	Caspase 3
CAR	Chimeric antigen receptor
CD	Cluster of differentiation
cDNA	Complementary deoxyribonucleic acid
cEC	Circulating endothelial cell
cEPC	Circulating endothelial progenitor cell
cGVHD	Chronic GVHD
CLS	Capillary leak syndrome
COX2	Cyclooxygenase-2
CTEM	Conventional transmission electron microscopy
CXCR4	C-X-C chemokine receptor type 4
DAH	Diffuse alveolar hemorrhage
DAMPs	Danger associated molecular patterns
DNA	Deoxyribonucleic acid
EDI	Endothelial damage index

ELI	Endothelial leakage index
eNOS	Endothelial nitrogen oxide
ES	Engraftment syndrome
ESAM	Endothelial cell adhesion molecule
FACS	Fluorescence activated cell sorting
FCS	Fetal calf serum
FGF	Fibroblast growth factor
G-CSF	Granulocyte-specific-colony-stimulating factor
GVHD	Graft-versus-host disease
GVT	Graft-versus-tumor
HLA	Human leukocyte antigen
HS	Heparin sulfate
HSCT	Hematopoietic stem cell transplantation
i.p.	Intraperitoneal
i.v.	Intravenous
ICAM1	Intercellular adhesion molecule 1
IL	Interleukin
INFγ	Interferon gamma
JAMs	Junction adhesion molecules
JAMA	Junction adhesion molecule-A
L-NAME	L-N^G-Nitroarginine methyl ester
LPS	Lipopolysaccharide
LSFM	Light sheet fluorescence microscopy
MAP	Mitogen-activated protein
MCEC	Mouse cardiac endothelial cell
MHC	Major histocompatibility complex
mTOR	Mechanistic target of rapamycin
NA	Noreadrenaline
NFAT	Nuclear factor of activated T-cells

NFκb	Nuclear factor kappa-light-chain-enhancer of activated B-cells
NG2	Neural/glia antigen 2
NK cell	Natural killer cell
non-RS	Non-responder
PAMPs	Pathogen-associated molecular patterns
PBS	Phosphate-buffered saline
PDF	Probability density function
PECAM	Platelet endothelial cell adhesion molecule
PGE2	Prostaglandin E2
PGI2	Prostaglandin I2
Phe	Phenylephrine
qPCR	Quantitative polymerase chain reaction
RNA	Ribonucleic acid
RS	Responder
SLC	Sneaking ligand construct
srGVHD	Steroid refractory GVHD
ß-APN	Beta-aminopropionitrile fumarate
Syn	Syngeneic
TAM	Transplant-associated thrombotic microangiopathy
T-cell	Thymus-derived lymphocyte
TCR	T-cell receptor
TEM	Transendothelial migration
T_{h17}-cells	T-helper cells type 17
T_{h1}-cells	T-helper cells type 1
T_{h2}-cells	T-helper cells type 2
Tie2	Tyrosine kinase with immunoglobulin- and epidermal growth factor-like domains 2
TM	Thrombomodulin
TNFα	Tumor necrosis factor alpha
T_{reg}-cells	Regulatory T-cells

VCAM1	Vascular cellular adhesion molecule 1
VE-cadherin	Vascular endothelial cadherin
VEGF	Vascular endothelial growth factor
VOD	Veno-occlusive disease
vWF	von Willebrand factor
ZO-1	Zonula occludens 1
αSMA	Alpha smooth muscle actin
β_2m	β_2-microglobulin

1 INTRODUCTION

1.1 HEMATOPOIETIC STEM CELL TRANSPLANTATION

Hematopoietic stem cell transplantation (HSCT) is an established procedure to transfer stem cells from donor to recipient. The aim of transplantation is to replace hematopoietic stem cells and thereby the immunological repertoire of the recipient by the transplant of the donor. Donor stem cell sources are autologous (auto) stem cells from the recipient, syngeneic (syn) stem cells from a twin, or allogeneic (allo) stem cells from another donor. In all HSCT settings, recipients are treated with high-dose chemotherapy and/or fractional radiation to eradicate malignant hematopoietic cells and to allow donor cells to repopulate the bone marrow niche[1,2]. The most common transplantation setting in malignant diseases is allo-HSCT, because of the wide donor pool and the beneficial graft-versus-tumor (GVT) effect[3,4]. GVT reaction is one major mechanism to cure hematopoietic malignancies, besides the myeloablative conditioning of the recipient[4]. Preferences of the type of donor source vary in different malignant and non-malignant diseases[5], in which HSCT could also serve as a cure. The number of HSCTs and therefore the number of allo-HSCTs performed in clinical HSCT-centers (Figure 1A) are increasing over the past two decades (Figure 1B)[6,7]. A drop in the number of auto-HSCTs after the year 1999 relates to the cease of rheumatoid arthritis as indication for auto-HSCT[8].

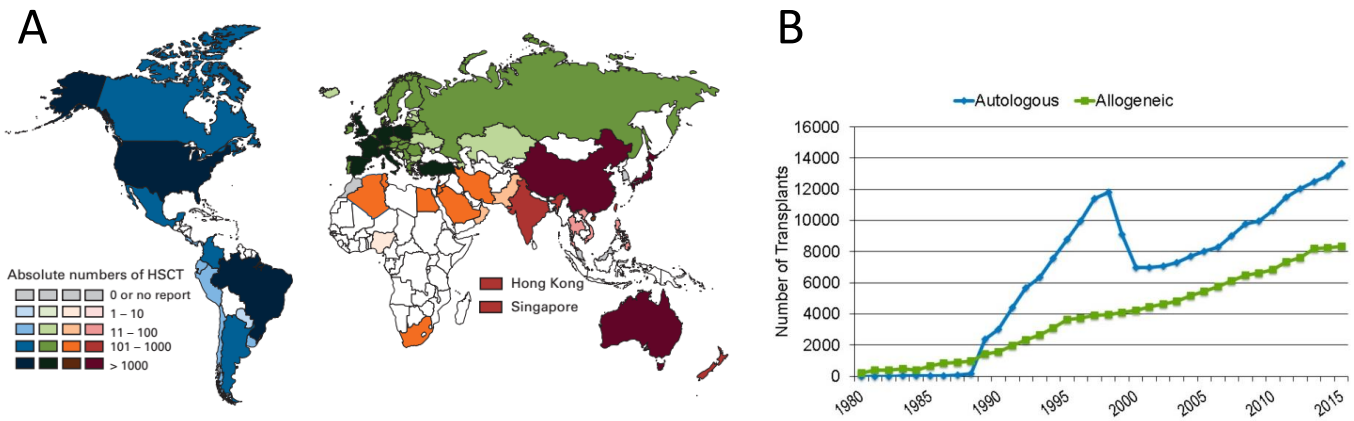

Figure 1| Total performed hematopoietic stem cell transplantations (HSCTs). A| Total numbers of HSCTs performed in 2014 worldwide. Modified according to Niederwieser et al.[9]. **B|** Total number of autologous and allogeneic HSCTs performed in the U.S.A. from 1980 to 2015 based on retrospective data. Modified according to D'Souza et al.[10].

A possible reason for the increasing number of allo-HSCTs is the increased lifespan of human population and thus increased incidence of hematopoietic malignancies in older patients. Additionally, the risk of complications after allo-HSCT decreased in the past decades and a better organized donor database with an increasing number of registered HSCT donors allows to find genetically matched

donors[11]. These factors are contributing to a broader application and increased number of allo-HSCTs performed worldwide.

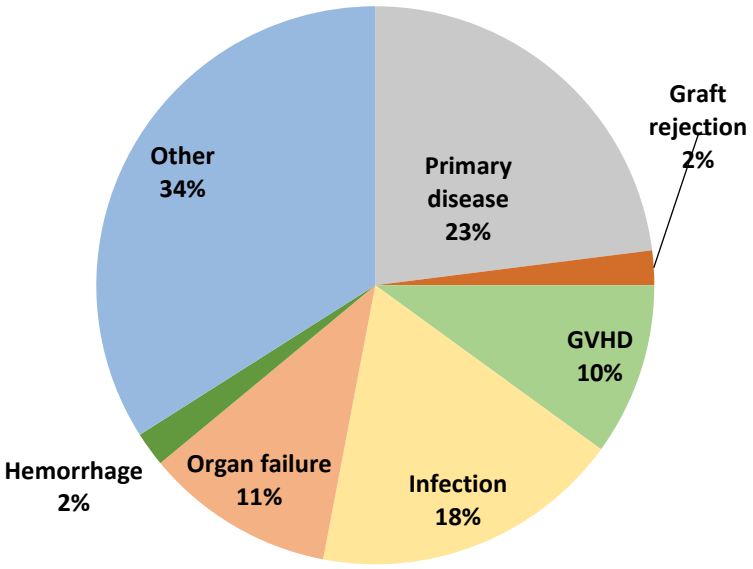

Figure 2| Cause of death after unrelated donor transplantation within 100 days after hematopoietic stem cell transplantation (HSCT) between 2013 and 2014. The pie chart shows the percentage of different causes of death within 100 days after HSCT. After allogeneic HSCT under the condition of unrelated donor and recipient, mortality related to graft-versus-host disease (GVHD), infection, organ failure and tumor relapse accounts for 62% of deaths. Modified according to D'Souza et al.[10].

The potential of allo-HSCT to cure leukemia was proven by Thomas et al. in 1971[12] and several improvements were made over the past four decades[2] leading to a better stem cell engraftment and reduced the risk of complications like GVHD. Improved engraftment and reduced incidence of GVHD is achieved by more advanced human leukocyte antigen (HLA) typing, based on deoxyribonucleic acid (DNA) sequencing[13]. GVDH treatment options such as engineered chimeric antigen receptor (CAR) T-cells are now in clinical studies[14]. Additionally, research progress in the isolation of hematopoietic stem cells[15] leads to larger donor databases[16]. Isolation of bone marrow is rare nowadays and only occasionally used for special indications. Instead, stem cells are usually isolated from peripheral blood[15]. Nevertheless, HSCT can lead to life threatening complications, including tumor relapse, GVHD, infections or organ failure, all together causing 62% of deaths within 100 days after allo-HSCT (Figure 2)[10,17]. GVHD, which is one of the major complications of HSCT, is likely to be associated with all other complications.

1.2 Indications for HSCT

The number of HSCTs performed in Europe 2014 reached a total of 40.829[18]. Among these, there were 15.765 allo-HSCTs and 20.704 auto-HSCTs. Main indications for 72% of allo-HSCTs were leukemias (acute myeloid leukemia (36%), acute lymphocytic leukemia (16%), chronic myeloid leukemia (3%), chronic lymphocytic leukemia (2%) and myelodysplastic syndromes (15%)). 87.3% of allo-HSCTs were performed because of malignant diseases, including plasma cell disorders (4%), Hodgkin's disease (3%), non-Hodgkin's lymphoma (8%) and solid tumors (0.3%). Non-malignant

diseases, such as bone marrow failure, primary immune deficits, inherent disorders of metabolism and autoimmune diseases present minor indications and make up 12.7% of all allo-HSCTs (Figure 3)[18].

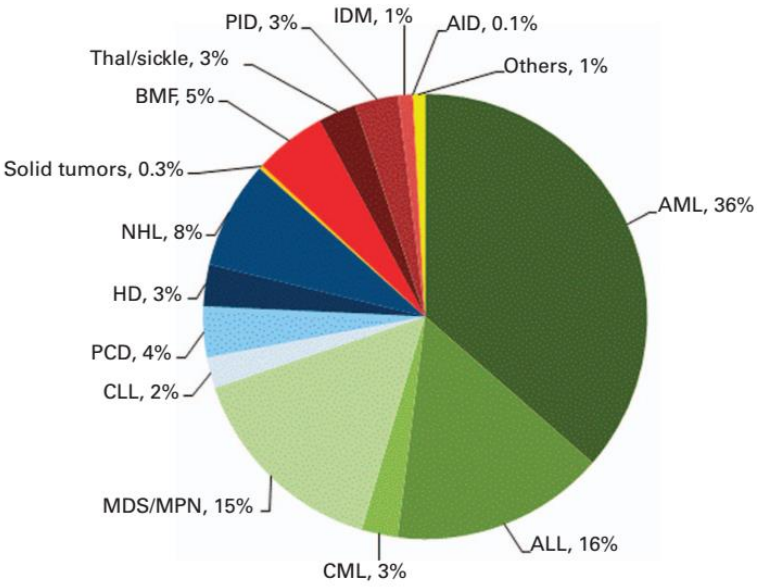

Figure 3| Indication for allogeneic hematopoietic stem cell transplantation (allo-HSCT). Pie chart representing the percentage of different disease entities among all allo-HSCTs. (AML, acute myeloid leukaemia; ALL, acute lymphoblastic leukaemia; CML, chronic myeloid leukaemia; MDS, myelodysplastic syndrome; MPN, myelo-proliferative neoplasm; CLL, chronic lymphocytic leukaemia; PCD, plasma cell disorders; HD, Hodgkin's disease; NHL, Non-Hodgkin's lymphoma; BMF, bone marrow failure; Thal/sickle, thalassemia/sickle cell disease; PID, primary immune diseases; IDM, inherited diseases of metabolism; AID, auto immune diseases). Modified according to Passweg et al.[18].

1.2.1 BENEFICIAL GRAFT VERSUS TUMOR EFFECT

The GVT effect is a desirable immune reaction after allo-HSCT against residual malignant cells, which survived myeloablative conditioning of the HSCT-recipient[4]. Although the underlying biological processes are not yet fully understood, the complex interaction of different kinds of effector cells and cytokines is considered to mediate the GVT effect. Allo-reactive T lymphocytes are mainly assigned for therapeutic success, with both, cluster of differentiation 4^+ ($CD4^+$) and $CD8^+$ T-cells acting as important effector cells[19,20]. Therefore, allo-reactive donor T-cells as well as tumor antigen-reactive T-cells are the main mediators of GVT response[20-23]. After transplantation of donor bone marrow, repopulation in the recipient and both, the activation by allo-response[4] and the activation by tumor reactive T-cells[24] mediate GVT effects. Cytokines such as interferon gamma (IFNγ)[25], tumor necrosis factor alpha (TNFα)[26] or interleukin 2 (IL-2)[27] further support the GVT reaction. In addition, natural killer cells (NK cells) have important functions in mediating GVT effects[28]. NK cells are cytotoxic to target cells lacking auto-major histocompatibility complex (MHC) class I molecules, such as recipient tumor cells[29].

The main mediators and processes of GVT reaction are displayed in Figure 4. Future research will focus on the optimization of the GVT effect/GVHD ratio: increasing GVT response while reducing GVHD.

1.3 COMPLICATIONS AFTER HSCT WITH ENDOTHELIAL INVOLVEMENT

HSCT remains the only available treatment option for several hematologic malignancies. As mentioned before, life-threatening complications of HSCT still make it a high-risk approach. Many of

these complications are associated with endothelium of the allo-HSCT recipient[30]. It is described that during conditioning, endothelial cells are damaged and activated[31]. Thereby, microbial and viral products enter endothelial cells more easily. During the process of engraftment after HSCT, additional stimuli such as cytokines released from immune cells, further activate and damage endothelial cells. It has been postulated that allo-reactivity plays a role in this cascade, which would explain the higher incidence of complications after allo-HSCTs[30]. Several complications occurring in the early phase after allo-HSCT are connected to endothelial abnormalities. It is likely that conditioning and hence damaging endothelial cells plays a critical role in the pathophysiology of these complications. The following chapters present an overview of possible complications.

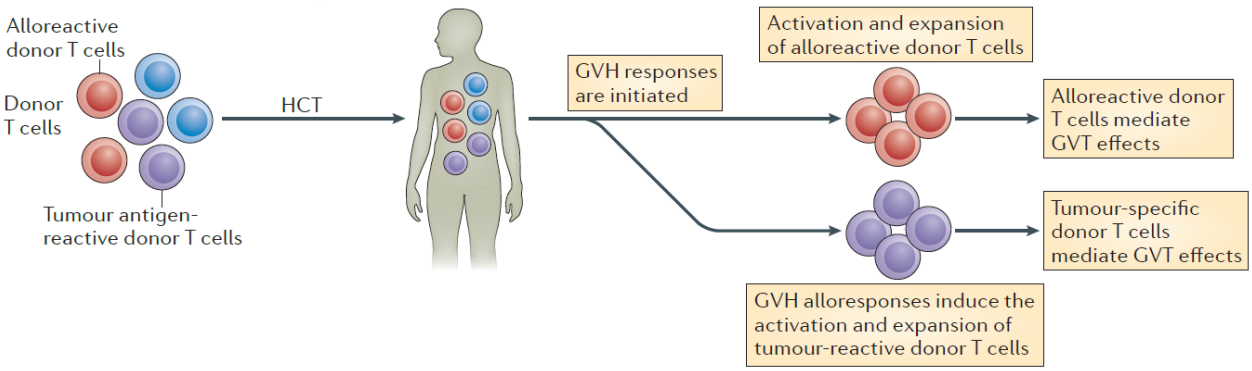

Figure 4| The main mediators of the graft-versus-tumor (GVT) effect. Transplants of allogeneic (allo) hematopoietic stem cells include donor T-cells, which can be divided in two main mediators of the GVT reaction. Allo-reactive donor T-cells and tumor antigen-reactive donor T-cells are suspected to mediate the GVT effect. Shortly after allo-HSCT, activation and expansion of allo-reactive donor T-cells by the graft-versus-host response are initiated. In parallel also the activation and expansion of tumor-reactive T-cells starts. Both cell types are supposed to contribute substantially to the GVT effect. (HCT, haematopoietic cell transplant: GVH, Graft-versus-host) Modified according to Li et al.[32].

1.3.1 INFECTIONS

One complication of HSCTs are infections. Around 11% of cases of death after HSCT are caused by infections[33,34]. Allo-HSCT recipients are prone to infections due to the cellular damage caused by the conditioning regime, but also because of their reduced immune status and the additional immune suppression[35]. Especially during the aplastic phase, before the successful engraftment of donor stem cells, there is an increased risk for infections. Bacterial sepsis, pneumonia or fungal infections are the main reasons for death in this phase[36]. Beginning three months after allo-HSCT, capsuled bacteria like streptococcus pneumoniae and haemophilus influenzae represent a major risk and reactivation of previous virus infections is possible[36]. Endothelial cell activation and damage is proposed to increase the infection rate, possibly due to weakened barrier function of the endothelial monolayer.

1.3.2 ENGRAFTMENT SYNDROME

Engraftment syndrome (ES) has usually been described in auto-HSCT settings[37]. The distinction between ES and GVHD in allo-HSCT is difficult. ES is often described as early GVHD or hyper acute

GVHD[38,39]. Experience with non-myeloablative conditioning in allo-HSCT revealed, that ES, independent from GVHD, may occur[38]. Clinical ES symptoms are fever, erythrodermatous skin rash and non-cardiogenic pulmonary edema. The pathomechanism is multifaceted and involves T-cells[40], monocytes[41] as well as complement activation[42] and pro-inflammatory cytokine release[41]. Epithelial and endothelial damage, resulting from cytotoxic conditioning, leads to the release of IL-1, TNFα and INFγ from damaged cells[43]. Effects of early cytokine production on immune cells activation have been well described[43].

1.3.3 THROMBOTIC MICROANGIOPATHY

Transplant-associated thrombotic microangiopathy (TAM) is mostly observed in allo-HSCT and has been rarely described in the setting of auto- or syn-HSCT [44]. Occurrence of grade two (or above) GVHD correlates with TAM after allo-HSCT[45]. Symptoms of TAM are thrombocytopenia, hemolysis and fragmentation of red blood cells accompanied by clinical manifestations like fever, renal dysfunction and neurological symptoms. Endothelial damage due to conditioning is likely to be the primary event causing TAM. Studies using plasma from TAM patients on endothelial cells showed that plasma was able to induce apoptosis of endothelial cells[46]. Biomarkers of endothelial damage, like thrombomodulin (TM)[47], intracellular adhesion molecule 1 (ICAM1)[48] and von Willebrand factor (vWF) antigen[47] serum levels were elevated in TAM patients. Additionally, increased levels of cytokines, like IL-1, TNFα, INFγ and IL-8 are observable[44]. It is likely that TAM pathobiology is triggered by cytokines, released from damaged endothelial cells, which in term activate allo-reactive T-cells.

1.3.4 VENO-OCCLUSIVE DISEASE

Veno-occlusive disease (VOD), also named hepatic sinusoidal obstruction syndrome (SOS), has the highest incidence rates in patients receiving allo-HSCT[49]. There are several risk factors for VOD such as abdominal irradiation[50], busulfan dose[51] and types of transplant and HLA mismatch[52]. GVHD and VOD represent different complications and may be difficult to distinguish. Clinical manifestations of VOD are ascites and an increased liver volume, accompanied by high bilirubin levels in the blood. First histopathologic changes during VOD include injury of hepatic sinusoids, subendothelial edema, red blood cell extravasation and fibrin deposits. Subsequently, sinusoid dilation and hepatocyte necrosis[53] might lead to a complete destruction of small hepatic vessels.

1.3.5 CAPILLARY LEAK SYNDROME

The incidence of the capillary leak syndrome (CLS) is highest in allo-HSCT setting[54]. High-intensity conditioning presents a major risk factor for the occurrence of the CLS[55]. Clinical manifestations of CLS are increased capillary permeability and generalized edema, accompanied by rapid weight gain. The pathobiology is unknown, but there is evidence that cytokines like IL-2[56] and granulocyte-specific-colony-stimulating factor (G-CSF)[57] as well as apoptosis of endothelial cells[58] are involved in the pathomechanism.

1.3.6 DIFFUSE ALVEOLAR HEMORRHAGE

Diffuse alveolar hemorrhage (DAH) is usually appearing during the engraftment phase in patients receiving allo-HSCT. Major risk factors for DAH development are allo-donor source and GVHD[59]. GVHD is closely related to terminal pulmonary hemorrhage. Symptoms of DAH include bloody cough and worsening of oxygenation, leading to cyanosis of limbs. Primary endothelial[60] and alveolar damage[61] due to chemotherapy, irradiation of lung and underlying infections are supposed to be crucial for the development of DAH.

1.4 GVHD; A MAJOR COMPLICATION

GVHD is one of the major problems after allo-HSCT with a high mortality rate[17,62,63]. Unrelated donor transplants, age of donor and recipient, conditioning regime intensity and prophylaxis of acute GVHD were identified as high-risk factors for GVHD development[64]. The severity of the symptoms varies and cutaneous, intestinal or hepatic affections are not mandatory. Involvement of the skin is most abundant and ranges from small, itchy, maculopapular exanthemata to confluent exanthemata. In severe cases, blistering of the skin and epidermolysis can occur. Hepatic involvement can be assessed by measurement of bilirubin, aspartate-aminotransferase and alanine-aminotransferase levels in serum. Intestinal GVHD is defined by degeneration of crypt cells and can proceed to total destruction of the intestinal mucosa. Clinical manifestations of intestinal GVHD are nausea, abdominal pain, vomiting as well as diarrhea. Most insights to the pathophysiology of GVHD are derived from animal experiments[2,63,65,66].

1.4.1 IMMUNOLOGICAL BACKGROUND OF GVHD

The classical MHC gene locus encodes highly polymorphic cell surface molecules, which are crucial for peptide presentation to immune cells. The discovery of MHC in mice, by Snell[67] and colleagues in the 1920's, was honored with the Nobel prize in 1980. They described the role of MHC molecules in tumor and skin rejection[68]. Detailed knowledge about the structure of MHC molecules, the genetic coding and their role in immune responses has been gathered in mice and human since then.

Classical MHC proteins, either class I or class II, present peptides of varying size to T-cells and are an integral part of vertebrate adaptive immunity[69]. Non-polymorphic MHCs are termed non-classical MHCs and are encoded by genes located within the MHC region[54]. MHC-like molecules are those encoded outside the MHC locus. Most of these non-classical and MHC–like proteins have other functions than peptide presentation and are involved in immune or non-immune related processes[70]. MHCs are critical in immune response and outcome of allo-HSCT. MHC differences between donor and recipient are the main cause of T-cell activation during GVHD[71].

The MHC molecule itself and peptides, presented by MHCs, are recognized by T-cells via their T-cell receptor (TCR). Allo-MHC and non-self MHC-peptide complexes can initiate T-cell responses, that lead to transplant rejection[72] and to the recruitment and modulation of other immune cells, subsequently resulting in GVHD[71].

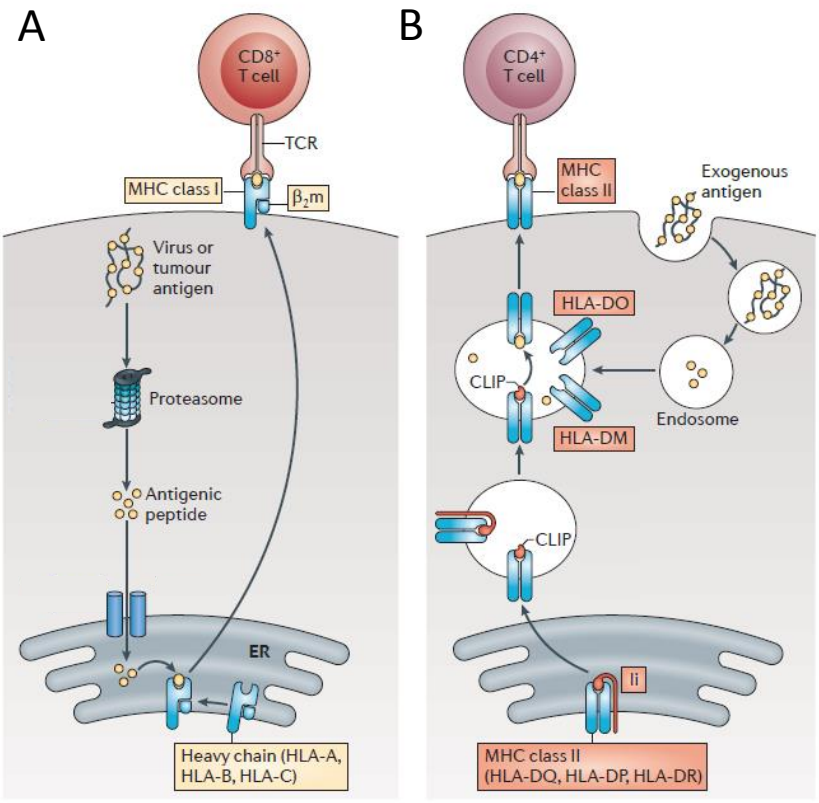

Figure 5| Major histocompatibility complex (MHC) class I and MHC class II antigen presentation to T-cells. A| Intracellular antigens are processed into peptides by proteasomes and transported to the endoplasmatic reticulum. There, antigens are loaded into the groove of MCH class I. MHC class I is composed of a heavy chain and a ß$_2$-microglubulin. On the cell surface, MHC class I presents antigens to CD 8$^+$ T-cells. **B|** Antigens from extracellular sources are processed by endolysosomal enzymes into peptides. These peptides bind to the groove of MCH class II complex and displace the class II-associated invariant chain peptide. The MHC class II presents antigens to CD4$^+$ T-cells. (TCR, T-cell receptor; ER, endoplasmatic reticulum; CLIP, class II-associated invariant chain peptide; HLA, human leukocyte antigen). Modified according to Kobayashi et al.[73].

Intracellular proteins, which are processed by proteolysis in proteasomes, are transported to the endoplasmatic reticulum, where MHC class I is loaded with peptides and transported to the cell surface[74]. MHC class I presents peptides to CD8$^+$ cytotoxic T-cells (Figure 5A) and is expressed by almost all nucleated cells[75]. Classical class I molecules have an MHC fold, derived from a single polypeptide chain (heavy chain), which is associated with the nonpolymorphic β_2-microglobulin (β_2m) subunit[76]. The heavy chain is composed of three extracellular domains ($\alpha_{1\text{-}3}$), a transmembrane region serving as anchor and an intracytoplasmic domain. The polymorphic α_1 and α_2 domains form a cleft, where 8-10 amino acid residues are presented to T-cells[76].

In contrast, MHC class II processes proteins from extracellular origin and presents peptides to CD4$^+$ T-helper cells. Thereby, exogenous proteins are entering the cell by endocytosis and undergo degradation in acidic endosomes[77]. The endosomes are fusing with vesicles, containing MHC class II and antigens, are loaded to the fold of MHC class II. When a vesicle reaches the cell membrane, it fuses with the lipid-double layer and the antigen MHC class II complex can be recognized by CD4$^+$ T-cells (Figure 5B). MHC class II molecules consist of two polypeptide chains (α and β). Both polypeptide chains consist of two extracellular regions (α_1 and α_2 or ß$_1$ and ß$_2$), a transmembrane region anchoring the molecule in the cell membrane and a cytosolic region. Polymorphic α_1 and ß$_1$ regions of MHC class II molecules form a fold and present peptides with 8 to 20 amino acids to CD4$^+$ T-cells[78]. MHC class II molecules are mainly expressed by professional antigen-presenting cells (APCs) such as dendritic

cells, macrophages and bone marrow-derived lymphocytes (B-cells)[79] but also by semiprofessional APCs like mast cells[80], basophils[81] and endothelial cells[82].

In the setting of HSCT, donor and recipient are screened for the major transplant antigens (HLA-A, HLA-B, HLA-C, HLA-DR and HLA-DQ). The standard for transplantation is the 8/8 match or if HLA-DQ is included, a 10/10 match of HLA loci[1].

Mouse MHC is very similar to the human MHC system. Mouse MHC also includes three types of MHC molecules (MHC class I, II and non-classical MHC molecules) with basically the same functions as in humans. The nomenclature, however, varies and MHC class I gene members are termed H-2D, H-2K and H-2L. MHC class II gene members, H-2A and H-2E and non-classical MHC genes from both classes include H-2Q, H2-M, H2-T, H2-M and H2-O[83].

1.4.2 MODEL OF GVHD PATHOBIOLOGY

GVHD is a complex orchestrated disease, including different cell types and a wide range of soluble factors. Investigation of mouse models revealed significant insights to GVHD pathobiology[66] and resulted in a generally accepted three-phased model[63,84]: first, activation of APCs, second, activation and proliferation of allo-reactive T-cells and third, damage and destruction of skin, liver and intestine (Figure 6)[63]. This model includes donor non-hematopoietic APCs (including endothelial cells) in the activation phase. Although the endothelium has been considered as a mediator of end organ damage[85,86], the potential role of endothelial cells as specific effector cells during GVHD is not well understood. Furthermore, damage and dysfunction of the endothelium is presumed to contribute to steroid refractory GVHD (srGVHD) pathobiology[87-89].

Phase 1: Activation of antigen-presenting cells

The first phase of GVHD is defined by strong activation of APCs. The conditioning regime is damaging tissues, specially epithelial and endothelial cells of the HSCT recipient, triggering the release of pro-inflammatory cytokines like TNFα, IL-6 and IL-1. Additionally, tissue damage of intestinal mucosa leads to translocation of pathogen-associated molecular patterns (PAMPs) like lipopolysaccharides (LPS) or flaggelin. Damage associated molecular patterns (DAMPs), like adenosinetriphosphate or uric acid, are released from cells undergoing apoptosis and necrosis. The orchestrated release of cytokines, PAMPs and DAMPs activates the recipient's APCs and leads to an increase in expression of adhesion molecules like ICAM1, MHC and co-stimulatory molecules like CD80 and CD86. Consequently, allo-donor T-cells are much more likely to be activated by the recipient's APCs[63,84,90-92].

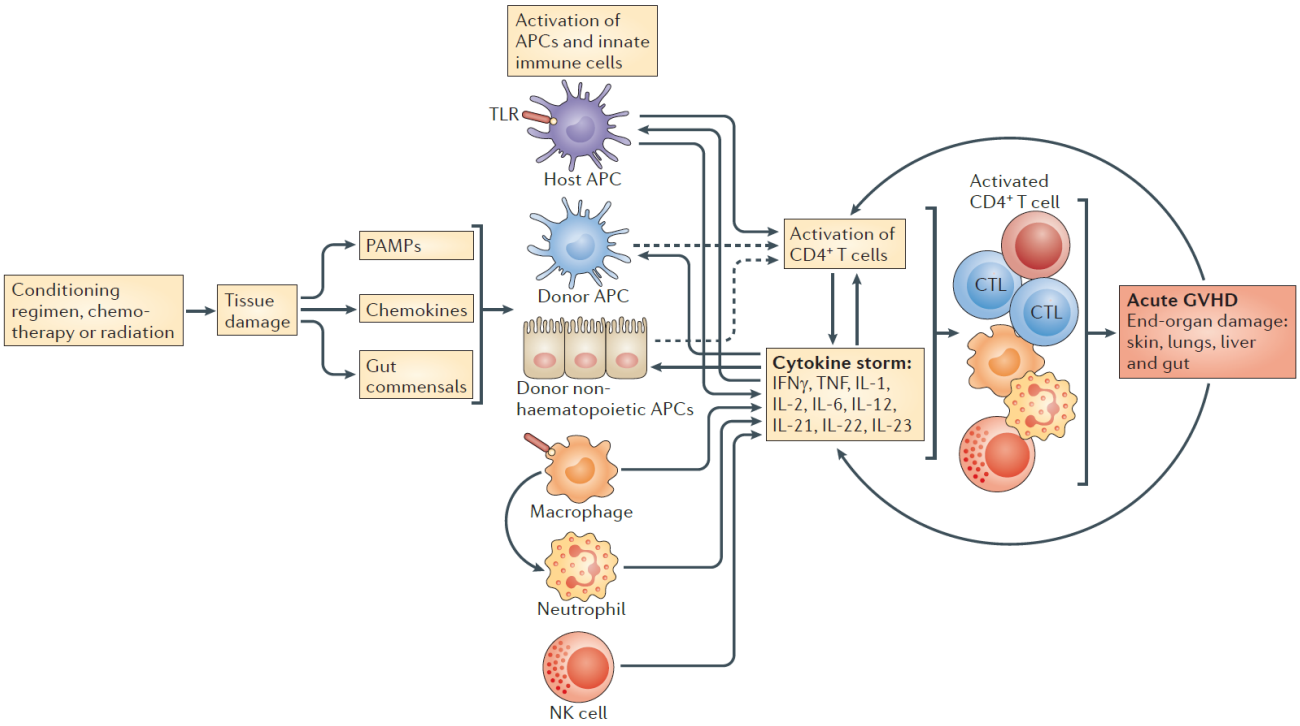

Figure 6| Three phases of the graft-versus-host disease (GVHD) cascade. The initial phase 1 is marked by activation of antigen-presenting cells (APCs), such as dendritic cells. Activation of APCs is further increased due to tissue damage and the release of gut bacteria, pathogen-associated molecular patterns (PAMPs) and pro-inflammatory chemokines by the conditioning regime. Phase 2 is marked by antigen presentation to T-cells, which in term initiates a strong cytokine response. These cytokines further promote antigen presentation and recruitment of innate immune cells as well as effector T-cells. In the third phase, the effector T-cells, natural killer cells, macrophages and pro-inflammatory cytokines result in end organ damage of the main target organs skin, liver and intestine. (NK cell, natural killer cell; INFy, interferon gamma; TNF, tumor necrosis factor; IL, interleukin; TLR, toll-like receptor; CTL, cytotoxic T lymphocyte). Modified after Blazar et al.[93].

Phase 2: Activation of T-cells

The second phase of GVHD is the activation of allo-donor T-cells. MHC and MHC peptide complexes on activated APCs are recognized by allo-donor T-cells by their TCR and they activate T-cells to proliferate and mature to cytotoxic T-cells or T helper cells[63,84]. This activation is promoted by the pro-inflammatory milieu, which is a result of the massive release of cytokines after the conditioning regime[91,92]. Activation and proliferation of T-cells is hypothesized to be mediated by a two-phased activation model. First, the TCR recognizes MHC or MHC peptide complexes presented by APCs. Second step is the co-stimulation of T-cells by binding of their CD28 receptor to CD80 and CD86 expressed on the APC. After binding of TCR to MHC and CD28 to CD80 and CD86, a signaling cascade in T-cells starts via nuclear factor kappa-light-chain-enhancer of activated B-cells (NFκb) pathway, the mitogen-activated protein kinase pathway and the calcium-calcineurin pathway. This results in the production of numerous factors including IL-2 and the CD40 ligand. Binding of IL-2 to its receptor CD25 activates the mechanistic target of rapamycin (mTOR) pathway resulting in clonal proliferation of T-cells. CD40 is expressed on all APCs and its ligand CD40L is expressed on activated $CD4^+$ T-cells and on a subset of $CD8^+$ T-cells and NK cells. Stimulation of CD40 on APCs

by CD40L triggers antibody production by B-cells and induces expression of co-stimulatory molecules (CD80 and CD86) and MHC expression on APCs via a positive feedback loop[91,92].

Investigation of mouse models of GVHD revealed that presentation of minor histocompatibility antigens by MHC class I on recipient APCs is substantially involved in activation of $CD8^+$ T-cells. Thereby antigen presentation is described as initial event in GVHD[94]. Additionally, donor APCs can further promote the GVHD reaction[95]. MHC class II expression on dendritic cells, activation of $CD4^+$ T-cells and even non-hematopoietic APCs are able to induce GVHD in mice[96-98]. On the effector site, $CD4^+$ T-cells, producing T-helper cells type 1 (T_{h1}-cells) specific cytokines like IFNγ, IL-2 and TNFα, are the dominant T-cell type during GVHD. T_{h1}-cells and their ability to produce IL-2 is critical to promote $CD8^+$ T-cell proliferation[94]. Production of IL-4, IL-5, IL-6, IL-10 and IL-13 is characteristic for T-helper cells type 2 (T_{h2}-cells), which are mainly involved in the humoral immune response. T_{h1}/T_{h2} polarization has a crucial influence on the severity of GVHD[99]. Mouse studies showed a significantly higher survival rate when transplanting T_{h2}-cells[100]. A third group to mention are T-helper cells type 17 (T_{h17}-cells), which are producing IL17a, IL-17f, IL-21 and IL-22. Recent studies showed pro-inflammatory but also anti-inflammatory properties of T_{h17}-cells during GVHD[101-103]. It is likely that they are capable of modulating GVHD in the different organs involved in GVHD[104].
GVHD in individual organs is caused by specific T-cell subsets, due to their specific chemokine release profile and the relative sensitivity of target tissues to these cytokines. In detail, T_{h1}-cells seem to be preferentially implicated in gastrointestinal, T_{h2}-cells in cutaneous and hepatic and T_{h17}-cells in cutaneous and pulmonary GVHD[105].

Phase 3: Effector phase with tissue damage

The third phase of GVHD involves the massive destruction of skin, intestine and liver tissue. Activated APCs and T-cells release cytokines like INFγ, TNFα and IL-1. These cytokines further fuel T-cell expansion and recruitment of innate immune cells like macrophages and monocytes to the site of inflammation.

$CD8^+$ allo-reactive T-cells are the main inflammation mediators during this phase of GVHD. Hepatic damage is mainly caused by Fas/Fas-Ligand signaling. In cutaneous and intestinal GVHD, $CD8^+$ T-cells mainly use perforin/granzyme signaling. Both pathways mediate cell lysis and induce caspase activation in target cells. Recruited innate immune cells, like macrophages, are enhancing cytokine release, especially release of TNFα. Additionally, LPS leaking through the damaged mucosa from skin and intestine, further increases release of pro-inflammatory cytokines. This results in an increased antigen presentation of APCs and thus a stronger activation and proliferation of $CD8^+$ T-cells[63,84,91,92].

1.4.3 TREATMENT OF GVHD

GVHD still remains a life threatening risk after allo-HSCT and patients receiving allo-HSCT are prophylactically treated with T-cell inhibitors like Cyclosporine A and Methotrexate[106]. Cyclosporine A is a calcineurin inhibitor and blocks the transcription factor, called nuclear factor of activated T-cells (NFAT) and thereby IL-2 secretion of T-cells[107]. Methotrexate is an inhibitor of dihydrofolate-reductase and reduces ribonucleic acid (RNA) and DNA synthesis[108]. Nevertheless, additional steroid treatment of GVHD is necessary in about 60% of allo-HSCT recipients[17,62,63].

Standard treatment of clinically manifested GVHD is aiming to reduce T-cell activation and to systemically suppress the immune system by high doses of corticosteroids, like methylprednisolone[109]. Response rates are poor and only 70% of patients are responding to steroids[106]. Steroids are acting on APCs, like dendritic cells, by blockade of transcription of co-stimulatory molecules, reduce MHC class II expression and the release of pro-inflammatory molecules. Additionally, anti-inflammatory IL-10 production is promoted[110]. On the site of effector cells, steroids are inhibiting intracellular signaling by blocking lymphocyte-specific protein tyrosine kinase and proto-oncogene tyrosine-protein kinase. The transcription factors NFκb, activator protein 1 and NFAT are inhibited by steroids (Figure 7)[111].

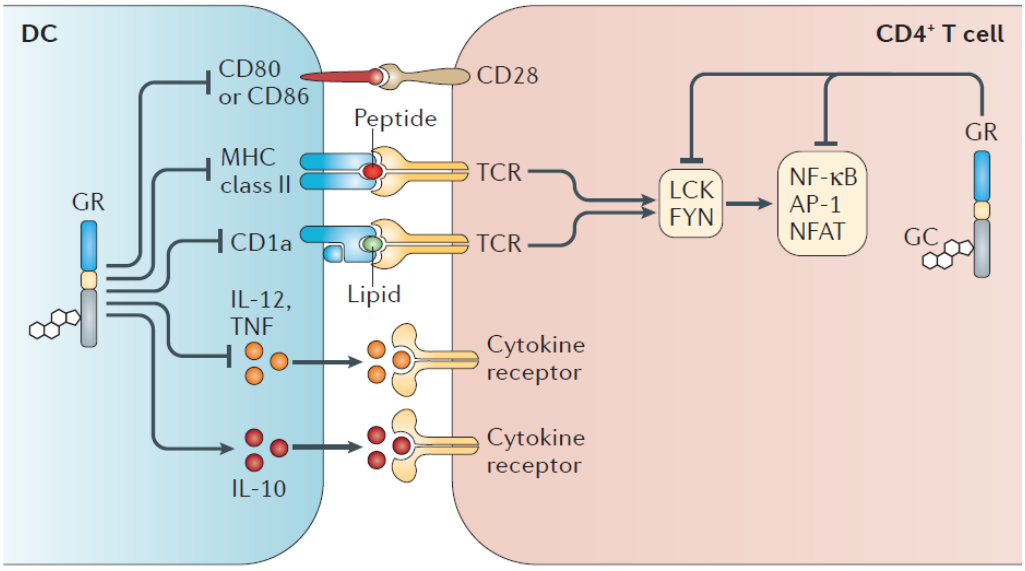

Figure 7| Glucocorticoids modulate T-cell activity. Glucocorticoids suppress T-cell activation indirectly by modulating antigen-presenting cells (APCs), such as dendritic cells (DCs), to decrease antigen presentation, expression of co-stimulatory molecules and pro-inflammatory cytokine release. Furthermore, glucocorticoids are regulating T-cell receptor (TCR) signaling, and inhibit transcription factors initiating T-cell activation, like NF-kB and NFAT. (MHC, major histocompatibility complex; LCK, lymphocyte specific protein tyrosine kinase; FYN, protein tyrosine kinase Fyn; GC, glucocorticoid; AP-1, activator protein 1; GR, glucocorticoid receptor; IL, interleukin; NFAT, nuclear factor of activated T-cells; NFκB, nuclear factor-κB; TNF, tumor necrosis factor). Modified according to Cain et al.[112].

The use of steroids and T-cell targeting drugs is problematic because systemic suppression of immune cells is resulting in higher infection rates[113] and a reduced GVT effect[114]. Although allo-reactive T-cells are the main mediators of GVHD, still 30% of patients are suffering from progressive GVHD despite treatment[115]. This clinical manifestation of GVHD is called srGVHD.

1.4.4 STEROID REFRACTORY GVHD

As mentioned previously, 30% of allo-HSCT recipients with GVHD are suffering from srGVHD and thus have a poor prognosis. Increase of steroid dosage, the use of other immune suppressive agents like Mycophenolate-mofetil[116], polyclonal antibodies against T-cells like Antithymocyte globulin[115], monoclonal antibodies against T-cells like anti-CD3[117] or anti-CD52[118], or monoclonal antibodies against soluble factors like anti-TNFα[119], anti-IL-2[120], anti-IL-25[121] or anti-IL-6[122] are only beneficial in small numbers of patients suffering from srGVHD[115]. The mortality rate of srGVHD did not change in the past decades. Despite the progress in GVHD understanding and the availability of multiple treatment options available, different studies state mortality rates of 70-100% for srGVHD patients[115,123].

All available therapies for GVHD and srGVHD aim to inhibit or reduce T-cell activation and proliferation, even risking severe side effects like increased infection rate and significant reduction of the GVT effect leading to tumor relapse.

T-cells are described to be the main mediators of GVHD, but recent data show the importance of the endothelium in different inflammatory disease like rheumatoid arthritis[124], early systemic lupus erythematosus[125] and inflammatory colitis[126], which share features with GVHD.

1.5 THE ENDOTHELIUM

The endothelium is a monolayer covering the tunica intima of blood and lymphatic vessels. Endothelial cells are the first barrier for cells, bacteria and viruses in the blood stream to enter the surrounding tissue during inflammation and infections. Blood vessels are categorized by the direction of blood flow. Arteries and capillaries are transporting oxygen enriched blood from the heart to the periphery, while veins and venules are transporting blood from the periphery back to the heart. Big blood vessels like aorta, arteries and veins consist of the tunica intima (the innermost cells of the vessel facing the lumen), the tunica media (a layer of smooth muscle cells) and the tunica externa (mainly composed of collagen and fixing the blood vessels to the surrounding tissue). The structure of small vessels like capillaries and venules differs from the structure of big vessels. They consist of an endothelial monolayer and surrounding pericytes, which are able to contract and communicate with endothelial cells[127].

There are three types of endothelial monolayers as shown in Figure 8: 1) the continuous endothelium, which is a tight barrier not permeable for soluble factors from the stream, 2) the fenestrated endothelium, which has pores of around 70nm in diameter and enables large molecules to pass through and 3) the discontinuous endothelium with gaps ranging from 100-200nm in diameter, which is permeable for cells[128].

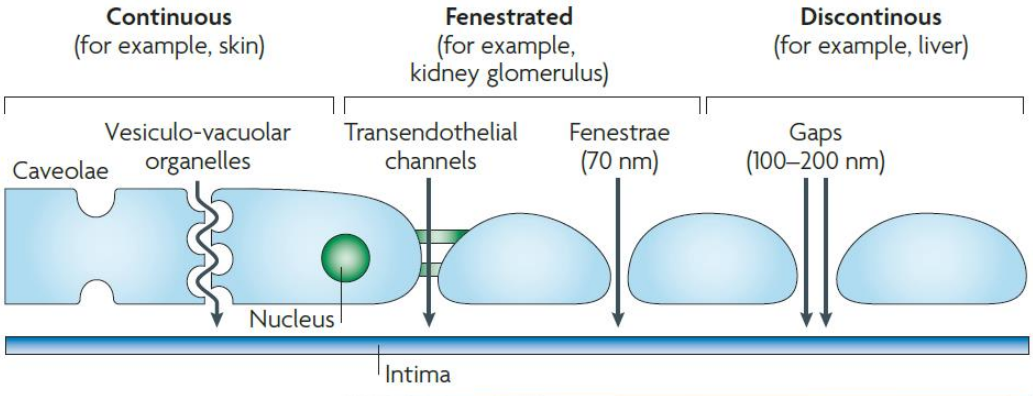

Figure 8| Different kinds of endothelial monolayers. The continuous endothelium is a tight barrier and not permeable for soluble factors in the blood. The fenestrated endothelium with transendothelial channels and pores from around 70nm in diameter is permeable for large molecules in the blood stream. The discontinuous endothelium with gaps ranging from 100-200nm in diameter is permeable for cells. Modified according to Lemichez et al.[128].

1.5.1 FUNCTIONS OF THE HEALTHY ENDOTHELIUM

Endothelial cells are not only covering the tunica intima, but play an important role in vascular biology (Figure 9). Angiogenesis, the formation of new blood vessels by sprouting of existing vessels, is mediated by endothelial cells responding to local vascular endothelial growth factor 2 (VEGF2)[129]. Blood clotting (thrombosis and fibrinolysis) is controlled by endothelial cells via production of heparin sulfate (HS)[130]. HS acts as a cofactor of antithrombin, an enzyme inactivating several factors in the coagulation cascade[131]. By production of endothelial nitrogen oxide (eNOS), endothelial cells are able to control vasoconstriction and vasodilation and thereby blood pressure[132]. The barrier function of the endothelial monolayer is essential for the control of material exchange and transit of immune cells into and out of the bloodstream. Zonula occludens 1 (ZO-1) and vascular endothelial cadherin (VE-cadherin) are important in maintaining the endothelial barrier function[133,134]. During inflammation, endothelial cells can recruit immune cells to the site of viral or bacterial infection, for example by up-regulation of adhesion molecules[135].

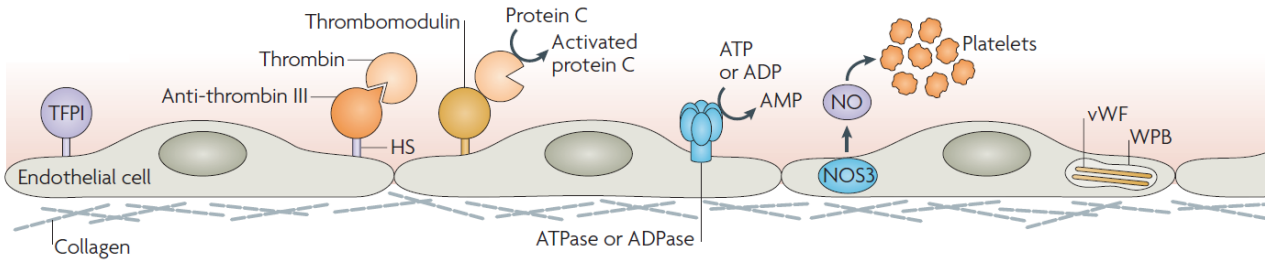

Figure 9| Functions of resting endothelial cells. Endothelial cells inhibit coagulation by expression and display of tissue factor pathway inhibitors (TFPIs). Subsequent actions of the factor VII-a-tissue factor complex are blocked. Endothelial cells also express heparin sulfate (HS) proteoglycans on their cell surface, causing anti-thrombin III to bind and inhibit thrombin molecule generation by the coagulation cascade. Thrombomodulin on endothelial cells binds thrombin and converts its substrate specificity from cleavage of fibrinogen to cleavage and activation of protein C. Endothelial cells also prevent platelet activation by conversion of adenosine triphosphate (ATP) to adenosine monophosphate (AMP) by adenosine triphosphatase (ATPase) and adenosine diphosphatase (ADPase). Nitric oxide (NO) generated by nitric

oxide synthase 3 (NOS3) mediates conversion of arginine and inhibits platelet activation. Von Willebrand factor (vWF) is stored in Weibel-Palade bodies (WPB) and therefore is not available to support the interaction of platelets with the basement membrane. (ADP, adenosine diphosphate) Modified according to Prober et al.[136].

Endothelial dysfunction affecting one or more functions of the healthy endothelium has significant systemic consequences for patients. Additionally, some inflammatory disease entities, like lupus erythematosus[125], arthritis[124], inflammatory colitis[126] and diabetes[137], are known to be associated with endothelial dysfunction.

1.5.2 ENDOTHELIAL ACTIVATION

Endothelial cells can be stimulated by different signals resulting in endothelial activation. Activation is divided in two types: type I activation is independent of gene expression, while type II implies gene expression changes[136].

Type I activation is mediated by ligands binding to G-protein-receptors on endothelial cells. This leads to Ras homologue activation (RHO), a small guanosine triphosphatase and cytosolic calcium release. Calcium release results in synthesis of prostaglandin I2 (PGI2), a potent vasodilator inducing relaxation of vascular smooth muscle cells. Production of nitric oxide is enhanced by cytosolic calcium release, which has a synergistic effect to PGI2. RHO signaling results in phosphorylation of the myosin light chain, inducing exocytosis of Weibel-Palade bodies. They deliver P-selectin to the endothelial cell surface. Concomitant contraction of actin filaments, connected to tight and adherence junctions, leads to increased leakage of the endothelial monolayer[136].

Type II activation is mainly mediated via the pro-inflammatory cytokines TNFα and IL-1ß. Cytokines are binding to its ligand (TNFα on TNFR1; and IL-1ß on IL-1R1) expressed on endothelial cells. Ligand binding induces a signaling cascade resulting in activation of the transcription factor NFκb. NFκb activation induces gene expression of vascular cellular adhesion molecule 1 (VCAM1), ICAM1, E-selectin, chemokines and cyclooxygenase-2 (COX2). While VCAM1, ICAM1 and E-selectin are adhesion molecules of leukocytes and play a critical role in recruitment of immune cells to the site of inflammation, COX2 increases the production of PGI2 resulting in vasodilatation. Chemokines and other unknown effector proteins lead to junction reorganization and thereby to increased vascular leakage[136].

1.5.3 RECRUITMENT OF IMMUNE CELLS BY ENDOTHELIAL CELLS

The endothelial monolayer is involved in immune cell trafficking. During inflammation and infection, expression of different adhesion molecules by activated endothelial cells is essential for transendothelial migration (TEM) of leukocytes. Initial contact of leukocytes to the endothelium via P-selectin glycoprotein ligand-1 is mediated by P-selectin on the surface of endothelial cells, called “capturing” of immune cells. E-selectin is expressed of the activated endothelium and T-cells get in closer contact via glycoprotein E-selectin ligand-1, causing the “rolling” of T-cells on the endothelial monolayer. Rolling is getting slower, if besides P- and E-selectin, ICAM1 and VCAM1 are expressed

at the endothelium. These adhesion molecules are recognized by leukocyte function associated antigen-1 and very late antigen-4 causing the "arrest" of leukocytes attached to the endothelium. ICAM2 recognition induces leukocytes to "crawl" along the endothelium and to find a possibility for transendothelial migration. ICAM2 is recognized by the same receptor as ICAM1 at the surface of leukocytes. There are two possible ways for the leukocytes to pass the endothelial monolayer. One is paracellular TEM. Tight and adherence junction proteins such as junction adhesion molecules (JAMs), endothelial cell adhesion molecule (ESAM), platelet endothelial cell adhesion molecule (PECAM), CD99 and CD99 antigen-like protein 2 and especially VE-cadherin are involved in this process. In case of transcellular TEM, leukocytes pass the endothelial cell itself. Important for this process is plasmalemmal vesicle-1. Also ICAM1, JAMA, PECAM and CD99 are involved in transcellular TEM (Figure 10). By passing the endothelial monolayer, leukocytes can reach the site of infection or inflammation and mediate cell damage[138,139].

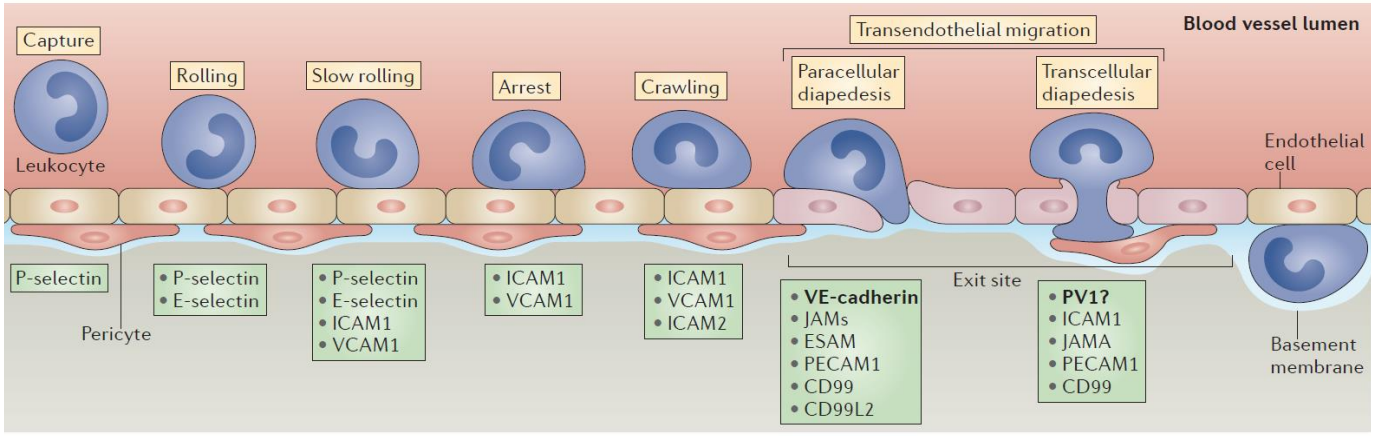

Figure 10| Steps of leukocyte recruitment to the site of inflammation. Steps of leukocyte migration are stated in the yellow boxes. Accordingly, molecules with specific function in the different steps are stated in the green boxes. (ICAM1, intracellular adhesion molecule 1, VCAM1, vascular cellular adhesion molecule 1, ICAM2, intracellular adhesion molecule 2, JAMs, junctional adhesion molecules, ESAM, endothelial cell-specific adhesion molecule, PECAM1, platelet endothelial cell adhesion molecule 1, CD99, cluster of differentiation 99, CD99L2, cluster of differentiation 99 like 2, PV1, plasmalemma vesicle protein 1). Modified according to Vestweber et al.[139].

1.5.4 Endothelial cells as APCs

As previously mentioned, endothelial cells can act like semi-professional APCs. Via surface expression of endothelial ICAM1, ICAM2, VCAM1 and leukocyte function activator-3, endothelial cells can be recognized by T-cells and thus establish the initial contact. These molecules also serve as co-stimulatory molecules for T-cell activation. Similar to professional APCs such as dendritic cells and macrophages, endothelial cells express MHC class I[140] and MHC class II[141], which is recognized by the TCR. Furthermore, co-stimulatory molecules like, CD40[142], OX40[143], CD80[144] and CD86[144] can be found on the surface of endothelial cells after stimulation (Figure 11).

Despite of multiple surface molecules expressed on endothelial cells, the microenvironment of T-cell-endothelial cell contact is critical. There is a heterogeneous expression pattern of MHC class I, MHC

class II, co-inhibitory and co-stimulatory molecules on endothelial cells, establishing various different local microenvironments[145]. Additionally, the fate of T-cells has to be considered, as T_{h1}-, T_{h2} -, T_{h17}- or regulatory T-cells (T_{reg}-cells) may interact in a different way with antigen presentation on endothelial cells.

Moreover, mouse and human endothelial cells differ in their expression pattern of co-stimulatory molecules. While human endothelial cells express constitutively P-selectin and its surface expression is not increased by inflammatory cytokines, murine endothelial cells are able to increase P-selectin expression upon pro-inflammatory cytokine stimulation. Other co-stimulatory molecules like CD40 are exclusively found on human endothelial cells[83,145].

As previously mentioned, time point, localization and T-cell fate are crucial for endothelial contact with T-cells with consequences for the activation of T-cells. Contradictory observations of alterations of migration, a stop or a delay of migration and the promotion of migration have previously been demonstrated as a result of T-cell endothelial cell interaction[140,146,147].

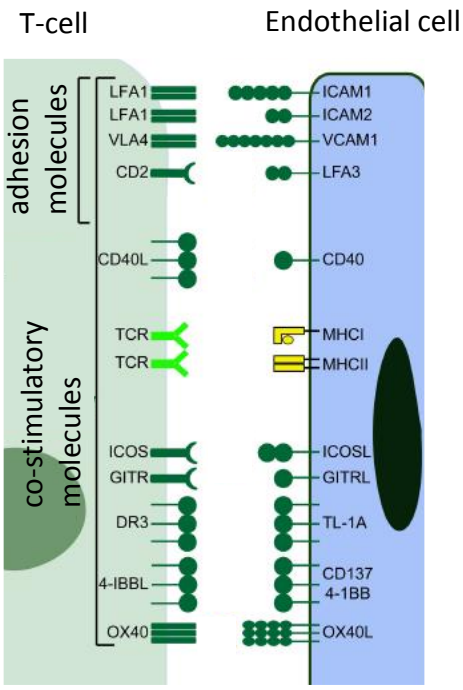

Figure 11| Endothelial cells as "semiprofessional" non-hematopoietic antigen-presenting cells (APCs). Scheme of the antigen presentation to T-cells (green), including co-stimulatory and adhesion molecules expressed by endothelial cells (blue). Endothelial cells share many surface proteins with professional APCs such as dendritic cells and macrophages. (ICAM1, intracellular adhesion molecule 1; LFA, lymphocyte function-associated antigen; VLA4, very late antigen 4; TCR, T-cell receptor; ICOS, inducible T-cell co-stimulator; GITR, glucocorticoid-induced tumor-necrosis-factor-receptor-related protein ; DR3, TNF-family receptor DR3; 4-IBBL, 4-1BB ligand; OX40, tumor necrosis factor receptor superfamily member 4; VCAM1, vascular adhesion molecule 1; MHC, major histocompatibility complex; ICOSL, inducible T-cell co-stimulator ligand; GITRL, glucocorticoid-induced tumor necrosis factor receptor-related protein ligand; TL-1A, TNF-family ligand TL1A; 4-1BB, co-stimulatory member of the TNF family; OX40L, OX40 ligand). Modified according to Carman et al.[148].

Other studies showed the ability of endothelial antigen presentation to promote inflammation. $CD4^+$ memory T-cells start to proliferate and secrete inflammatory cytokines upon endothelial antigen presentation via MHC class II *in vitro*[142,143] and *in vivo*[149]. MCH class I antigen presentation by endothelial cells promotes $CD8^+$ cytotoxic T-cell activation and killing of endothelial cells[144]. In context of inflammation there are also studies suggesting that endothelial cells provide peripheral tolerance[150]. It has been shown that liver sinusoidal cells promote tolerance towards $CD8^+$ cytotoxic T-

cell, suppress $CD4^+$ pro-inflammatory T_{h1}- and T_{h17}-cell response and the differentiation of T_{reg}-cells[151].

1.5.5 ENDOTHELIUM IN GVHD

As mentioned in chapter 1.3, endothelial cells are involved in many complications of HSCT, amongst them GVHD. There is a consensus that the endothelium is damaged by the conditioning regime in advance to HCST and thus, prone to pro-inflammatory cytokines. Recent data from Riesner et al. suggest a potent role of angiogenesis in the pathophysiology of GVHD, as increased angiogenesis is observable before immune cells are migrating to GVHD target organs[152].

Angiogenesis

Angiogenesis and inflammation are closely linked to each other. Angiogenesis is involved in cancer growth[153], rheumatoid arthritis[154], inflammatory bowel disease[155] as well as in ocular disorders[156]. Angiogenesis is a process where new blood vessels are formed. Main components in angiogenic signaling are fibroblast growth factor (FGF) and vascular endothelial growth factor (VEGF), which are recognized by endothelial cells in pre-excisting blood vessels via surface receptors. After binding to their receptor, a complex cascade is initiated, resulting in matrix degradation. Finally, proliferation of endothelial cells leads to formation of sprouts. If two sprouts get in contact, they can form a new blood vessel[157-159]. Assessment of angiogenesis can be performed for example, by measuring serum levels of VEGF and FGF.

In context of GVHD, angiogenesis had been described in the mid1970s' for the first time[160]. Thenceforth, there has been little research activity in the field of angiogenesis in GVHD. In 2010, a study of Penack et al. described an increased vessel density during GVHD in the target organs skin, liver and colon in murine GVHD models[161]. The association of increased vessel density and GVHD was confirmed in human biopsies of patients suffering from GVHD[161-164]. These findings brought up the idea of the endothelium as a possible effector cell type in GVHD. Penack et al.[163] hypothesized a versatile role of endothelial cells in the context of GVHD. After initial endothelial damage caused by the conditioning regime, significant neovascularization is initiated during inflammation of T-cells. Furthermore, vasculature itself is a target of allo-reactive T-cells[163]. Active involvement of endothelial cells in the pathobiology of GVHD is supported by mechanistic studies, targeting VE-cadherin and α_v integrin in murine GVHD models. Blockade of VE-cadherin or α_v integrin led to amelioration of GVHD symptoms and reduced mortality, while GVT reaction was unaffected[161-163]. These finding shed light to compounds targeting endothelial function in the treatment of GVHD.

Endothelial damage

Endothelial damage and dysfunction is involved in many inflammatory diseases, like inflammatory bowel disease[165] and multiple sclerosis[166]. The assessment in humans is quite easy to perform by measuring blood pressure, circulating endothelial cells (cECs) and serum levels of soluble factors like TM and angiopoeitin-2 (ANG2). ANG2 and angiopoeitin-1 (ANG1) were shown to be involved in the

maintenance of the endothelium in a quiescent state by phosphorylation of the transmembrane protein tyrosine kinase with immunoglobulin- and epidermal growth factor-like domains 2 (Tie2)[167]. In the healthy and quiescent endothelium, endothelial cells are covered by a layer of glycocalyx, they produce physiological amount of nitric oxygen and are in close contact to pericytes (Figure 12A).

Upon damage and dysfunction, redox signaling in endothelial cells leads to direct damage and cell lysis mediated by T-cells. Consequently, endothelial cells lose their glycocalyx layer and their contact to the basement membrane is disturbed. This results in the detachment of endothelial cells out of their endothelial monolayer. cECs could serve as marker of endothelial damage[168]. Additionally, the loss of pericytes also serves as a marker for endothelial damage (Figure 12B)[169].

The endothelium is considered to be actively involved in early complications of HSCT. Late complications after HSCT are cardiovascular events such as cardiomyopathy and atherosclerosis[170]. Recent studies found increasing evidence for endothelial damage during GVHD. Endothelial changes in cutaneous GVHD[171,172] and soluble markers of endothelial damage (soluble adhesion molecules[173], TM[87,174,175] and cECs[176]) have been investigated. Furthermore, the amount of endothelial damage correlates to the mortality rate of patients suffering from GVHD in clinical studies[174,175].

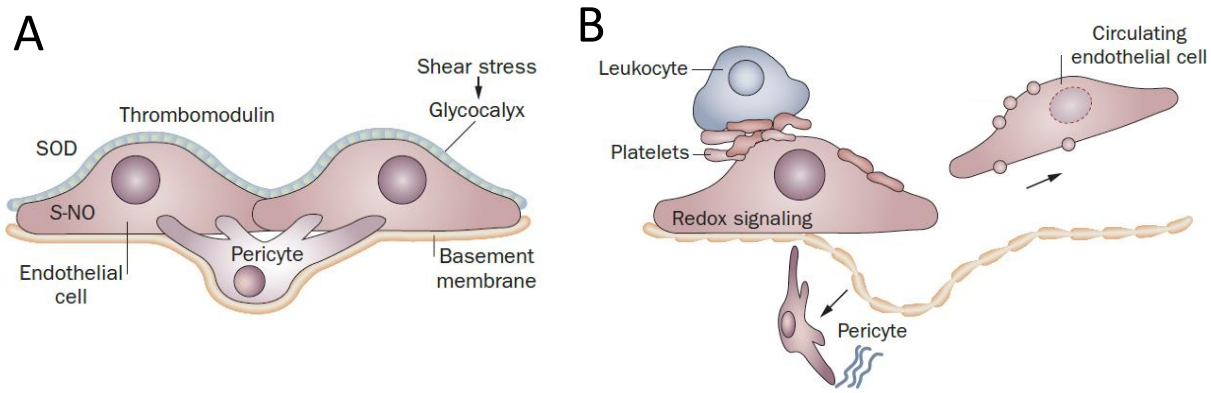

Figure 12| Process of endothelial damage. A| In the quiescent state, the antithrombotic, anti-inflammatory and anti-proliferative properties of the endothelium are maintained. The glycocalyx layer and pericytes are preserved and functional. **B|** Factors inducing damage or activation of endothelial cells lead to a release of glycocalyx fragments and adhesion molecules like ICAM1 into the blood flow. This process causes platelets and leukocytes to bind to the endothelial surface. Binding is initiating the formation of pro-inflammatory factors, like thrombin and the caspase activation complex. This further activates the endothelium and micro particles from the endothelium, platelets and leukocytes are released into the circulation. Furthermore, the stabilizing endothelial cell-pericyte interaction is disturbed, and pericytes start to produce proteases leading to damage of the basement membrane. Redox signaling of the endothelial cells may lead to apoptosis or necrosis of the endothelial cells and pericyte signaling is disturbed, leading to detachment and finally to release of endothelial cells to the circulation. (S-NO, S-nitrosyl; SOD, superoxide dismutase). Modified according to Rabelink et al.[168].

1.6 AIM OF THIS STUDY

Allo-HSCT is the only curative treatment option for the many patients suffering from hematological malignancies. Currently used prophylactic and therapeutic strategies are only successful in 30-60% of the cases of GVHD[106]. Especially in srGVHD patients, the mortality rate is high[115,123]. GVHD treatment strategies aim to suppress and reduce effector T-cell expansion. This approach has many disadvantages and increases complications after HSCT, in particular the higher risk of infections and tumor relapse[177,178]. In srGVHD, further immune suppression is insufficient to stop disease progression. No standard treatment for srGVHD is currently available, and the pathobiology is poorly understood. Recent studies suggest a critical role of the endothelium in GVHD. It has been shown that early angiogenesis is important during GVHD, however, factors mediating this process remain unknown[152]. In established GVHD, endothelial damage is suspected to play a crucial role in the pathophysiology and may be relevant in srGVHD as well[174,175].

As shown in the schematic overview (Figure 14) we hypothesize that endothelial damage and dysfunction is elevated during GVHD with consequences for alloantigen presentation to T-cells. This might promote the expansion and migration of T-cells and thereby fueling the GVHD cascade. Therefore, aiming the endothelium with protective substances may be an optimal treatment strategy to reduce GVHD symptoms by maintaining GVT effects. Additionally, this study aims to establish a murine srGVHD model and to study endothelial alterations in this condition to shed light on the contribution of endothelial cells in srGVHD. A better understanding of endothelial cell involvement to the pathophysiology of GVHD may add additional markers to assess GVHD onset and may lead to new treatment strategies to reduce GVHD and srGVHD.

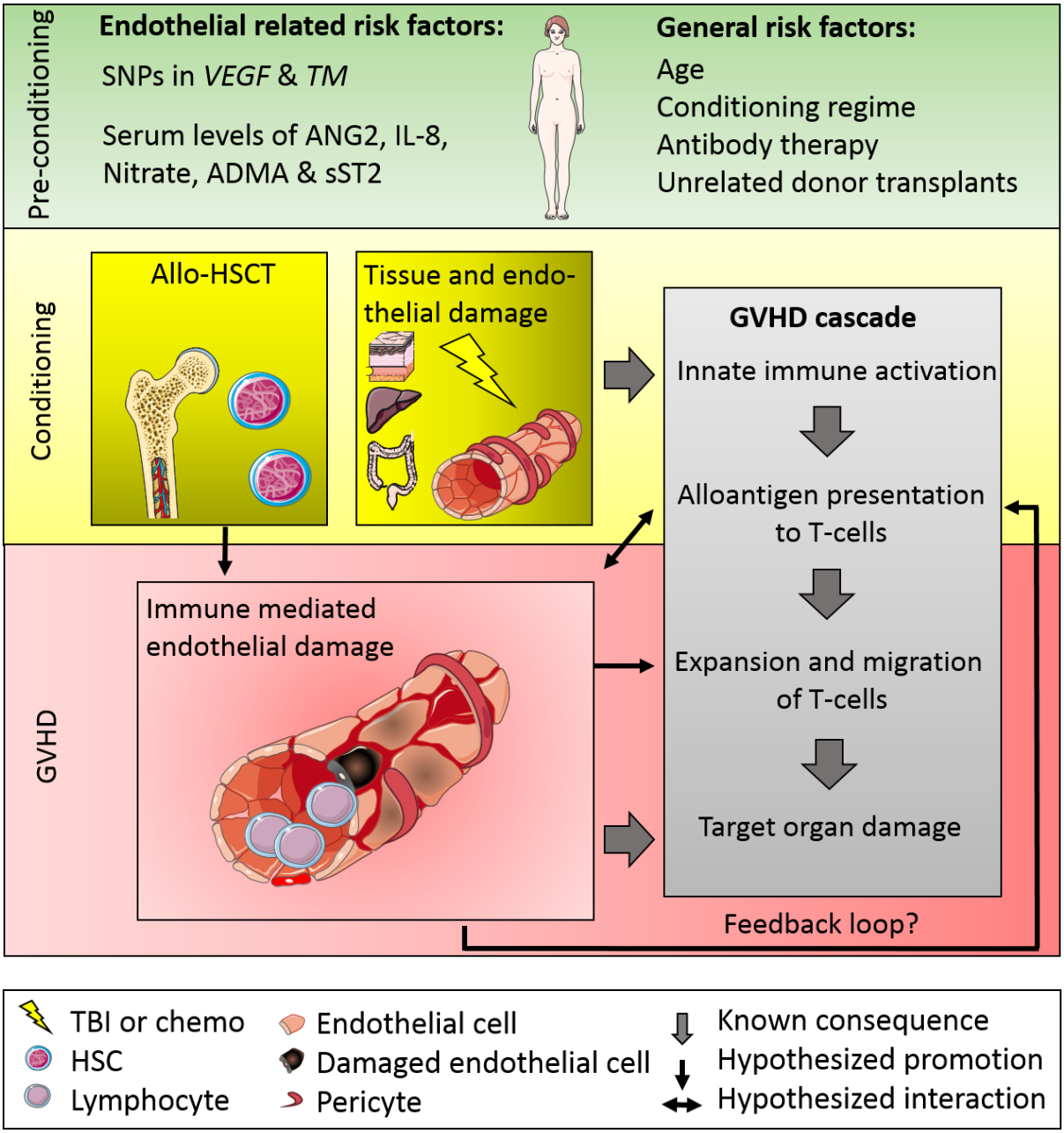

Figure 13| Graft-versus-host disease (GVHD) cascade including risk factors before hematopoietic stem cell transplantation (HSCT) and endothelial involvement in GVHD cascade. Risk factors previous (pre-) to conditioning for developing GVHD are listed within the green box. Besides known risk factors like age and conditioning regime, single nucleotide polymorphisms (SNPs) in the genes of *vascular endothelial growth factor* (*VEGF)* and *thrombomodulin (TM)*, markers for endothelial dysfunction such as angiopoietin 2 (ANG2), asymmetric dimethyl arginine (ADMA) and soluble ST2 (a member of the interleukin-1 receptor family) serum levels are included. Conditioning is leading to tissue damage and damage of endothelial cells (displayed in the yellow boxes), while allogenic (allo) HSCT is supposed to contribute to endothelial damage. The phases of classical GVHD cascade are displayed in the gray box. In GVHD, endothelium might be a direct target of allo-reactive T-cells. Endothelial damage is associated with target organ damage and may be connected with increased activation of the endothelium. Increased activation status of endothelial cells may be involved in the process of antigen presentation to T-cells. This may have an impact on expansion and migration of T-cells. (IL, interleukin; sST2, soluble ST2; TBI, total body irradiation; chemo, chemotherapy; HSC, hematopoietic stem cell). I created the schematic overview with templates from http://smart.servier.com/.

2 MATERIAL AND METHODS

2.1 *IN VIVO* METHODS

2.1.1 ANIMALS

C57BL/6 (B6) (H-2K^b), LP/J (H-2K^b) and B6D2F1 (BDF) (H-2K$^{b/d}$) mice were purchased from Charles River Laboratories (Sulzfeld, Germany). BALB/cByJRj (BALB/c) (H-2K^d) mice were purchased from Janvier Laboratories (St. Berthevin Cedex, France). All animals used in the experiments were female and 10-12 weeks old, housed in the Charité University Hospital Animal Facility under pathogen-free controlled conditions and 12h-light/dark cycle. Mice had access to food and water *ad libitum*. All experiments were approved by the Regional Ethics Committee for Animal Research (State Office of Health and Social Affairs Berlin).

2.1.2 ANALYSIS OF ACTIVATION STATUS OF THE DONOR ADAPTIVE IMMUNE SYSTEM

Donor mice were checked for activation of the adaptive immune system to ensure proper GVHD. Blood samples were collected via retro orbital bleeding of the animals and erythrocytes were lysed with ammonium chloride (Sigma Aldrich, USA). Cells were stained with CD25, CD62L, CD69 and CD3 as described in 2.2.3 and quantified by flow cytometry. Only donors with a maximum of 15-20% CD25$^+$ and 1-2% CD62l$^-$, CD69$^+$ of CD3$^+$ cells were used for transplantation experiments to prevent hyper-acute GVHD by pre-activation of donor T-cells.

2.1.3 RADIATION CONDITIONING

Female BALB/c recipient mice received 800 centigray (cGy) total body irradiation from a ^{137}Cs source (GSR D1, Gamma Service Medical, Germany) with a maximum of 0.85cGy per min as a split dose with a 4h interval and were injected with bone marrow (BM) and splenic T-cells at the same day, up to 2h after the last radiation dose.

Analogously to radiation of BALB/c recipients, female B6 recipient mice received 1200cGy total body irradiation.

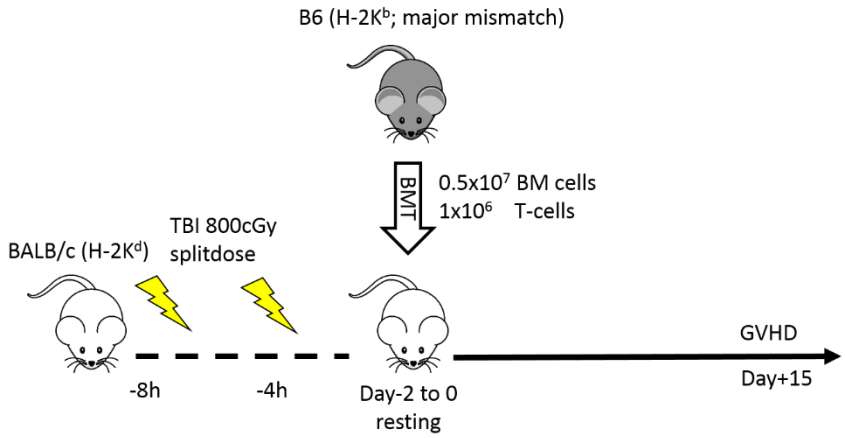

Figure 14| Schematic procedure of total body irradiation (TBI) and transplantation of B6→BALB/c major mismatch graft-versus-host disease (GVHD) model. (cGy, centigray; BMT, bone marrow transplantation; BM, bone marrow; H-2K^b, major histocompatibility complex 2K^b)

2.1.4 CHEMOTHERAPEUTIC CONDITIONING

7 days before bone marrow transplantation (BMT), female B6 mice received 20mg/kg/day busulfan (Sigma Aldrich, USA) on 5 consecutive days. Stock solution of 40mg/ml of busulfan in dimethyl sulfoxide (Carl Roth, Germany) was diluted in sterile phosphate-buffered saline (PBS) (Life Technologies, CA, USA) and applied by intraperitoneal injection (i.p.). Additionally, 5 days before BMT, 100mg/kg/day cyclophosphamide monohydrate (Sigma Aldrich, USA) dissolved in sterile water was applied by i.p. injection on 3 consecutive days. There was a 6h time interval between both injections. Conditioning protocol ended two days before BMT and T-cell injection[179].

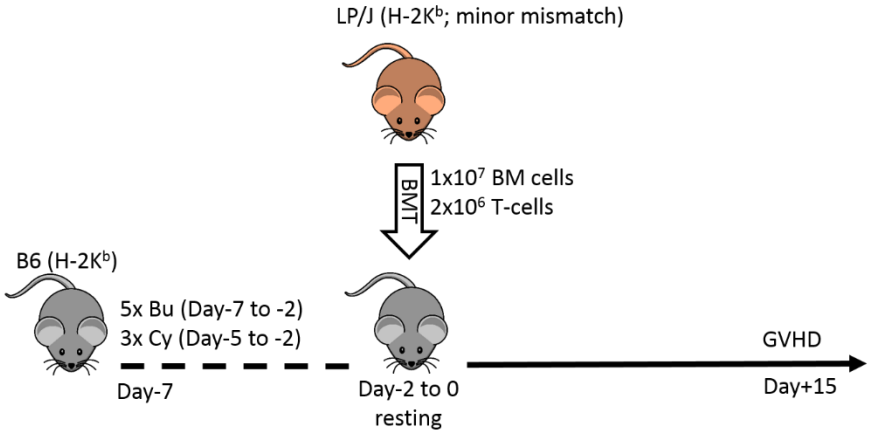

Figure 15| Schematic procedure of chemotherapy and transplantation of LP/J→B6 minor mismatch graft-versus-host disease (GVHD) model. (Bu, busulfan; Cy, cyclophosphamide; BMT, bone marrow transplantation; BM, bone marrow; H-2K^b, major histocompatibility complex 2K^d)

Analogously to B6 conditioning, chemotherapy was performed in B6D2F1 mice, with the exception that treatment started 6 days before BMT. Chemotherapy consisted of busulfan injections (20mg/kg/day) on 4 consecutive days. Additionally, mice received 100mg/kg/day of cyclophosphamide monohydrate injections on two consecutive days.

2.1.5 BONE MARROW ISOLATION

BM from the tibia, femur and humerus of donor mice was flushed out with isolation buffer (PBS/2% FCS/1mM EDTA). Single cell suspensions were prepared by passing the BM gently through a 23G needle and a 70µm cell strainer (BD Biosciences, USA) under sterile conditions. Erythrocytes were lysed with ammonium chloride (Sigma Aldrich, USA), washed with PBS and again passed through a 70µm cell strainer. After a final washing step, cell viability was quantified using Trypan blue (Sigma Aldrich, USA) staining and counting with a Neubauer chamber (Marienfeld Superior, Germany).

2.1.6 ISOLATION OF T-CELLS

Spleens were grounded with a sterile syringe plunger and passed through a 40µm cell strainer (BD Bioscience, USA). Erythrocytes in the single cell suspension were lysed with ammonium chloride. Cells were passed through another 40µm cell strainer and washed twice with PBS before resuspension in MACS buffer. Splenic T-cell suspension was obtained using Pan T-cell isolation Kit II for mouse (Miltenyi Biotec, Germany) according to manufacturer's instructions. T-cell viability was tested using

trypan blue staining. Purity of the T-cell suspension was evaluated by CD3 staining and flow cytometry analysis (at least 90% $CD3^+$ cells per isolation). The number of T-cells was calculated before injection according to purity.

2.1.7 INJECTION OF BONE MARROW AND T-CELLS

Mice were injected with different numbers of cells according to the GVHD model applied (see. Table1). Briefly, cells were stained with Trypan blue and viable cells were counted with a Neubauer counting chamber (Marienfeld Superior, Germany). Cells were washed twice with sterile PBS and resuspended in PBS for injection. Injection volume was 100µl of BM and 100µl of T-cells, resulting in a total injection volume of 200µl. For intravenous (i.v.) injection of cell suspensions, recipient mice were placed under a heat lamp for 10min before injection. Subsequently, mice were placed in an immobilization tube (TV-150 small, Braintree Scientific, USA) and one injection was applied i.v.: for syn-BMT recipients only syn-BM and for allo-BMT recipients, allo-BM and allo-T-cells. Cell numbers and conditioning regime for the different GVHD models are listed in Table 1. All animal models used in this study are comparable in the course of GVHD. Weight loss, score and survival as shown in supplemental Figure 1 are similar in the GVHD major mismatch models. Clinical parameters for the LP/J→B6 GVHD minor mismatch model (with mortality of 75% at day 40 after BMT) are described by Riesner et al.[179]. The used major mismatch models predominantly have hepatic and intestinal involvement, while cutaneous GVHD is less dominant. The used minor mismatch model predominantly has hepatic and cutaneous GVHD, while the intestinal GVHD is less dominant.

Table 1| GVHD models used in the study. (Bu, busulfan; Cy, cyclophosphamide; cGy, centigray; BM, bone marrow; H-$2K^b$, major histocompatibility complex $2K^b$)

Model	Conditioning	Cell numbers	Missmatch
LP/J - B6	5x Bu, 3xCy	$1x10^7$ BM, $2x10^6$ T-cells	minor mismatch (H-$2K^b$, H-$2K^b$)
B6 - BDF	4x Bu, 2xCy	$1x10^7$ BM, $5x10^6$ T-cells	major mismatch (H-$2k^b$, H-$2k^{bd}$)
BALB/c - B6	1100cGy splitdose	$0,5x10^7$ BM, $2x10^6$ T-cells	major mismatch (H-$2K^d$, H-$2K^b$)
B6 - BALB/c	800cGy splitdose	$0,5x10^7$ BM, $1x10^6$ T-cells	major mismatch (H-$2K^b$, H-$2K^d$)

2.1.7 GVHD MONITORING

Mice were individually scored at least twice a week regarding five clinical parameters (posture, activity, fur, skin and weight loss) on a scale from 0-2. Clinical GVHD score was assessed by summation of the individual score-numbers for each parameter. Animals were sacrificed when exceeding a total score of 6, or if one parameter reached a score of 2. Survival was monitored daily. At day 15 after BMT, chimerism of BMT donors was checked by staining of blood cells and analysis was performed by flow cytometry. Blood was collected via retro orbital bleeding. Erythrocytes were lysed with ammonium chloride (Sigma Aldrich, USA) and samples were washed with PBS afterwards. After resupending the single cell suspension, staining for H-$2K^b$, H-$2K^d$, Ly9 (for LP/J→B6 model) and CD3 according to the donor in the chosen GVHD model was performed as described in 2.2.3. Chimerism was confirmed by 80- 90% donor cells in the blood of BMT recipients.

2.1.8 TREATMENT OF GVHD

Dexamethasone (Merck, Germany) stock solution was diluted with PBS and daily applied i.p.. Dosage and starting point of treatment is indicated at each experiment. For the non-responder group (non-RS) 1mg/kg/day, for the responder group (RS) 2mg/kg/day were applied i.p. starting at day 4 after BMT. Defibrotide, a kind gift from JAZZ Pharmazeuticals (Ireland) was applied i.p. (700mg/kg/day in PBS) starting at day 4 after BMT. Beta-Aminopropionitrile fumarate (ß-APN), purchased from Sigma Aldrich (USA) was applied i.p. (2mg/kg/day in PBS) starting at day 4 after BMT. Plerixafor, a kind gift from Genzyme (USA) was applied i.p. (10mg/kg/day, in PBS) starting at day 4 after BMT.

2.1.9 ANESTHESIA OF MICE

Anesthesia was prepared in 1:1:2 dilution with 100mg/ml Ketavet (Pfizer, USA), 2% Xylavet (CP Pharma, Germany) and PBS. Depending on the size and weight of mice, 120-160µl were injected i.p.. 5min after injection, anesthesia was tested by tail and food pad reflexes.

2.1.10 EVANS BLUE ASSAY

For assessment of endothelial leakage, Evans blue assay was performed as described in detail elsewhere[180]**.** Evans blue was purchased from Sigma Aldrich (USA). Briefly, mice received an i.v. injection of a sterile 1% (w/v) Evans blue solution. 30min after injection, mice were sacrificed by cervical dislocation and the animal was perfused with PBS through the left ventricle for 5min with a flow rate of 5ml/min (PLP300, DüLab, Germany). After perfusion, organs were harvested, weighted and placed in tubes containing formalin solution (Roth, Germany). Samples were incubated at 56°C for 24h and supernatant was collected. The amount of Evans blue in the supernatant was determined at a wavelength of 610nm with a Benchmark plus microplate spectrometer system (BioRad, USA). To calculate the amount of Evans blue in the supernatant, a series of dilutions was measured for a standard curve. The extravasation of Evans blue from the blood vessels was calculated as mg of organ.

2.1.11 FITC-LECTIN PERFUSION

To determine the integrity of blood vessels we performed FITC-Lectin perfusion. FITC-Lectin was purchased from Vector Labs (USA) and dissolved in sterile PBS. A final concentration of 20µg FITC-Lectin was i.v injected into the tail vein. 10min after injection, mice were sacrificed by cervical dislocation and the animal was perfused with PBS as described in 2.1.10. After Perfusion, organs were harvested, placed into Tissue-tek optimum cutting temperature compound (Sakura Finetek, Netherlands) and stored at -80°C. The tissues were cut with a NX78 cryotome (ThermoScientific, USA) into 7µm thick slides and stained with anti CD31 antibody according to the protocol for immune histology. In addition to the secondary antibody (α-hamster), anti-FITC antibody was used to amplify the FITC-Lectin signal. Image analysis was performed with Fiji and my self-written macro CLDS (Appendix). For assessment of vessel perfusion, the ratio of total vessels to perfused vessels ($CD31^+$ area/FITC-$Lectin^+$ area) was calculated.

2.1.12 IMMUNOLABELING AGAINST VE-CADHERIN FOR LIGHT SHEET FLUORESCENCE MICROSCOPY

Analysis of blood vessel structure in colon was performed by vascular endothelial cadherine (VE-cadherin) perfusion. VE-cadherin antibody was purchased from eBioscience (USA). 25µg/mouse VE-cadherin antibody was injected i.v. into the tail vein. 30min after injection, mice were anesthetized as described in 2.1.9 and perfused with PBS at a flow rate of 5ml/min for 5min (PLP300, DüLab, Germany) and afterwards with a solution containing 4% paraformaldehyde for another 5min at the same flow rate. After perfusion, colon was harvested and placed in 4% paraformaldehyde solution overnight. The next day, colons were transferred in PBS and sent to our cooperation partner in Würzburg, where sample preparation and analysis was performed. Samples were dehydrated with increasing concentrations of ethanol (30%; 50%; 70%; 90%; 96%; 100%) for 2h each. Afterwards, they were placed for another 2h in n-hexane and finally cleared by incubating for 2h in 1x benzyl alcohol: 2x benzyl benzoate solution. Imaging of whole organs was performed by light sheet fluorescence microscopy (LSFM). LSFM allows imaging of transparent samples. Images were acquired using an in house-built scanner light-sheet fluorescence microscope, which was constructed according to a similar system described earlier[181]. A detailed description of the microscope setup can be found in the appendix. Control of all devices including galvanometer scanner, sCMOS camera, and motorized sample stage were managed using IQ 2.9 software (Andor, UK). Z-stack imaging of the sample was performed by moving the sample in the z-direction across the light sheet. Finally, obtained images were saved and processed by image analysis software for further analysis and 3D reconstruction. Analysis of vasculature and its segmentation were performed using Imaris 8.1 software (Bitplane, USA). Diameter, length, straightness as well as branch level were calculated for each dendrite and the results are presented as histograms.

Branch level is determined by the new branching point and diameter changes of the vasculature. The branch level increases as soon as the dendrite diameter at the branching point decreases. Straightness is defined as a ratio between dendrite length and the radial distance between two branch points.

2.2 *EX VIVO* METHODS

2.2.1 SMALL VESSEL WIRE MYOGRAPHY

Contraction of isolated mesenteric arteries was measured using a conventional small vessel wire DMT 610M myograph (Danish Myo Technology, Denmark). To isolate mesenteric arteries, animals were sacrificed by cervical dislocation and the intestine was removed without destroying the mesenteric bed. The mesenteric bed was transferred to cold (4°C), oxygenated (95% O_2, 5% CO_2) salt solution. Perivascular fat and connective tissue were removed from the arteries with precision tweezers (Dumont Nr. 5, Schwitzerland) and a microscissor (Aesculap OC498R, Aesculap AG & CO, D) using a stereomicroscope (Type MZ6 Leica, Germany). The arteries were then dissected into 2mm rings and each ring was mounted on two stainless steel wires (diameter, 0.0394mm) in a 2 ml organ bath[182]. The

organ bath was filled with PSS. The composition of PSS was 119mM NaCl, 4.7mM KCl, 1.2mM KH_2PO_4, 25mM $NaHCO_3$, 1.6mM $CaCl_2$, 1.2mM Mg_2SO_4 and 11.1mM D-glucose. The bath solution was continuously oxygenated with a gas mixture of 95% O_2 and 5% CO_2 and kept at 37°C (pH 7.4). The software Chart5 (AD Instruments Ltd.) was used for data acquisition and display. After an equilibration period of 60min and before starting the experiment, vessel constriction was provoked by 60mM KCl to assess viability and maximum contraction. The increased potassium concentration leads to membrane depolarization and contraction of the vascular smooth muscle cells. Afterwards the high potassium solution is washed out and replaced by physiologic PSS solution. Subsequently, the vessel constriction was provoked by noradrenaline (NA) and phenylephrine (Phe) at the concentrations indicated. After NA and Phe were washed out, we examined vasorelaxation by pre-constriction of arterioles with 35mmol/l K^+ and administration of acetylcholine (ACh). ACh causes endothelial cells to release nitric oxygen. This in turn causes relaxation of vascular smooth muscle cells. Again, after washing out K+ and ACh, we examined inhibitory effects of L-N^G-Nitroarginine methyl ester (L-NAME) on vasorelaxation. After pre-constriction with 35mmol/l K^+ and ACh administration L-NAME was added. L-NAME reserves vasodilation of ACh by inhibition of nitric oxygen synthase. Calibration and details are described elsewhere[182,183].

2.2.2 ENDOTHELIAL CELL ISOLATION

Hepatic endothelial cells were isolated to perform flow cytometry and gene array analysis. Single cell suspensions were generated via digestion. 2mg/ml collagenase D (Roche Diagnostics, Switzerland) and 5µl deoxyribonuclease (Sigma Aldrich, USA) in 1ml PBS were injected in the liver. The liver was cut into small pieces and incubated at 37°C for 45min with constant shaking. The cell suspension was passed two times through a 70µm cell strainer and washed with PBS and PBS/0.5 % bovine serum albumin (BSA). Hepatic endothelial cell fraction was enriched by gradient centrifugation using 30% histodenz (Sigma Aldrich, USA) according to manufacturer's instructions. This obtained single cell suspension was used for fluorescence staining and flow cytometry.

For gene expression analysis, the obtained single cell suspension was further enriched for endothelial cells ($CD11b^-$, $CD45^{dim/-}$, $CD31^+$) by fluorescence-activated cell sorting (FACS) using a Bio-Rad S3 cell Sorter (Bio-Rad, USA). Endothelial cell purity was checked via flow cytometry analysis of $ICAM1^+$ and $CD31^+$ cells.

2.2.3 FLUORESCENCE STAINING OF CELLS FOR FLOW CYTOMETRY

Single cell suspensions were prepared as described before. For blood samples, erythrocytes in the single cell suspension were lysed with ammonium chloride. For isolation of hepatic endothelial cells, erythrocytes were removed via density gradient centrifugation as described above. Single cell suspensions were washed twice with PBS/0.5mM EDTA/0.5% BSA and stained for 20min at 4°C in the dark with the rat anti-mouse antibodies from BD Biosciences (USA) listed in Table 2.

After staining, samples were washed twice with PBS and collected in MACS buffer. Samples were measured by BD FACSCanto II (BD Biosciences, USA) and analyzed with FlowJo 7.6.5 software (TreeStar Inc., USA).

Table 2| Antibodies for fluorescence staining of single cell suspensions for flow cytometry. (CD, cluster of differentiation; c-kit, tyrosine-protein kinase Kit; H-2K^b, major histocompatibility complex 2K^b; ICAM1, intracellular adhesion molecule 1; Ly9.1, T-lymphocyte surface antigen Ly9; MHC class II, major histocompatibility complex class II; Sca-1, Stem cell antigen 1; VEGFr2, vascular endothelial growth factor receptor 2; PE, phycoerythrin; APC, allophycocyanin; PerCp, peridinin chlorophyll protein complex; FITC, fluorescein isothiocyanate; Cy7, cyanine dye 7)

Name	Clone	Flourchrome	Company	Country
CD11b	M1/70	PE/APC-Cy7	BD Bioscience	USA
CD25	PC61	PE/APC/PerCp	BD Bioscience	USA
CD25	7D4	FITC	BD Bioscience	USA
CD31	MEC13.3	PE/APC	BD Bioscience	USA
CD3e	145-2c11	FITC/PE/APC/APC-Cy7	BD Bioscience	USA
CD4	RM4-5	PE/APC/PerCp/Pecy-7/Pac blue	BD Bioscience	USA
CD44	IM7	FITC/PE/APC/PerCp	BD Bioscience	USA
CD45	30-F11	FITC/PerCp	BD Bioscience	USA
CD62l	MEL-14	FITC/PE	BD Bioscience	USA
CD69	H1.2F3	PE/APC	BD Bioscience	USA
CD80	16-10AA	PE	BD Bioscience	USA
CD86	GL1	APC	BD Bioscience	USA
CD8a	53-6.7	FITC/APC/PerCp/APC-Cy7/Pac blue	BD Bioscience	USA
c-Kit	2B8	PE/APC/PE-Cy7	BD Bioscience	USA
H-2K^b	AF6-88.5.5.3	FITC/PE	BD Bioscience	USA
H-2K^d	SF1-1.1	FITC/PE	BD Bioscience	USA
ICAM1	3E2	APC/PerCp	BD Bioscience	USA
Ly9.1	30C7	FITC/PE	BD Bioscience	USA
MHC class II	OX-6	PerCp	BD Bioscience	USA
Sca-1	D7	FITC/PE-Cy7	BD Bioscience	USA
Ter119	TER119	PE-Cy7	BD Bioscience	USA
VEGFr2	AVAS 12a1	FITC/PE	BD Bioscience	USA

2.2.4 HISTOLOGY OF MURINE TISSUE

At the indicated time points (day 2; day 7; day 15) after BMT, large bowel and liver of allo- and syn-BMT recipients were harvested and cryoembedded in Tissue-tek optimum cutting temperature compound (Sakura Finetek, Netherlands). 7µm thick sections were cut with a NX78 cryotome (ThermoScientific, USA) and acetone-fixed for 10min at -20°C. The sections were blocked in blocking buffer (PBS/3% BSA/5% FCS) for 1h and stained over night at 4°C with primary rat anti-mouse antibodies. Sections were washed twice with blocking buffer and were then incubated for 2h at room temperature with secondary antibodies. For nuclear counterstaining, 4´.6-Diamidino-2-phenylindole (DAPI) from Sigma Aldrich (USA) was used. All antibodies (including the concentrations) are listed in Table 3. To determine positive staining, a minimum of five images per

sample was recorded with a Motic BA410 epifluorescence microscope (Motic, Hong Kong). Images were analyzed and the staining was quantified with a self-written macro (see Appendix) and predetermined threshold using Fiji Software (NIH, USA).

Single staining was analyzed with macro CLSS found in the appendix.

Pericyte and endothelial area was measured by the macro CLDS and pericyte-coverage was calculated by the formula:

$$\frac{pericyte\ marker\ positive\ pixel\ (\alpha SMA\ or\ NG2)}{endothelial\ cell\ marker\ positive\ pixel\ (CD31)}$$

ZO-1 pixel from $CD31^+$ pixel and total $CD31^+$ pixel were measured by the macro CLZE and percent of ZO-1 expressed by endothelial cells was calculated by the formula:

$$\frac{ZO-1\ positive\ pixel\ from\ CD31\ positive\ pixel}{total\ CD31\ positive\ pixel} * 100$$

Endothelial damage index (EDI) in colonic mucosa was calculated by the formula:

$$\frac{pericyte-coverage}{area\ CD4\ positive\ pixel}$$

Endothelial leakage index (ELI) in colonic mucosa was calculated by the formula:

$$\frac{percent\ ZO-1\ from\ endothelial\ cells}{area\ CD4\ positive\ pixel}$$

Table 3| Primary and secondary antibodies used for mouse immunohistology. (αSMA, alpha smooth muscle actin; CD, cluster of differentiation; NG2, neural/glial antigen 2; VE-cadherin, vascular endothelial cadherin; ZO-1, zonula occludens 1; IgG, immunoglobulin G; FITC, fluorescein isothiocyanate; Cy3, cyanine dye 3; Conc., concentration; µg, microgram)

Primary antibodies	Clone	Conjugated	Scource	Conc.	Company	Country
αSMA	1A4	Cy3	mouse	1:250	Sigma Aldrich	USA
CD31	2H8	purified	hamster	1:200	Thermo Scientific	USA
CD31	MEC 13.3	purified	rat	1:200	BD Pharmingen	USA
CD4	H129.19	purified	rat	1:500	BD Pharmingen	USA
CD8a	53-6.7	purified	rat	1:500	BD Pharmingen	USA
NG2	polyclonal	purified	rabbit	1:200	Millipore	USA
VE-cadherin	polyclonal	purified	goat	1:100	R&D Systems	USA
ZO-1	polyclonal	purified	rabbit	1:250	Thermo Scientific	USA

Secondary antibodies	Clone	Conjugated	Scource	Conc.	Company	Country
anti goat IgG	goat IgG	Cy3	donkey	1:1000	Millipore	USA
anti hamster	hamster	Cy3	goat	1:1000	Jackson Immuno Research	USA
anti rabbit	rabbit	Alexa Flour 488	donkey	1:1000	Life Technologies	USA

anti rabbit	rabbit IgG (H+L)	Alexa Flour 555	goat	1:1000	Invitrogen	USA
anti rat	rat	Cy3	goat	1:1000	Biolegend	USA
anti rat	rat	Alexa Flour 488	donkey	1:1000	Life Technologies	USA
anti FITC	polyclonal	FITC	goat	1:100	Abcam	UK

Antibodies used *in vivo*	**Clone**	**Conjugated**	**Scource**	**Conc.**	**Company**	**Country**
VE-cadherin	eBioBV13	eFluor660	rat	25µg/mouse	eBioscience	USA
FITC-Lectin	-	FITC	from tomato	100µg/mouse	Vector Labs	USA

2.2.5 PATIENT MATERIAL AND HISTOLOGY OF HUMAN BIOPSIES

The protocol to collect human samples was approved by the institutional ethics committee of the Charité and was in accordance with the Declaration of Helsinki. Intestinal biopsies were collected from patients with suspected intestinal GVHD after written informed consent was obtained. We performed a search in the biobank of our center to identify intestinal biopsies with GVHD versus no GVHD after allo-HSCTs performed between 2007 and 2016. We identified 12 duodenal biopsies from patients with GVHD grade III-IV and 19 duodenal biopsies from allo-HSCT recipients without histological evidence of GVHD. Furthermore, we identified 11 colon biopsies from patients with GVHD grade III-IV and 10 colon biopsies from allo-HSCT recipients without GVHD. The histological GVHD score was assessed by applying Lerner´s criteria.

Immunohistochemistry was performed on formalin fixed tissue sections. Tissue sections were incubated in 3% H_2O_2 to block endogenous peroxidases. Heat-induced antigen retrieval was performed in a pressure cooker, using citrate buffer, pH6 (Dako Cytomation, Denmark). The primary antibody was applied overnight at 4°C. Incubation with biotinylated secondary antibodies against the host species of the first antibody (Vector Laboratories, CA, USA) for 30min was followed by the ABC reagent (Vector Laboratories, CA, USA). 3,3′-Diaminobenzidine (Dako Cytomation, Denmark) was used for detection. Antibody diluent without primary antibody was used for negative control. Nuclei were counterstained with haematoxylin Harris (Leica, Germany). Antibodies applied to human biopsies are listed in Table 4. The sections were digitalized by the Institute of Pathology in Heidelberg and images were analyzed by Image Scope version 11 (Leica, Germany).

Table 4| Primary and secondary antibodies used for immunohistochemistry on human biopsies. (IgG, immunoglobulin G; Conc., concentration; µg, microgram)

Primary antibody	**Clone**	**Conjugated**	**Scource**	**Conc.**	**Company**	**Country**
cleaved caspase 3	Asp175	purified	rabbit	1:1000	Cell Signaling	USA

Secondary antibody	**Clone**	**Conjugated**	**Scource**	**Conc.**	**Company**	**Country**
anti-rabbit	rabbit IgG	biotinylated	goat	1:1000	VectorLabs	USA

Analysis was manually performed by a blinded investigator. Therefore, at least six high-power fields (HPF) for each patient were analyzed for the total number of vessels and the number of vessels with at least one caspase 3^+ (Casp3) endothelial cell. Percentage of $Casp3^+$ vessels in relation to total amount of vessels was calculated for each high-power field. Afterwards the mean for each patient of all high-power fields was calculated. Vessels without a distinct lumen were excluded from the analysis.

2.2.6 CONVENTIONAL TRANSMISSION ELECTRON MICROSCOPY

For assessment of ultrastructural changes, we harvested liver and colon from allo- and syn-BMT recipients at day 15 after BMT. Organs were cut with a razor blade in small 1mm thick pieces and were placed in 0.1M sodium-cacodylate/2.5% glutaraldehyde buffer and washed twice. Conventional transmission electron microscopy (CTEM) core facility took care of sample preparation. Briefly, another fixation step with 0.1M cacodylate buffer/1% OsO4 /0.8% K4(Fe(CN)6) for 1.5h and dehydration with increasing ethanol series (50%; 70%; 80%; 95%; 100%) was carried out two times for 10min. Embedding was performed by incubation of samples with propyleneoxide (SERVA, Germany) and epoxy resin (SERVA, Germany) in a ratio of 2:1 for 1h, followed by incubation in a 1:1 and 1:2 ratio for 1h each. Samples were kept overnight with epoxy resin and placed in molds, followed by incubation for 48h at 60°C. 0.5µm thick semi-thin sections were cut with a RM2065 microtome (Leica, Germany) and stained with methylene blue according to Richardson. The region of interest was determined by light microscopy and 70nm thick ultra-thin sections were prepared with an Ultracut S ultramicrotome (Leica, Germany). Staining was performed with uranyl acetate and lead citrate according to Reynolds. Microscopy was performed with an EM 906 electron microscopy (ZEISS, Germany).

2.3 MOLECULAR BIOLOGY METHODS

2.3.1 RNA ISOLATION FROM WHOLE ORGANS

Isolation of ribonucleic acid (RNA) was performed by freezing 30mg of the respective tissue in liquid nitrogen directly after harvesting at indicated time points after BMT. The tissue was homogenized with an ultra Thurax (IKA-Werke, Germany). RNA was isolated with RNeasy Mini Kit (Qiagen, Netherlands) following the manufacturer's instructions. Concentration and quality of the isolated RNA was determined by NanoDrop 1000 spectrophotometry (PEQLAB, Germany).

2.3.2 CDNA TRANSCRIPTION AND QUANTITATIVE PCR

1µg of total RNA was used for complementary deoxyribonucleic acid (cDNA) synthesis using the RNeasy Mini Kit (Qiagen, Netherlands) following the manufacturer's instructions. Primers and probes were designed using the Primer Express 1.5 software (Life Technologies, USA) and were ordered from BioTez GmbH (Germany). Quantitative polymerase chain reaction (qPCR) was performed using the TaqMan probe-based chemistry. qPCR amplification reaction was performed on a DNA Engine Opticon (BioRad, USA) using the TaqMan Gene Expression Master Mix (Life Technologies, USA) according to manufacturer's instructions. Thermal cycling conditions were as follows: 50°C for 2min,

95°C for 10min followed by 49 cycles of 95°C for 10s and 60°C for 1min. Data were collected and analyzed with the Opticon Monitor 3.1 analysis software (BioRad, USA) and the comparative CT Method (ΔΔCT Method). Primer and probe sequences are listed in Table 5.

Table 5| Primer and probes used for quantitative polymerase chain reaction. (FAM, 6-carboxyfluorescein; TAMARA, 6-caboxytetramethyl-rohdamine)

Gene Name	Abbreviation	Primer Sequence	
Angiopoietin-2	*ANG2*	Forward	5'-CTGCAAGTGTTCCCAGATGCT-3'
		Reverse	5'-TGTGGGTAGTACTGTCCATTCAAGTT-3'
		Probe	FAM-5'-AGGAGGCTGGTGGTTTGACGCATGT-3'-TAMRA
E-selectin	*E-sel*	Forward	5'-TGAACTGAAGGGATCAAGAAGACTT-3'
		Reverse	5'-GCCGAGGGACATCATCACAT-3'
		Probe	FAM-5'-ACAGCTGAACACGTGGGCTTCTT-3'-TAMRA
Intra cellular adhesion molecule 1	*ICAM1*	Forward	5'-GTCCGCTGTGCTTTGAGAACT-3'
		Reverse	5'-CGGAAACGAATACACGGTGAT-3'
		Probe	FAM-5'-TGGCACCGTGCAGTCGTCCG-3'-TAMRA
P-selectin	*P-sel*	Forward	5'-CGTCTCAGAAAGAAAGATGATGGA-3'
		Reverse	5'-GCAGCGTTAGTGAAGACTCCGTAT-3'
		Probe	FAM-5'-CCTTGAACCCTCACAGCCACCTAGGAA-3'-TAMRA
Thrombomodulin	*TM*	Forward	5'-CACCCAAGCCGGATGAAC-3'
		Reverse	5'-CAAACAGTAGGAGAGTTAGGGTCACA-3'
		Probe	FAM-5'-AAGTGCGAAATGTTCTGCAATGAAA-3'-TAMRA
Tyrosine kinase with immunoglobulin- and epidermal growth factor-like domains 2	*Tie2*	Forward	5'-GGGACAGTGCTCCAACCAAA-3'
		Reverse	5'-AGACTCGGTTGACAGTGAATATGG-3'
		Probe	FAM-5'-ACTTCAACTATACAGATCGTTTCTCAGTG-3'-TAMRA
Vascular cell adhesion protein 1	*VCAM1*	Forward	5'-TAAGACTGAAGTTGGCTCACAATTAAG-3'
		Reverse	5'-TGCGCAGTAGAGTGCAAGGA-3'
		Probe	FAM-5'-AAAGAACATAACAAGAACTATTTTTCGCCC-3'-TAMRA
Von Willebrand factor	*vWF*	Forward	5'-CCTTCTCCATTCTCGGGAACT-3'
		Reverse	5'-TCAAAAAACTCCCCAAGATACACA-3'
		Probe	FAM-5'-CCAAGATGGCAAGAGAATGAGCCTG-3'-TAMRA

2.3.3 MICROARRAY ANALYSIS

Total RNA from hepatic endothelial cells harvested at day 15 after BMT was isolated with the mirVana™ miRNA Isolation Kit (Life Technologies, USA) and subjected to microarray analysis (GeneChip® Mouse Gene 2.0 ST Array, Affymetrix, USA) at Max Dellbrück Center core facility for Genomics. The raw data were normalized with Expression Console Software and analyzed with Transcriptome Analysis Console (TAC) Software (Affymetrix, USA) using the following parameters: Fold change (linear) < -2 or > 2, ANOVA *P*-value (Condition pair) < 0.05.

2.4 CELL CULTURE

2.4.1 IMMORTALIZED MOUSE CARDIAC ENDOTHELIAL CELLS

Mouse cardiac endothelial cells (MCECs) were purchased from Cedarline (Canada) and cultured in DMEM medium supplemented with 10mmol/l penicillin/streptomycin, 10mmol/l HEPES and 5% fetal calf serum (FCS) in T75 cell culture flasks. Medium was changed every second day. Cells could grow till 80% confluency before they were passaged. The adherent monolayer was washed twice with PBS, incubated with 0.5% trypsin in PBS at 37°C for 5min, washed twice with DMEM medium supplemented with 10mmol/l penicillin/streptomycin, 10mmol/l HEPES and 5% FCS and $1x10^6$ MCECs were seeded on T75 cell culture flasks. For *in vitro* assays, cells were used in passage 3-6.

2.4.2 SERUM CO-CULTURE WITH MOUSE CARDIAC ENDOTHELIAL CELLS

For measuring activation of endothelial cells by soluble factors, we performed co-culture of MCECs with serum obtained from animals at day 15 after BMT. Blood was collected by retro orbital sampling. Around 800-1000µl were obtained per BMT recipient. The blood was stored for 20min at room temperature. After clotting, the samples were centrifuged for 10min at 13000 rpm in a centrifuge (Eppendorf, Germany). The supernatant was removed with a pipette and stored at -20°C. MCECs were cultured as described before and serum starved for 24h before the co-culture experiments. $5x10^4$ cells per well were placed in 24well plates and DMEM with 10mmol/l penicillin/streptomycin, 10mmol/l HEPES and 5% mouse serum either from syn- or allo-BMT recipients were added. After 24h, cells were detached from the flask with 0.5% trypsin as described before and stained for MHC class I, MCH class II, ICAM1, CD80 and CD86 as described in chapter 2.2.3. Phenotypic changes were analyzed by flow cytometry.

2.5 STATISTIC ANALYSIS

2.5.1 *IN VIVO* AND *EX VIVO* STATISTICS

Survival data were analyzed using the Kaplan-Meier-method and statistical significance was tested with Mantel-Cox log-rank test. For statistical analysis of all other data, except for the LFSM approach, the Student´s unpaired *t*-test was used. Values are presented as mean ± SEM (standard error of the mean) *P*-value ≤ 0.05 was considered as statistically significant. All statistical analyses were performed using GraphPad Prism software (GraphPad software Inc, USA).

2.5.2 PROBABILITY DENSITY FUNCTION FOR BLOOD VESSEL STRUCTURE

Probability density function (PDF) was used as a method for structural comparison of blood vessels. This function gives a set of possible values assigned to the random variable and provides a relative likelihood that a value would equal the sample. The value of the PDF of two different samples can be used to test, how much more likely it is that the random variable would equal one sample compared to the other sample.

2.6 MATERIAL

2.6.1 INSTRUMENTS

Table 6| Instruments used.

Name	Company	Country
Neubauer counting chamber	Marienfeld Superior	Germany
Ultra turrax t25 basic	IKA®-Werke GmbH & CO. KG	Germany
DNA Engine Opticon	BioRad	USA
Motic BA410 epifluorescence microscope	Motic	Hong Kong
Inverted microscope	ZEISS	Germany
Objective inverter	LSM Tech	USA
Stepper motor–controlled stage	Standa	Lithuania
Bio-Rad S3 cell sorter	BioRad	USA
BD FACSCanto II	BD Biosciences	USA
RM2065 microtom	Leica	Germany
Ultracut S ultramicrotome	Leica	Germany
EM 906 electron microscopy	Zeiss	Germany
DNA Engine Opticon	BioRad	USA
Fiber coupled laser combiner	BFI OPTiLAS GmbH	Germany
Objective lens	A10/0.25 Hund	Germany
Dichroic beam splitter DCLP 660	AHF Analysentechnik	Germany
Galvanometer scanner 6210H	Cambridge Technology	USA
Theta lens VISIR f. TCS-MR II	Leica	Germany
Objective lens EC Plan-Neofluar 5x/0.16 M27	ZEISS	Germany
HCX APO L20x/0.95 IMM objective	Leica	Germany
MAC 6000 Filter Wheel Emission TV 60 C 1.0x with a MAC 6000 Controller	ZEISS	Germany
Metal holder for translation	Newport	Germany
Rotator	Standa	Lithuania
Fixation tube TV-150 small	Braintree Scientific	USA
sCMOS camera	Andro	UK
DMT 610M myograph	Danish Myo Technology	Denmark
Precision tweezers	Dumont Nr. 5	Switzerland
Microscissor Aesculap OC498R	Aesculap AG & CO	Germany
Stereomicroscope Type MZ6	Leica	Germany
NX78 cryotome	Thermo Scientific	USA
GSR D1	Gamma Service Medical	Germany

2.6.2 CONSUMABLES

Table 7| Consumables used.

Product	Company	Country
3,3′-Diaminobenzidine (DAB)	Dako Cytomation	Denmark
4-(2-hydroxyethyl)-1-piperazineethanesulfonic acid (HEPES)	Invitrogen	USA
4´,6-Diamidino-2-phenylindole (DAPI)	Sigma Aldrich	USA
40µm cell strainer	BD Biosciences	USA

70µm cell strainer	BD Biosciences	USA
ABC reagent	Vector Laboratories	USA
Aceton	Sigma	USA
Acetylcholine (ACh)	Sigma-Aldrich	USA
Albumin fraction V (BSA)	Roth	Germany
Ammonium chloride	Sigma	USA
Antigen retrieval citrate buffer, pH6	Dako Cytomation	Denmark
Benzyl alcohol	Roth	Germany
Benzyl benzoate	Agar Acientific	UK
Beta-Aminopropionitrile fumerate (ß-APN)	Sigma	USA
Busulfan (Bu)	Sigma Aldrich	USA
BZO seal film	Biozym Scientific GmbH	USA
Calcium chloride ($CaCl_2$)	Sigma	USA
Cell culture dishes, 60x15mm	Greiner bio one	USA
Chloroform	Roth	Germany
Collagenase D	Roche Diagnostics	Schwitzerland
Cyclophosphamide monohydrate (Cy)	Sigma	USA
D(+) glucose	Merck	Germany
Defibrotide	JAZZ Pharmaceuticals	Ireland
DEPC-H2O	Ambion	USA
Dexamethasone (DEX)	Merck	Germany
d-Glucose	Roth	Germany
Dimethyl sulfoxide (DMSO)	Roth	Germany
DMEM medium	Gibco	USA
DNase	Sigma Aldrich	USA
Dodium chloride (NaCl)	Sigma-Aldrich	USA
Epoxy resin	SERVA	Germany
Ethanol rotipuran >99,8%	Roth	Germany
Ethylenediaminetetraacetic acid (EDTA)	Sigma	USA
Ethylene-glycol-bis(2-amino-ethylether) -N,N,N´,N´-tetraacetic acid (EGTA)	Fluka	USA
Evans blue	Sigma	USA
Falcon 15ml	VWR	Germany
Falcon 50ml	SPL Lifesciences	Korea
Fetales calf serum (FCS)	Invitrogen	USA
Formalin solution	Roth	Germany
Glutaraldehyde	Roth	Germany
Haematoxylin Harris	Leica	Germany
Histodenz	Sigma-Aldrich	USA
Hydrogen peroxide	Sigma	USA
Isopropanol	J.T. Baker	USA
Ketavet	Pfizer	USA
L-glutamin stock solution (200mM)	Gibco	USA
L-N^G-Nitroarginine methyl ester (L-NAME)	Sigma	USA

MACS separation columns, MS columns	Milteny Biotec	Germany
Magnesium sulfate (Mg_2SO_4)	Sigma	USA
Monopotassium phosphate (KH_2PO_4)	Merck	Germany
Needles (20G, 23G, 27G)	Braun	Germany
n-Hexane	Roth	Germany
Noreadrenalin (NA)	Sigma-Aldrich	USA
Osmium tetroxide (OsO_4)	Sigma	USA
Paraformaldehyd (PFA)	Sigma	USA
Pasteur pipettes	VWR	Germany
PCR 96-well plates	BioRad	USA
Penicillin/Streptomycin 10x	Invitrogen	USA
Phenylephrine (Phe)	Sigma	USA
Phosphate-buffered saline (PBS)	Life Technologies	USA
Plerixafor	Genzyme	USA
Potassium chloride (KCl)	Roth	Germany
Potassium hexacyanoferrate(II) trihydrate ($K_4(Fe(CN)_6)$)	Sigma	USA
Potassium hygrogen carbonate ($KHCO_3$)	Fluka	USA
Propyleneoxide	SERVA	Germany
Serological pipettes 10ml	Sarstedt	Germany
Serological pipettes 25ml	Sarstedt	Germany
Serological pipettes 5ml	Sarstedt	Germany
Sodium bicarbonate ($NaHCO_3$)	Sigma	USA
Sodium-cacodylate	Roth	Germany
ß-Mercaptoethanol	Sigma-Aldrich	USA
Syringe 1ml	Braun	Germany
Syringe 5ml	Braun	Germany
TaqMan Gene Expression Master Mix	Applied Biosystems	USA
Tissue-tek O.C.T.TM compound	Sakura Finetek	Netherlands
TRI Reagent	Ambion	USA
Trypan blue	Sigma	USA
Trypsin	Invitrogen	USA
Uranyl acetate	Sigma	USA
Xylavet	CP Pharma	Germany

2.6.3 KITS

Table 8| Commercially available Kits used.

Name	**Company**	**Country**
GeneChip® Mouse Gene 2.0 ST Array	Affymetrix	USA
mirVana™ miRNA isolation Kit	Life Technologies	USA
Pan T-cell Isolation Kit II for mouse	Milteny Biotec	Germany

QuantiTect Reverse transcription Kit	Quiagen	Netherlands
RNeasy Mini Kit	Quiagen	Netherlands
TaqMan Gene Expression Master Mix	Life Technologies	USA

2.6.4 CELL LINE

Table 9| Commercially available cell line used.

Name	Company	Country
Mouse cardiac endothelial cell line (MCEC)	Cedarline	Canada

2.6.5 SOFTWARE

Table 10| Software used.

Name	Company	Country
Primer Express 1.5 software	Applied Biosystems	USA
LabView software	National Instruments	USA
Software package MetaMorph 7.1	Molecular Devices	USA
ImageJ	National Institute of Health	USA
Volocity	PerkinElmer	USA
IQ 2.9 software	Andor	UK
FlowJo 7.6.5 software	TreeStar Inc.	USA
Fiji software	National Institute of Health	USA
Opticon Monitor 3.1 analysis software	BioRad	USA
Expression Console software	Affimetrix	USA
GraphPad Prism software	GraphPad Software Inc.	USA
Imaris 8.1 software	Bitplane	USA
Microplate Manager 6 software	BioRad	USA
Chart5	AD Instruments Ltd.	Australia
Image Scope version 11	Leica	Germany
Transcriptome Analysis Console	Affimetrix	USA

3 RESULTS

3.1 CASPASE 3 STAINING IN HUMAN BIOPSIES

To obtain information about endothelial apoptosis for indirect analysis of endothelial damage during the acute phase of GVHD, we retrospectively analyzed human colon and duodenum biopsies for endothelial damage with the apoptotic cell marker Casp3, up to 100 days after HSCT. Patient samples diagnosed for either no GVHD or GVHD grade III-IV were used for the analysis. Exemplary pictures of human colon section show no GVHD (Figure 16A) and grade III-IV GVHD (Figure 16B). The dotted white line marks vessel lumen in colonic mucosa and black arrows indicate endothelium-specific Casp3 events. In biopsies of patients diagnosed with no GVHD, endothelial Casp3$^+$ cells were rare events, while in biopsies of grade III-IV GVHD patients, Casp3$^+$ endothelial cells were quite common. Quantification revealed a significant increase in percentage of Casp3$^+$ vessels in duodenal (Figure 16C) and colonic mucosa (Figure 16D) of grade III-IV GVHD compared to noGVHD.

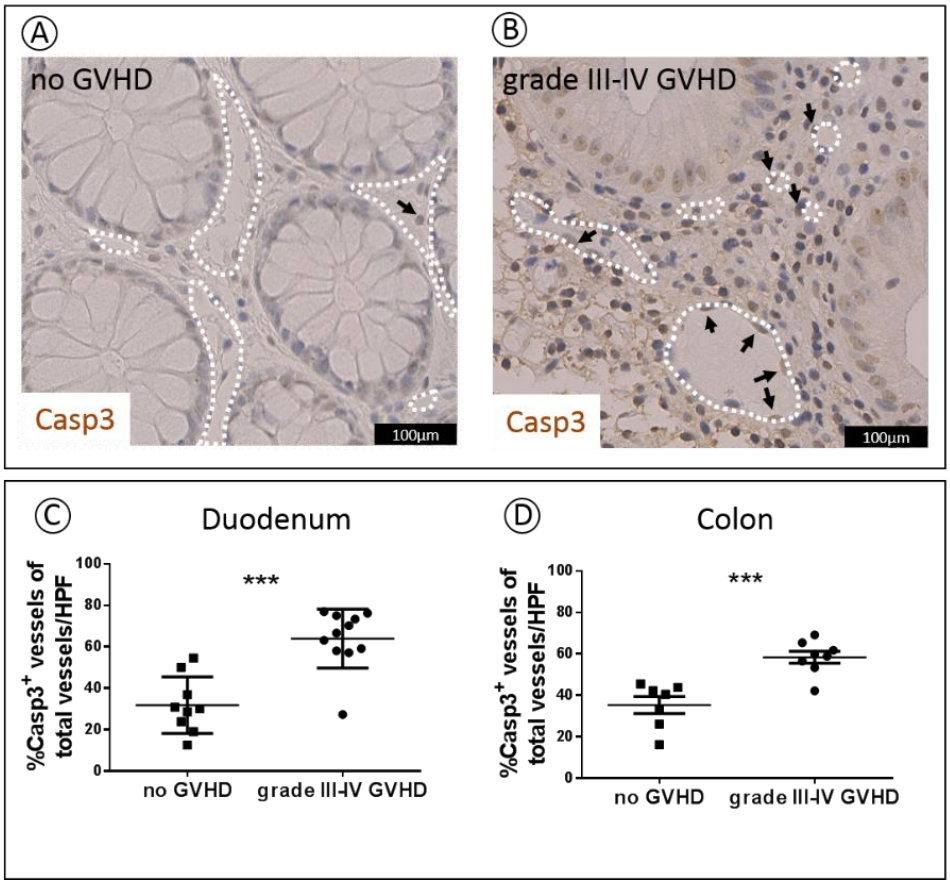

Figure 16| Endothelial damage in human intestinal biopsies. A| Exemplary picture of colon biopsy of a patient with no GVHD. The white dotted line indicates vessel lumen and the arrows indicate apoptotic caspase 3 (Casp3$^+$) endothelial cells. **B|** Exemplary picture of colon biopsy of a patient with grade II-IV GVHD. The white dotted line indicates vessel lumen and the arrows indicate apoptotic Casp3$^+$ endothelial cells. **C|** Quantification of Casp3$^+$ events in colonic endothelium given in percent per high-power field (HPF). **D|** Quantification of Casp3$^+$ events in duodenal endothelium given in percent per HPF. Percentage of Casp3$^+$ vessels was tested for significance by student's *t*-test (***$P < .001$; n=7-11 patients per group). Error bars indicate mean ± standard error of the mean (SEM).

These data provide strong evidence of increased endothelial damage during GVHD. To get a better understanding of the pathophysiologic role of endothelial damage during GVHD, we hereafter used mouse models of GVHD. In murine tissue, Casp3 staining in the endothelium is hardly distinguishable from Casp3$^+$ cells in the surrounding. For that reason, we decided to describe endothelial damage of microstructure by CTEM, cECs, pericyte-coverage, vascular structure, vascular leakage and physiological functions of endothelial cells.

3.2 DAMAGE OF ENDOTHELIAL CELLS AND ULTRASTRUCTURAL CHANGES DURING GVHD

To address the question of microstructural changes of endothelium during GVHD, we performed CTEM of the GVHD target organs liver (Figure 17) and colon (Figure 18) at day 15 after BMT. Endothelium of hepatic sinusoidal endothelium in syn-BMT recipients was inconspicuous. The endothelial monolayer and endothelial cell-cell contacts were intact (Figure 17A, B). Fenestration of the endothelial monolayer in hepatic sinusoids was observed (Figure 17B). In contrast, hepatic sinusoidal endothelium of allo-BMT recipients was significantly damaged. We detected close immune cell-endothelial cell interactions (Figure 17C) in allo-BMT recipients. Furthermore, the discontinuous endothelial monolayer at the contact zone with immune cells (Figure 17D) was observed in allo-BMT recipients.

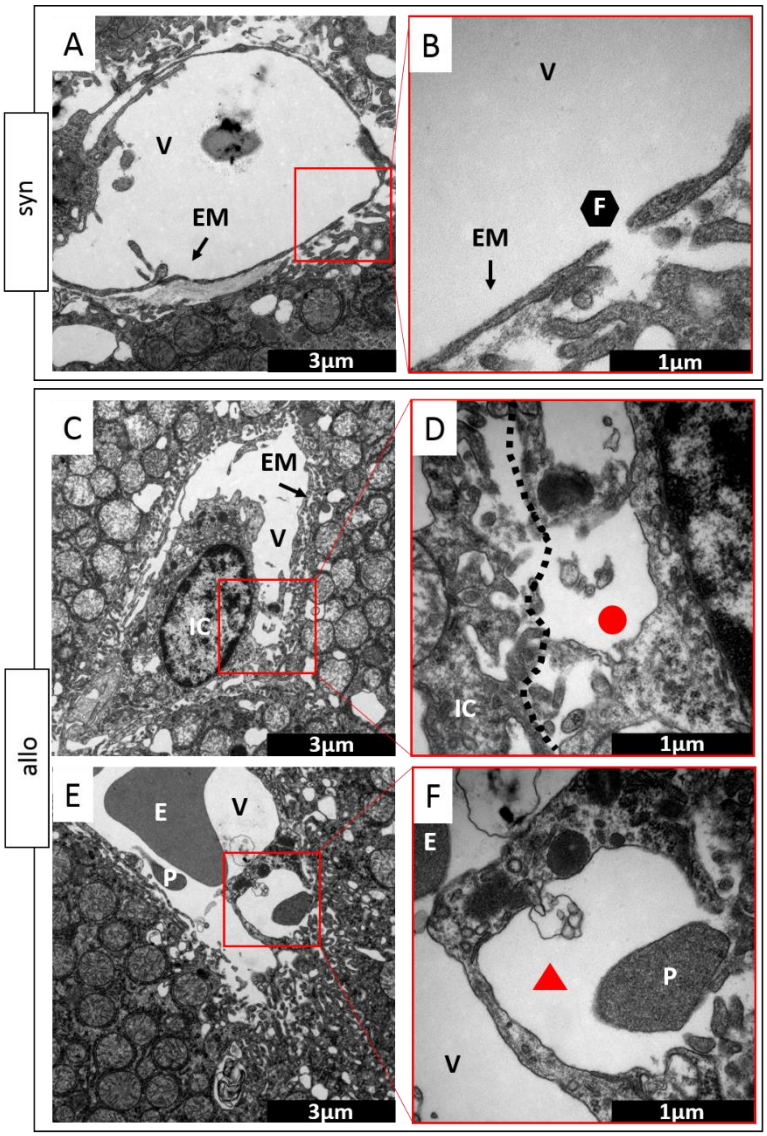

Figure 17| Visualization of ultrastructural changes in the liver by conventional transmission electron microscopy. A-B| Liver sinusoidal endothelial monolayer of a syngeneic (syn) transplanted animal day 15 after bone marrow transplantation (BMT). **A|** Normal, fenestrated sinusoidal blood vessel completely covered with endothelial monolayer. **B|** Higher magnification of a 100nm large fenestration of endothelium in the liver. **C-F|** Sinusoidal liver endothelial monolayer of an allogeneic (allo) BMT recipient day 15 after BMT. **C|** Liver sinusoidal vessel with an immune cell in contact with destroyed and unregularly shaped endothelial monolayer. **D|** Magnification of contact zone from immune cell-endothelial cell, revealing loss of endothelium. **E|** Blistering of endothelial monolayer with a platelet in the region of injury, **F|** higher magnification of endothelial blistering. Perivascular space is marked by a red triangle. Experiment was performed in the B6→BDF graft-versus-host disease model. (V, vessel lumen; EM, endothelial monolayer; F, fenestrated endothelium; IC, immune cell; E, erythrocyte; P, platelet; red circle, loss of endothelium; red triangle, endothelial blister)

We detected blistering of the endothelial monolayer in liver samples of allo-BMT recipients (Figure 17E). Also, platelet adhesion on sinusoidal endothelial monolayer (Figure 17E) and platelet adhesion in the blistered endothelium was detectable at the side of injury (Figure 17F).

In colonic mucosa, vessels were inconspicuous in syn-BMT recipients as well. We noted a well-structured, smooth endothelial monolayer surrounded by a pericyte (Figure 18A) with intact tight junctions (Figure 18B). In contrast, allo-BMT recipients had an activated, ruffled endothelial monolayer (Figure 18E) with perivascular fibrinogen deposits (Figure 18C, D and F). Endothelial cytoplasm was enriched with vesicles and discontinuous endothelial monolayer was observable (Figure 18D). We detected clotting in the colonic microvasculature as well as convolution of the endothelial monolayer (Figure 18E).

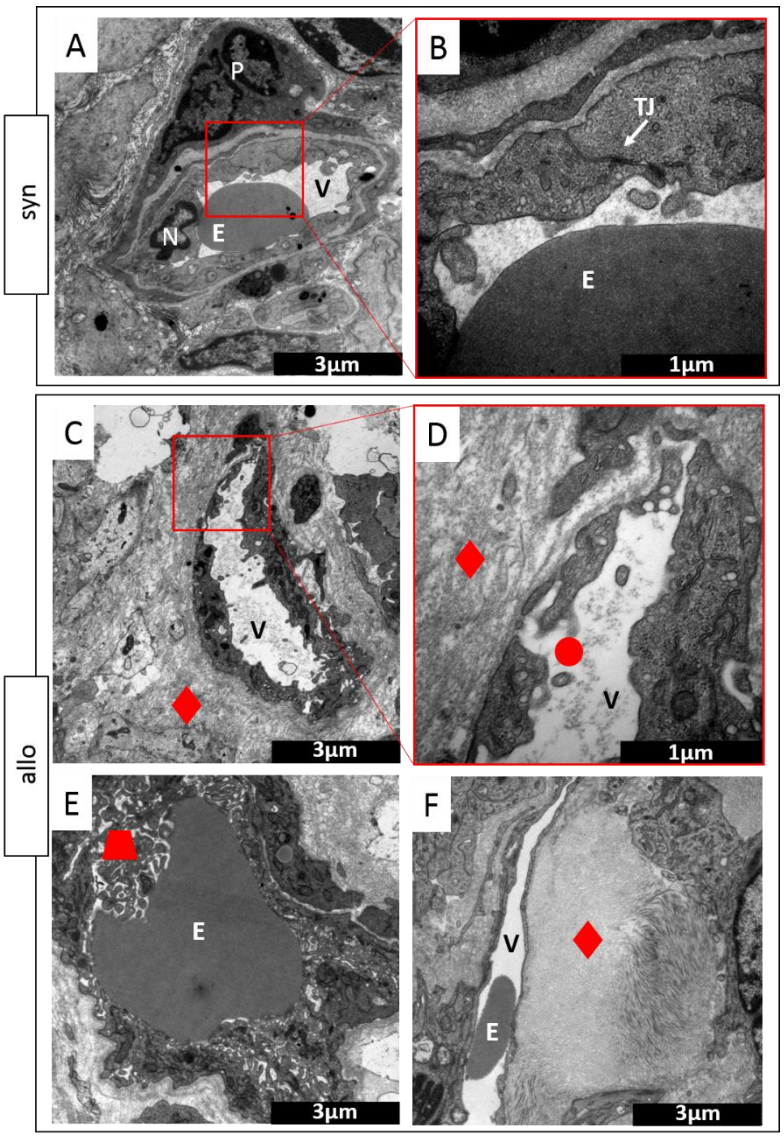

Figure 18| Visualization of ultrastructural changes in colon by conventional transmission electron microscopy. A-B| Colonic mucosa endothelium in a syngeneic (syn) transplanted recipient day 15 after bone marrow transplantation (BMT). **A|** Unaltered endothelial monolayer with a prominent endothelial-endothelial cell contact. The vessel is surrounded by a pericyte. **B|** Higher magnification of an intact endothelial-endothelial cell contact. **C-F|** Colonic mucosa endothelium of an allogeneic (allo) transplanted animal day 15 after BMT. **C|** Ruffled, activated endothelium with many vesicles in endothelial cytoplasm and reduced thickness of endothelial monolayer. The vessel is surrounded by perivascular fibrinogen deposits marked by a red rhombus. **D|** Magnification of endothelial monolayer, showing vesicles and irregular thickness of endothelium marked by a red circle. Perivascular fibrinogen deposits are marked by a red rhombus. **E|** Vessel in mucosa filled with an erythrocyte; the endothelial monolayer is strongly convolved, marked with a red trapezoid. **F|** Large vessel in colonic mucosa with prominent perivascular fibrinogen accumulation marked by a red rhombus. Experiment was performed in the B6→BDF graft-versus-host disease model. (V, vessel lumen; E, erythrocyte; P, pericyte; N, nucleus; TJ, tight junction; red rhombus, perivascular fibrinogen deposits; red circle, irregular, activated endothelium; red trapezoid, endothelial convolution)

These data show that in murine GVHD many changes occurred, which are connected to increased endothelial damage in allo-BMT recipients. The micro-structural changes are in line with the increase of Casp3^{+} endothelial cells in human GVHD biopsies.

3.3 cECs AS ENDOTHELIAL DAMAGE MARKER DURING GVHD

To quantify endothelial damage during GVHD, we analyzed the amount of cECs in blood samples of syn- and allo-BMT recipients. An increase in cECs has been demonstrated as marker for endothelial damage[168].

We took blood by retro orbital bleeding of recipients and stained the blood cells for CD45, Ter119, VEGFr2 and CD11b. cECs were defined as CD45$^{dim\ to\ -}$, Ter119^{-} CD11b^{-} and VEGFr2^{+} as shown in Figure 19A. Quantification was performed by flow cytometry. The amount of cECs per µl blood revealed a trend of increased cECs in allo- compared to syn-BMT recipients at day 15 after BMT (Figure 19B).

These data put further evidence to an increased endothelial damage during the course of GVHD.

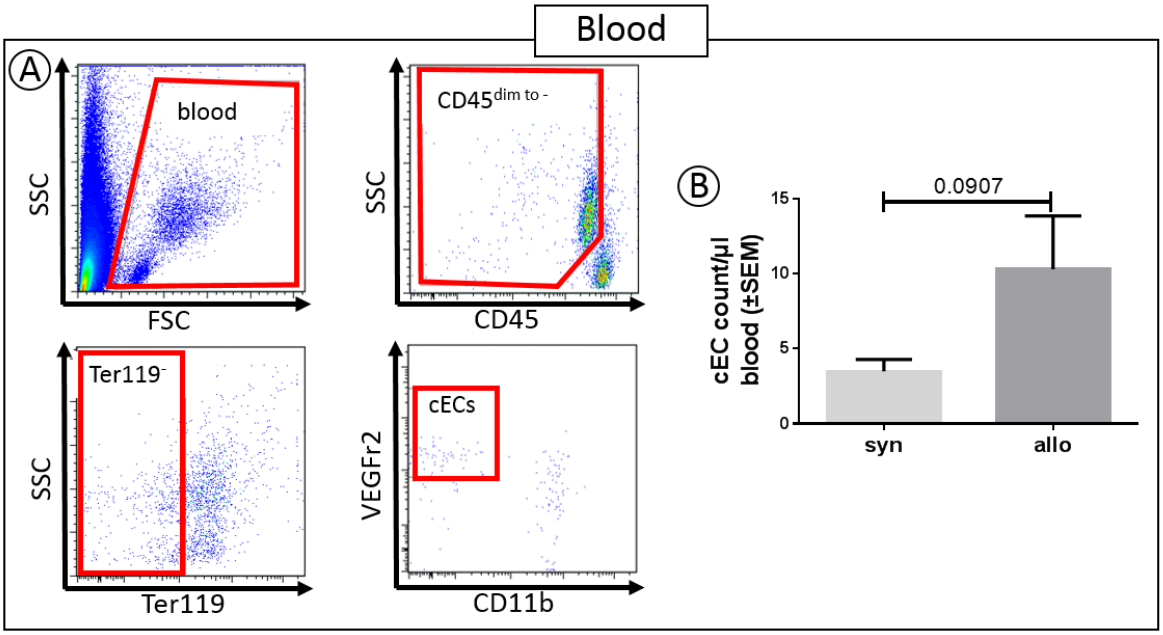

Figure 19| Gating strategy of circulating endothelial cells (cECs) in blood and quantification of cECs. A| Gating strategy of endothelial cells in blood. Stained blood single cell suspension was analyzed by flow cytometry. CD45$^{dim\ to\ -}$, Ter119^{-} CD11b^{-} and VEGFr2^{+} cells were defined as cECs. **B|** Quantification of cECs in blood of allogeneic (allo) and syngeneic (syn) transplanted recipients at day 15 after bone marrow transplantation. Experiments were performed in B6→BALB/c graft-versus-host model. Amount of cECs was calculated per µl blood and tested for significance by student's *t*-test (n=6 animals per group). Error bars indicate mean ± standard error of the mean (SEM).

3.4 PERICYTE-COVERAGE IN GVHD

As an additional method to quantify endothelial damage in murine GVHD, we quantified pericyte-coverage in colon and liver. Pericyte-coverage was defined as the amount of αSMA^{+} area divided by the amount of CD31^{+} area of colonic mucosa. We first compared animals that underwent chemotherapy to untreated control mice in order to show a correlation of endothelial damage to loss of

pericytes in mice. As shown in Figure 20, we could demonstrate a significant loss of pericytes in colonic mucosa (Figure 20A) and an almost significant loss in the sinusoidal hepatic endothelium (Figure 20D) of chemotherapeutically treated animals compared to untreated controls. We then checked colon and liver of allo- and syn-BMT recipients for reduced pericyte-coverage. Exemplary pictures of colonic mucosa (Figure 20B) and sinusoidal hepatic endothelium (Figure 20E) depict pericytes (αSMA, red) and endothelial cells (CD31, green). Reduced pericyte-coverage was detectable comparing tissue from syn-BMT recipients to allo-BMT recipients for both GVHD target organs. Quantification of pericyte-coverage in transplanted animals showed a significant loss of pericyte-coverage in allo- compared to syn-BMT recipients. This significant reduction of pericyte-coverage was observable in colonic mucosa (Figure 20C) and sinusoidal hepatic endothelium (Figure 20F) during the acute phase of GVHD. This reduction was only observable during the acute phase of GVHD and was reproducible in another GVHD mouse model (supplemental Figure 2D). The pericyte marker neural/glial antigen 2 (NG2) only showed a trend to be reduced (supplemental Figure 2C). In the colonic mucosa of allo- and syn-BMT recipients at earlier time points (day 2 and day 7 after BMT) we did not find significant differences in pericyte-coverage (supplemental Figure 2A and B).

We could show a loss of pericytes during GVHD, indicating a damaged endothelial monolayer.

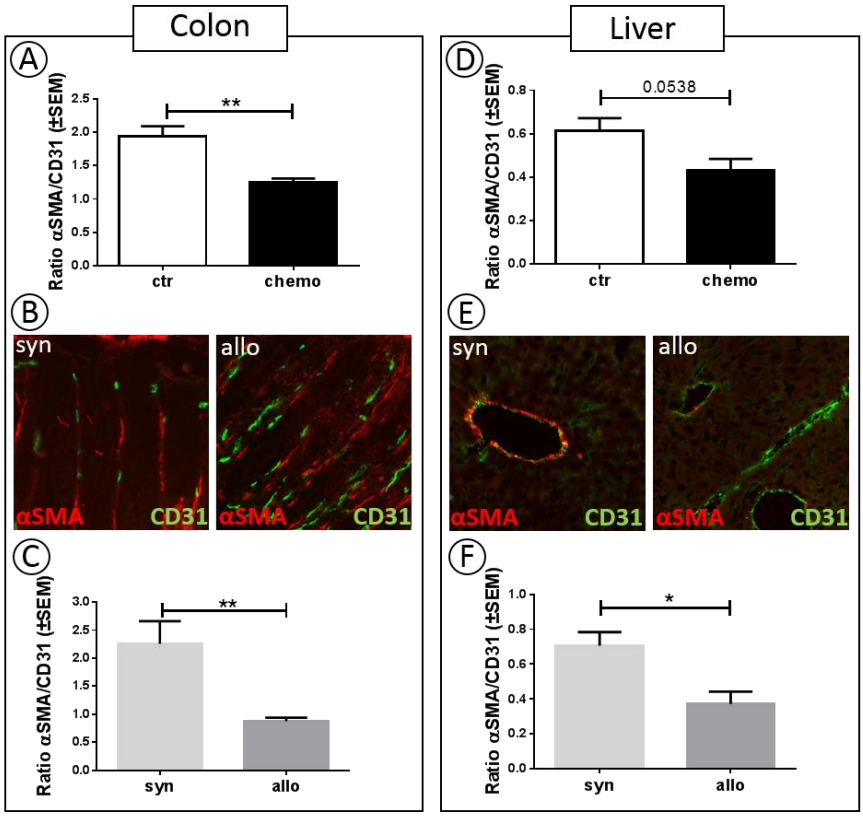

Figure 20| Quantification of vessel-surrounding pericytes as marker of endothelial damage. A-C| Quantification in colonic mucosa. **A|** Ratio of pericyte marker alpha smooth muscle actin (αSMA) positive area and endothelial cell marker CD31 positive area in colonic mucosa in B6 animals that underwent chemotherapy (chemo) versus untreated B6 control (ctr) animals. **B|** Exemplary pictures of αSMA CD31 staining in colonic mucosa of syngeneic (syn) and allogeneic (allo) bone marrow transplantation (BMT) recipients. **C|** Ratio of pericyte marker αSMA and endothelial marker CD31 in colonic mucosa of allo- and syn- BMT recipients, in LP/J→B6 graft-versus-host disease (GVHD) model at day 15 after BMT. **D-F|** Quantification of pericytes in liver sinusoidal endothelium. **D|** Ratio of pericyte marker αSMA and endothelial cell marker CD31 in sinusoidal liver endothelium of B6 animals after chemo versus ctr animals. **E|** Exemplary pictures of αSMA CD31 staining in hepatic tissue of syn- and allo-BMT recipients. **F|** Ratio of pericyte marker αSMA and endothelial marker CD31 in sinusoidal liver endothelium of allo- and syn-BMT recipients, in LP/J→B6 GVHD model at day 15 after BMT. Ratios of αSMA/CD31 were tested for significance by student's *t*-test (*P < .05; **P < .01; n=5 animals per group). Error bars indicate mean ± standard error of the mean (SEM).

3.5 STRUCTURE AND ORGANIZATION OF BLOOD VESSELS

To address the question whether the microcirculation in colon is affected by endothelial dysfunction, we performed FITC-Lectin perfusion. In this manner, perfused vessels ($CD31^+$ and $FITC^+$) can be distinguished from vessels not connected to the circulation (only $CD31^+$) by calculating the ratio of $CD31^+$ area to FITC-$Lectin^+$ area. Both groups (allo-BMT and syn-BMT recipients) showed normal blood perfusion. We found no differences in blood circulation during GVHD (Figure 21).

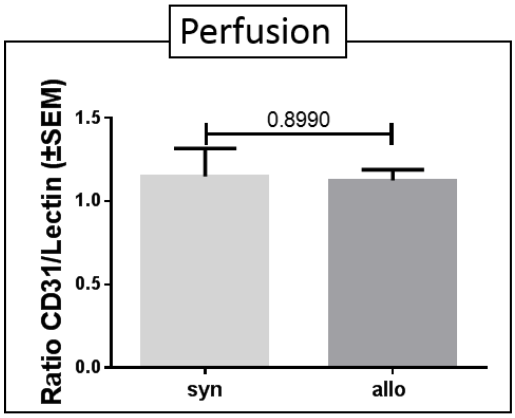

Figure 21| Perfusion of microvasculature in colon tissue. Assessment of endothelium (CD31) and perfusion of vessels (FITC-Lectin) in colon at day 15 after bone marrow transplantation (BMT) in B6→Balb/c graft-versus-host disease model. Colonic mucosa from syngeneic (syn) and allogeneic (allo) BMT recipients was analyzed. Significance was checked by student's *t*-test (n=5 animals per group). Error bars indicate mean ± standard error of the mean (SEM).

As blood vessel perfusion is unaffected during GVHD, we checked changes of vessel structure and organization by scanning light sheet fluorescence microscopy. Therefore, VE-cadherin in vivo perfusion was performed and our cooperation partner in Würzburg analyzed the structure of blood vessels in colonic samples. In Figure 22A, exemplary raw data of the colon from one BMT recipient are shown. Raw data were processed and a 3D model was created (Figure 22B). This model was used to calculate vessel diameter, length, straightness and branch level of vasculature in colon. The diameter of vasculature slightly shifted towards a higher diameter in allo- compared to syn-BMT recipients (Figure 22C), which was not significant. Vessel length was unaffected in allo- and syn-BMT recipients (Figure 22D). The parameter straightness, defined as continuous staining of non-collapsed vessels, showed a not significant shift towards lower straightness in allo- compared to syn-BMT recipients (Figure 22E). Branching of vessels in colonic microvasculature was not significantly reduced in allo- compared to syn-BMT recipients (Figure 22F). The structure of the microvasculature in GVHD was similar in allo- and syn-BMT recipients. We found no evidence of structural changes in microvasculature during established GVHD.

Since direct endothelial dysfunction was observed during GVHD, we further looked for endothelial leakage. For this purpose we examined extravasation with Evans blue assay and analyzed frozen sections for endothelial junction protein expression.

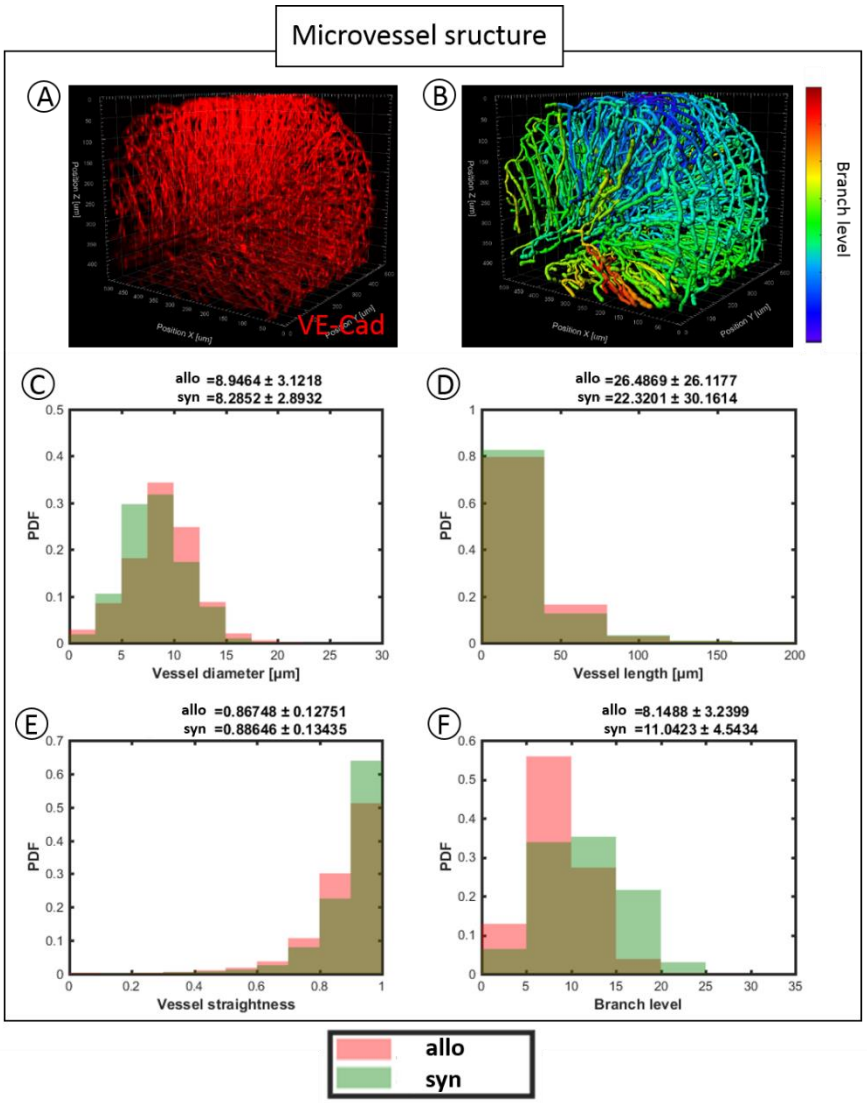

Figure 22| Visualization of microvascular structure in colon of syngeneic (syn) and allogeneic (allo) transplanted recipients by scanning light sheet fluorescence microscopy A| Exemplary picture of whole microvasculature in colon with red vascular endothelial cadherin (VE-cad) signal. **B|** Computed model of microvasculature in colon with the amount of branches per dendrite (blue= low branch levels; red= high branch levels). **C-F|** Analysis of microvasculature parameters of colon at day 12 after bone marrow transplantation (BMT) in B6→Balb/C graft-versus-host disease model (n=3 animals per group). **C|** Assessment of vessel diameter, **D|** vessel length, **E|** vessel straightness and **F|** vessel branching in allo- and syn-BMT recipients. Distribution was calculated with probability density function (PDF).

3.5 ENDOTHELIAL LEAKAGE IS INCREASED DURING GVHD

To address the question whether endothelial barrier function is altered during GVHD, we analyzed vessel leakage by performing Evans blue assay and staining GVHD target organs for the tight junction protein ZO-1 and the intercellular junction protein VE-cadherin. Evans blue assay revealed a significant increase in endothelial leakage in allo-BMT recipients compared to syn-BMT recipients in colon (Figure 23A), liver (Figure 23B) and skin (Figure 23C) during the acute phase of GVHD. The increase in leakage in allo-BMT recipients was also observable in another GVHD model. Increased leakage was significant in the colon (supplemental Figure 3G). A trend of increased leakage was observable in liver (supplemental Figure 3H) and skin (supplemental Figure 3I). Increased leakage was specific to GVHD target organs and was not detectable in non-target tissues such as kidney (supplemental Figure 4A and C) muscle (supplemental Figure 4B and D) in two different GVHD models. Furthermore, increased leakage was only present at day 15 after BMT. In the liver, first hints of increased leakage were detected at earlier time points (day 2 and day 7 after BMT) in allo-

compared to syn-BMT recipients (supplemental Figure 3B and E), whereas in colon (supplemental Figure 3A and D) and skin (supplemental Figure 3C and F) no remarkable increase was observed.

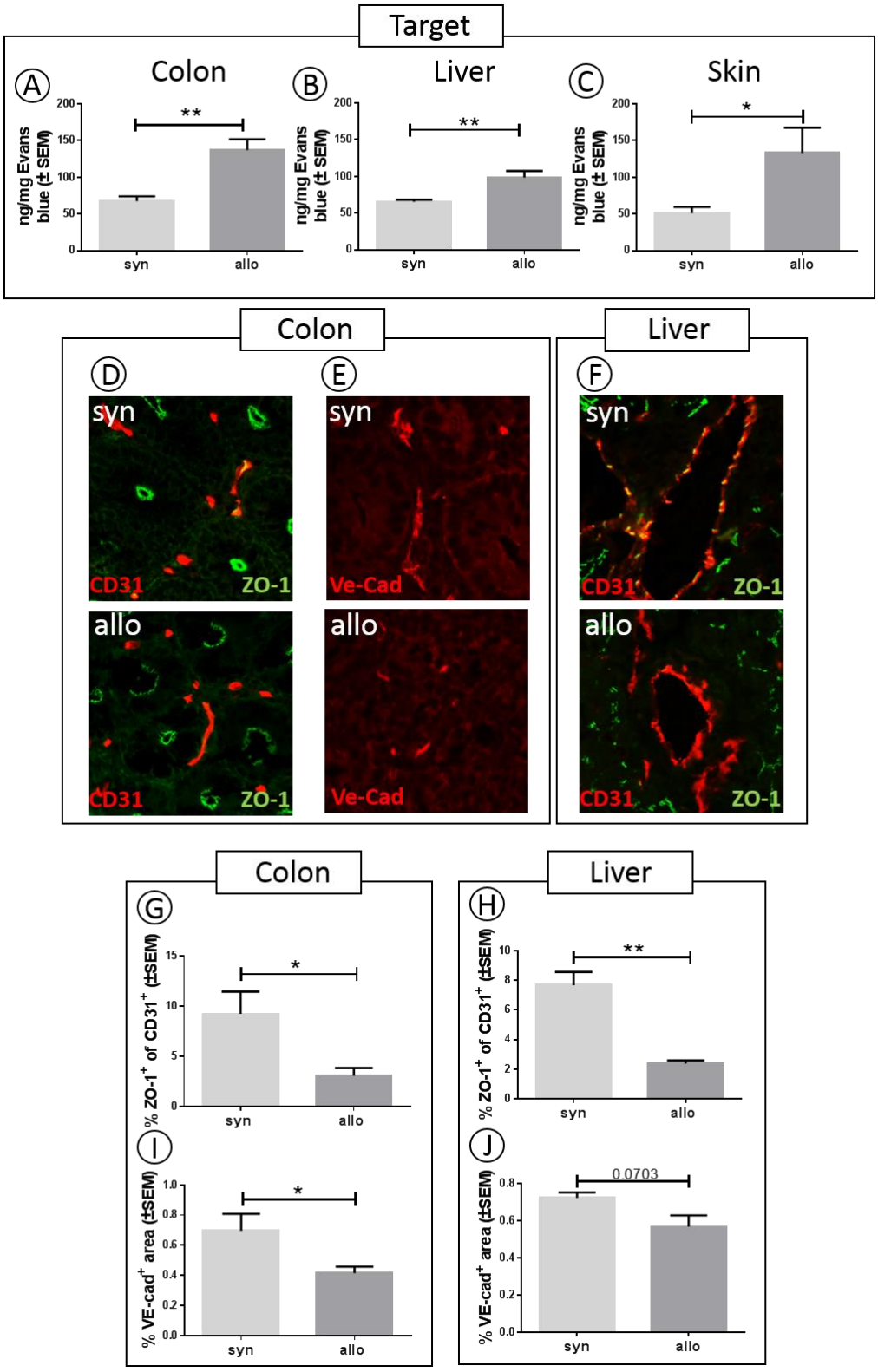

Figure 23| Assessment of endothelial leakage in graft-versus-host disease (GVHD) mouse models. A-C| Measurement of Evans blue extravasation form GVHD target organs (colon, liver and skin) at day 15 after bone marrow transplantation (BMT) in B6→BDF GVHD model. **A|** Evans blue extravasation in colon **B|** liver and **C|** skin of allogeneic (allo) and syngeneic (syn) recipients. **D-F|** Exemplary pictures of GVHD target organs liver and colon of LP/J→B6 GVHD model. **D|** Merge of tight junction marker zonula occludes 1 (ZO-1) expression and endothelial cell marker CD31 expression in colonic mucosa of syn- and allo-BMT recipients. **E|** Intercellular adherens junction marker

vascular endothelial cadherin (VE-cad) expression in colonic mucosa of syn- and allo-BMT recipients. **F|** Merge of ZO-1 expression and CD31 expression in sinusoidal liver endothelium of syn- and allo-BMT recipients. **G-J|** Quantification of ZO-1 expression and VE-cad expression in colon and liver at day 15 after BMT in LP/J→B6 GVHD model. **G|** VE-cad expression and **H|** expression of ZO-1 in endothelium in colonic mucosa of allo- and syn-BMT recipients. **I|** VE-cad expression and **J|** ZO-1 expression in liver endothelium of allo- and syn-BMT recipients. Significance was tested by student's *t*-test (*P < .05; **P < .01; n=5 animals per group). Error bars indicate mean ± standard error of the mean (SEM).

The findings of Evans blue assay were confirmed by analyzing endothelial ZO-1 expression and VE-cadherin expression in immunostainings of sections of allo- and syn-BMT recipients. A remarkable reduction of ZO-1 expression of endothelial cells was detected, as shown in the exemplary pictures of colon (Figure 23D) and liver (Figure 23F) in allo-BMT recipients. For quantification of endothelial tight junctions, $CD31^+$ and $ZO\text{-}1^+$ (double positive) area was measured and the percentage of double positive area to total $CD31^+$ area was calculated.

Endothelial ZO-1 expression was significantly decreased in colonic mucosa (Figure 23G) and hepatic sinusoidal endothelium (Figure 23I) of allo- compared to syn-BMT recipients. Moreover, the expression of VE-cadherin (red) was remarkably reduced in colonic mucosa of allo-BMT recipients as shown in the exemplary pictures (Figure 23E). Quantification of VE-cadherin (red) expression in colonic mucosa and hepatic sinusoidal endothelium revealed a significant reduction in allo-BMT recipients in colonic mucosa (Figure 23H) and an almost significant reduction in hepatic sinusoidal endothelium (Figure 23J) when compared to syn-BMT recipients. In another model of GVHD endothelial ZO-1 was significantly reduced (supplemental Figure 3J). VE-cadherin expression only showed a slight, not significant, decrease in colonic mucosa of allo- compared to syn-BMT recipients (supplemental Figure 3K).

There is evidence that integrity and barrier function of the endothelium is disturbed during GVHD, allowing immune cells to pass the endothelial barrier. Loss of pericytes and increased leakage lead to the question whether the physiologic function of endothelial cells might be disturbed in GVHD.

3.7 PHYSIOLOGICAL CHANGES DURING GVHD

Under physiologic conditions, the interplay between endothelial cells and pericytes is essential for the perfusion of organs with blood. We examined different physiological functions of the vasculature by measuring blood vessel contraction and relaxation in mouse mesenteric arteries from BMT recipients by myo-graphic measurements.

A maximum contraction of mesenteric arteries from allo- and syn-BMT recipients was induced by different compounds and calculated as fold of untreated control animals. Potassium-induced contraction was significantly increased in mesenteric arteries from allo- compared to arteries from syn-BMT recipients (Figure 24A). Stimulation with NA (Figure 24B) and Phe (Figure 24C) resulted in an increase of maximum contraction of mesenteric arteries of allo- compared to syn-BMT recipients. Partial contraction induced by different concentrations of NA (Figure 24D) and Phe (Figure 24E) resulted in contraction at lower dose of mesenteric arteries of allo- compared to syn-BMT recipients.

Fractional relaxation after maximum contraction of the arteries was induced by ACh. Response to ACh was faster in arteries from syn-BMT recipients compared to allo-BMT recipients (Figure 24F). Inhibition of relaxation by L-NAME to assess communication between endothelial cells and pericytes did not show significant differences among the groups (Figure 24G).

Physiological data only show minor alterations in arteries in terms of contraction and relaxation that seem not to be critical during established GVHD.

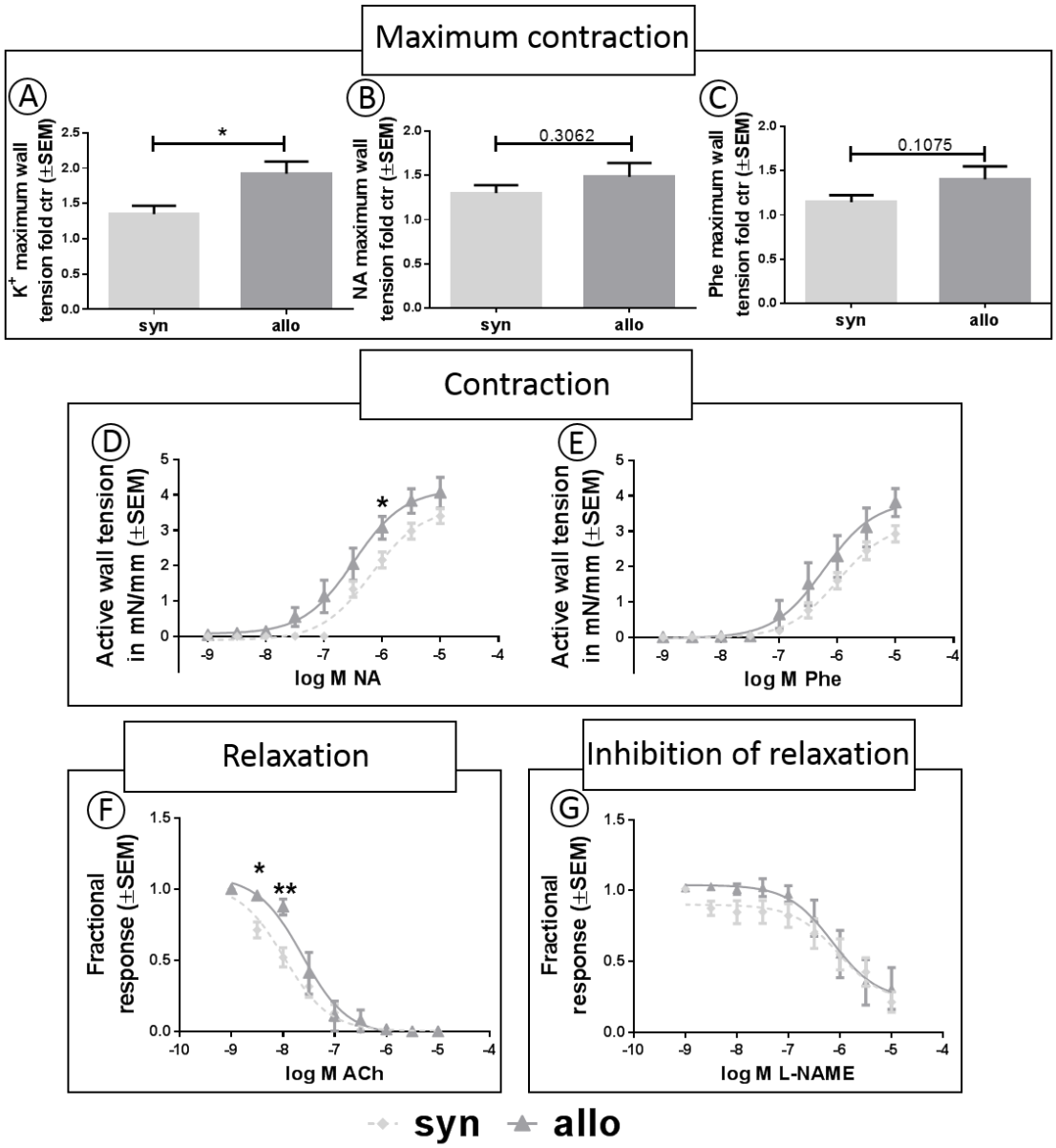

Figure 24| Physiological functions of mesenteric arteries. A-C| Maximum contraction of mesenteric arteries upon different stimuli at day 27 after bone marrow transplantation (BMT) in LP/J→B6 graft-versus-host disease (GVHD) model. **A|** Maximum contraction of mesenteric arteries in response to potassium (K^+), **B|** noradrenaline (NA) and **C|** phenylalanine (Phe) from allogeneic (allo) and syngeneic (syn) BMT recipients as fold increase to untreated control (ctr) animals. **D-E|** Partial contraction of mesenteric arteries upon different stimuli. **D|** Partial contraction of mesenteric arteries upon increasing concentrations of NA and **E|** increasing concentrations of Phe from allo- and syn-BMT recipients. **F|** Partial relaxation of mesenteric arteries induced by acetylcholine (ACh) after maximum contraction with potassium. **G|** Inhibition of relaxation by L-N^G-nitroarginine methyl ester (L-NAME) after maximum contraction of mesenteric arteries by potassium and addition of ACh. Significance was tested by student's *t*-test (*P < .05; **P < .01; n=6 to 8 mesenteric arteries from 3 to 4 animals). Error bars indicate mean ± standard error of the mean (SEM).

3.8 ENDOTHELIAL ADHESION MOLECULES AND IMMUNE CELL INTERACTION DURING GVHD

To determine the activation status of endothelial cells leading to increased inflammation in the target organs liver and colon, we checked interaction of immune cells with endothelial cells by CTEM, performed expression analysis by qPCR of whole organ lysates and checked immune stimulatory capacity of hepatic endothelial cells. During GVHD, we observed tight immune cell-endothelial cell contact in allo-BMT animals, whereas in syn-BMT recipients no contact of immune cells to endothelial cells was observed. In colon, immune cells were detected in close contact to endothelial cells (Figure 25A) forming podocytes that invade the perivascular space (Figure 25B). Also in the liver we found immune cells and endothelial cells in close contact (Figure 25C). A high magnification CTEM image of the contact zone reveals direct contact of the immune cell with the hepatic sinusoidal endothelial monolayer (Figure 25D). Analysis of mRNA expression of endothelial adhesion and activation markers of whole colon- and liver lysates from transplanted animals puts more evidence to an activated inflammatory status of endothelial cells. Expression of *ICAM1* (Figure 25E), *VCAM1* (Figure 25F) and *P-selectin* (Figure 25G) in whole colon lysates was increased in allo- compared to syn-BMT recipients but only P-selectin showed significant results.

Comparable results were obtained when analyzing whole liver lysates of transplanted animals. *ICAM1* (Figure 25H) and *VCAM1* (Figure 25I) mRNA expression tended to be increased when comparing allo- to syn-BMT recipients. Again, *P-selectin* mRNA expression was significantly up-regulated when comparing allo- to syn-BMT recipients (Figure 25J). Expression of co-stimulatory proteins of hepatic endothelial cells fitted into this pattern. Fluorescence flow cytometry analysis and quantification revealed an increase of antigen presentation by MHC class I and MHC class II, co-stimulatory proteins CD86 and CD80 as well as the expression of the adhesion protein ICAM1 in allo-BMT recipients. Hepatic endothelial cells were isolated from transplanted animals at day 15 after BMT. Endothelial cell fraction was determined by the following characteristics: $CD45^{dim\ to\ -}$, $Ter119^{-}$ $CD11b^{-}$ and $VEGFr2^{+}$. The percentage of MHC class I and MCH class II co-expressing hepatic endothelial cells was significantly higher in allo- compared to syn–BMT recipients (Figure 25K). The same applied for hepatic endothelial cells co-expressing CD80 and CD86 (Figure 25L). The amount of ICAM1 protein expression on the endothelial cell surface was analyzed by mean fluorescence intensity of ICAM1 positive endothelial cells. There was an almost significant increase in ICAM1 expression of hepatic endothelial cells in allo- compared to syn-BMT recipients (Figure 25M).

In summary, endothelial cells play an active role during GVHD by increasing the expression of adhesion molecules to allow immune cell efflux from the circulation and may directly contribute to immune cell activation by acting as APCs.

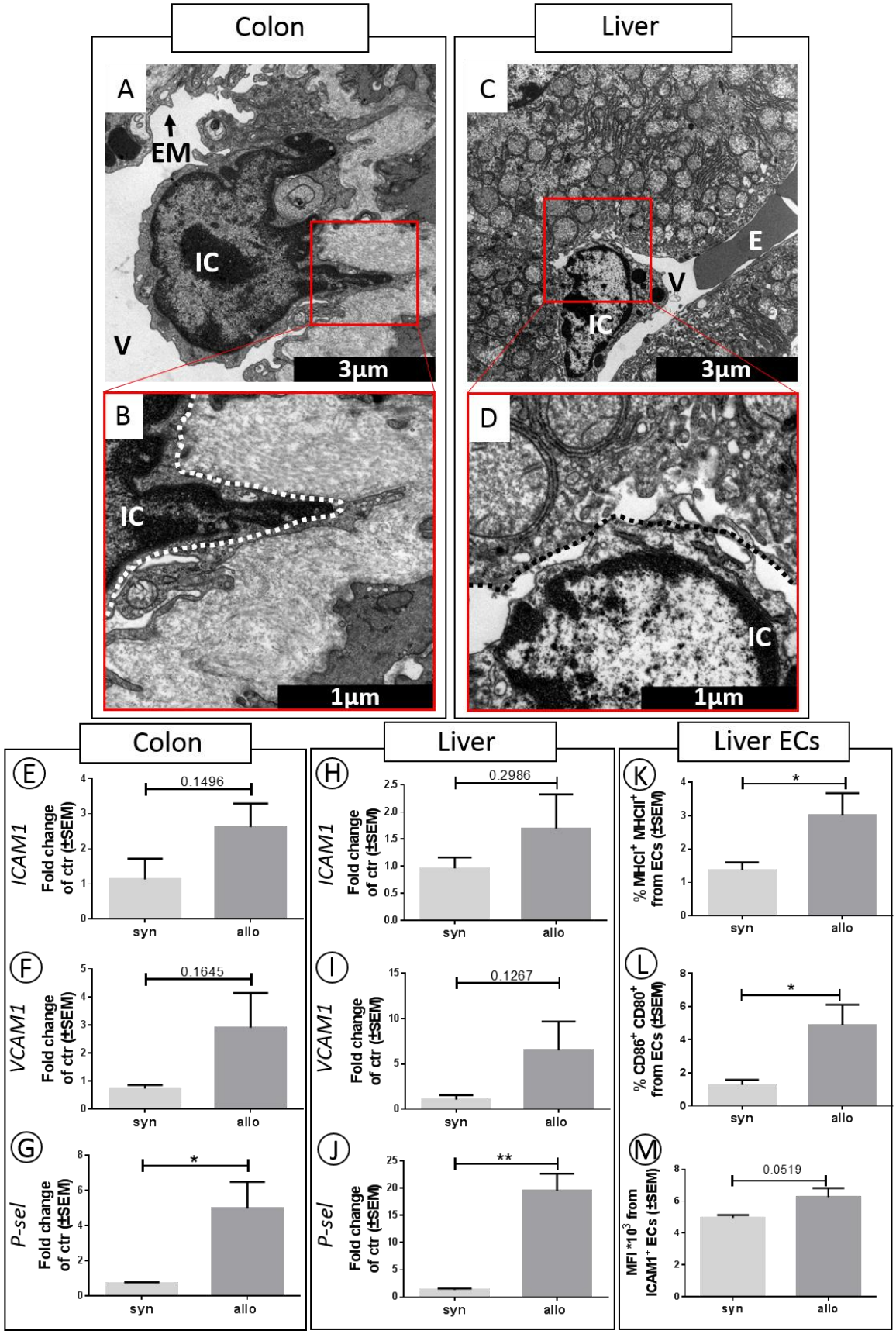

Figure 25| Immune cell adherence and interaction with the endothelial cell monolayer. A-D| Conventional transmission electron microscopy pictures of allogeneic (allo) bone marrow transplantation (BMT) recipients from liver and colon at day 15 after BMT in B6→BDF graft-versus-host (GVHD) model. **A|** Immune cell attached to colonic endothelium forming podocytes. **B|** Higher magnification of podocyte showing close contact of an immune cell with the endothelial monolayer. **C|** Sinusoidal liver endothelium with an immune cell in close contact to the endothelial monolayer. **D|** Higher magnification of the contact zone from immune cell and endothelium with the

discontinuous endothelial monolayer. **E-J|** mRNA expression of whole organ lysates at day 15 after BMT in LP/J→B6 GVHD model. Values are normalized to *Gapdh* mRNA expression and to the expression of untreated wildtype controls (ctr) of the studied gene. **E|** *Intercellular adhesion molecule 1* (*ICAM1*) mRNA expression, **F|** *vascular cellular adhesion molecule 1* (*VCAM1*) mRNA expression and **G|** *P-selectin* (*P-sel*) mRNA expression in colon lysates of allo- and syn-BMT recipients. **H|** *ICAM1* mRNA expression, **I|** *VCAM1* mRNA expression and **J|** *P-sel* mRNA expression in liver lysates of allo- and syn-BMT recipients. **K-M|** Antigen presentation, co-stimulatory capacity and expression of ICAM1 of hepatic endothelial cells measured by flow cytometry at day 15 days after BMT in B6→Balb/C GVHD model. **K|** Percentage of the major histocompatibility complex (MHC) class I (MHCI) /MHC class II (MHCII) co-expressing and **L|** percentage of CD80/CD86 co-expressing hepatic endothelial cells in allo- and syn-BMT recipients. **M|** Mean fluorescence intensity (MFI) of ICAM1 expression from hepatic endothelial cells in allo- and syn-BMT recipients. Significance was tested by student's *t*-test (**P* < .05; ***P* < .01; n=6 animals per group). Error bars indicate mean ± standard error of the mean (SEM).

3.9 SOLUBLE FACTORS DURING GVHD AND EFFECT ON ENDOTHELIUM

We addressed the question whether soluble factors in serum of allo- or syn-BMT recipients are able to change the endothelial phenotype. Therefore, we used MCECs *in vitro* and added 5% serum from either allo- or syn-BMT recipients for 24h in the culture medium. Cells were analyzed for surface protein expression of the co-stimulatory molecules CD86 (Figure 26A) and CD80 (Figure 26B), the activation markers MHC class II (Figure 26C) and ICAM1 (Figure 26D) by flow cytometry. For all markers we found no difference in surface expression on endothelial cells upon serum co-culture.

Activation of endothelial cells was not achieved by soluble factors from serum of animals with GVHD.

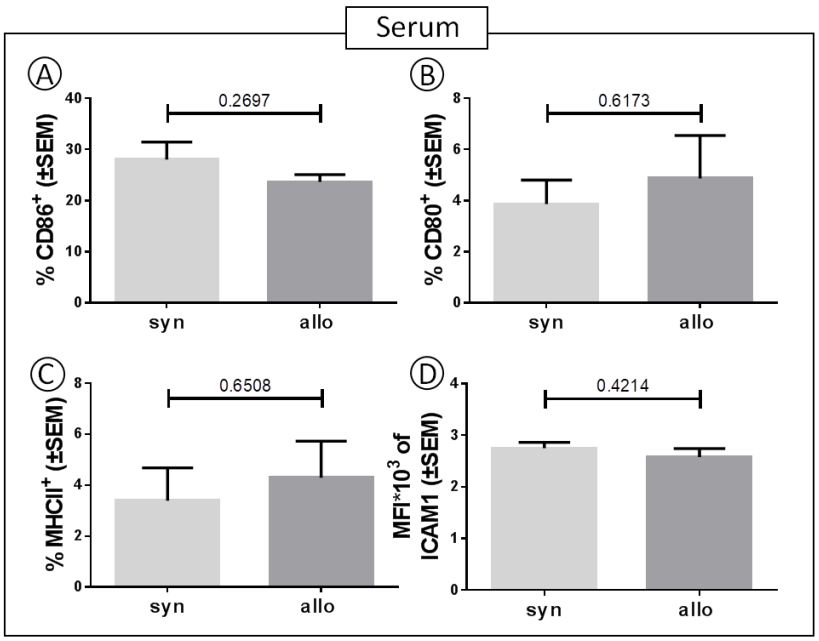

Figure 26| Impact of soluble factors in serum on endothelial cells. Serum from either syngeneic (syn) or allogeneic (allo) bone marrow transplantation (BMT) recipients was isolated at day 15 after BMT in LP/J→B6 graft-versus-host disease model. Serum starved mouse cardiac endothelial cells were co-cultured for 24h with 5% mouse serum from either syn- or allo-BMT recipients and checked for **A-B|** co-stimulatory capacity by CD80 and CD86 expression, **C|** activation and antigen presentation by the major histocompatibility complex (MHC) class II (MHCII) and **D|** adhesion by mean fluorescence intensity (MFI) of ICAM1 expression by flow cytometry. Significance was tested by student's *t*-test (n=5 animals per group). Error bars indicate mean ± standard error of the mean (SEM).

3.10 ENDOTHELIUM-MODIFYING AGENTS DURING GVHD

The obtained results encouraged us to look for a pathophysiological function of endothelial cells during GVHD. Therefore, we tried to ameliorate GVHD by agents targeting the endothelium.

To address the question whether altered endothelial function is a critical pathological feature of GVHD, we performed *in vivo* experiments and treated allo-BMT recipients with either Defibrotide

(700mg/kg/d), ß-APN (2mg/kg/d) or Plerixafor (10mg/kg/d). Defibrotide has antithrombotic, anti-ischemic and pro-fibrinolytic effects on the endothelium and is applied as therapeutic agent in VOD[184]. ß-APN is a lysyl oxidase 1 (LOX1) inhibitor, which catalyzes the formation of aldehydes from lysine in collagen and elastin precursors, resulting in cross-linking of collagen and elastin[185]. Plerixafor is an antagonist of C-X-C chemokine receptor type 4 (CXCR4) and an allosteric agonist of C-X-C chemokine receptor type 7[186]. Through the interaction with SDF-1, an important hematopoietic stem cell homing receptor, Plerixafor promotes stem cell recruitment to the periphery. Protection of endothelium and prevention of thrombus formation with Defibrotide did not show differences in clinical score (Figure 27A) and mortality rates between treatment and control groups (Figure 27B).

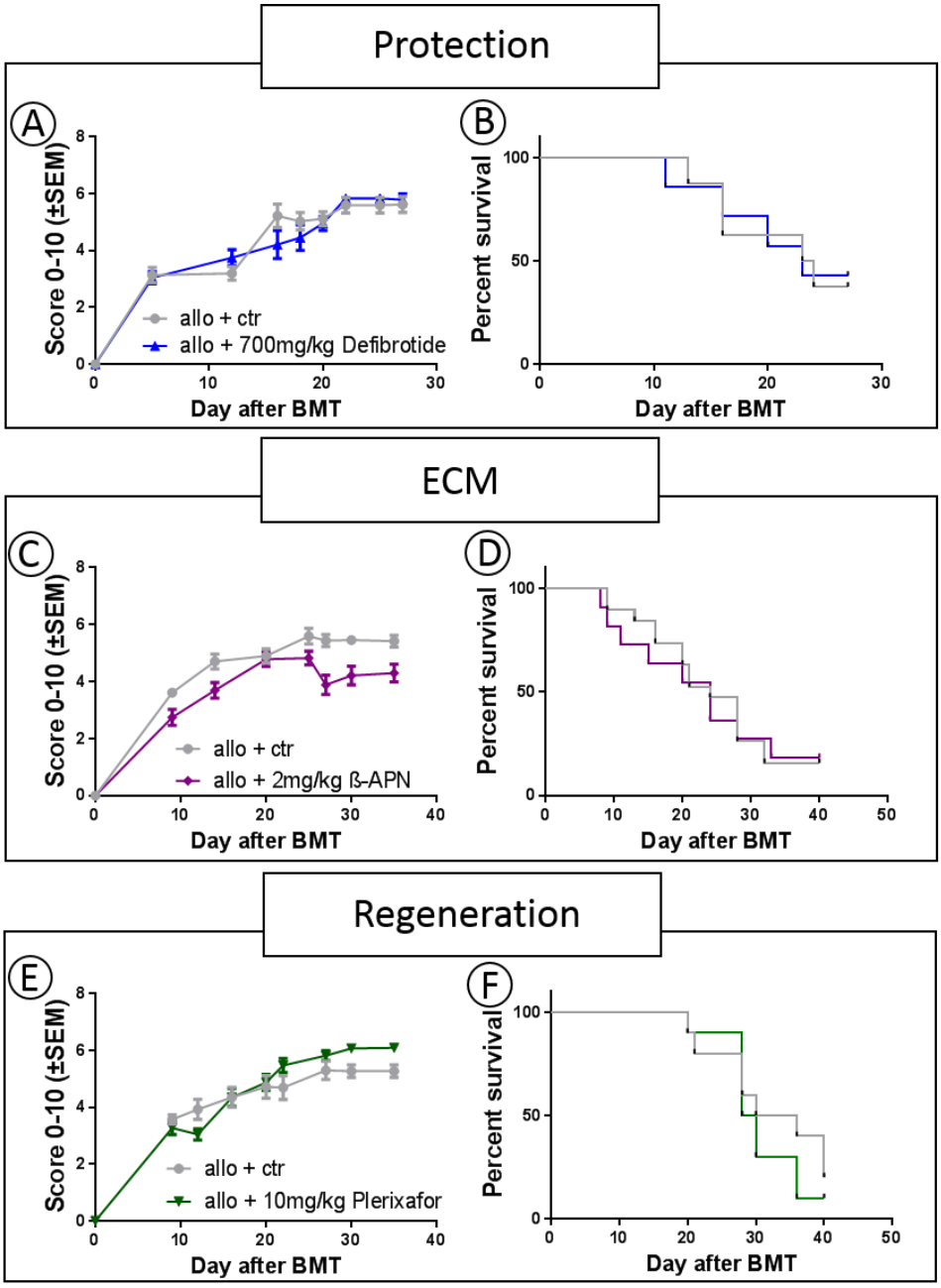

Figure 27| Endothelial modulating agents as therapeutic strategy to ameliorate graft-versus-host disease (GVHD) symptoms in B6→BDF GVHD model. A-B| Score and survival in GVHD with protection of endothelium by Defibrotide treatment versus PBS (ctr) treatment (n=10 animals per group). **C-D|** Score and survival in GVHD by modulating extracellular matrix (ECM) crosslinking by beta-aminopropionitrile fumarate (ß-APN) treatment versus PBS (ctr) treatment (n=20 animals per group). **E-F|** Score and survival in GVHD with higher regeneration of endothelium by Plerixafor treatment versus PBS (ctr) treatment (n=10 animals per group). Significance of score was tested by student's *t*-test, survival was tested by Mantel-Cox log-rank test. Error bars indicate mean ± standard error of the mean (SEM).

By modulating the extracellular matrix of the endothelium with LOX1 inhibitor ß-APN, there was also no difference in score (Figure 27C) and survival (Figure 27D) between the treatment and control

GVHD group. In addition, the approach to stimulate endothelial regeneration by mobilizing hematopoietic stem cells with the CXCR4 antagonist Plerixafor was not able to ameliorate GVHD symptoms (Figure 27E) and survival (Figure 27F).

Thus, we were not able to find a suitable compound or appropriate treatment protocol to ameliorate GVHD.

3.11 Gene array to identify new targets to ameliorate endothelial cell damage in GVHD

Since we failed to improve GVHD by endothelial protection, we wanted to investigate endothelial gene expression during GVHD. Aim of this approach was the revelation of specific endothelial pathways regulated during GVHD to get hands on new targets and to get a better understanding of the process of endothelial damage. Therefore, we performed gene array expression analysis of FACS purified hepatic endothelial cells from either syn- and allo-BMT recipients. Clustering analysis revealed specific gene expression patterns in syn- and allo-BMT recipients (Figure 28A). The variance between individual animals was adequate. Specific gene expression is shown as hierarchical clustering (Figure 28C). Profound differences in gene expression of syn- versus allo-BMT recipients was observable. Volcano plot (Figure 28B) shows 214 down-regulated genes in green and 1064 up-regulated genes in red. Down- and up- regulation was defined as 2-fold decrease or increase of expression.

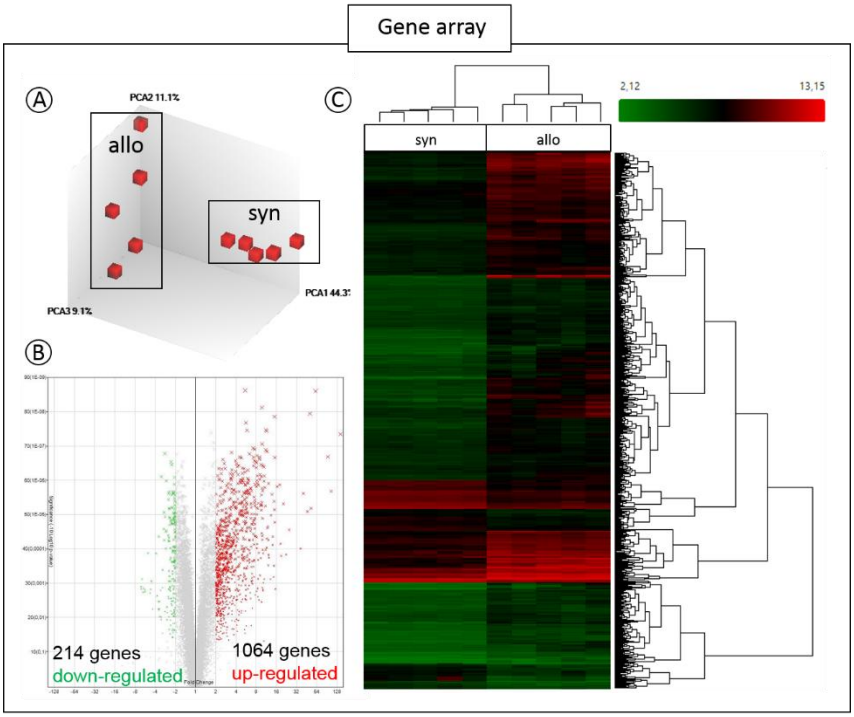

Figure 28| Microarray analysis of sorted hepatic endothelial cells during graft-versus-host disease (GVHD). A| Transcriptome clustering from isolated colonic endothelial cells at day 15 after bone marrow transplantation (BMT) in LP/J→B6 GVHD model from allogeneic (allo) and syngeneic (syn) BMT recipients. **B|** Volcano plot of the expression of total genes; red and green crosses represent 1064 up-regulated and 214 down-regulated genes, respectively. **C|** Hierarchical clustering of microarray data. Green and red represent low and high levels of gene expression (n= 5 animals per group).

For the total number of 1278 regulated genes, we screened for pathways, which were 1) altered and 2) associated to damage and specific for endothelial cells. Gene alterations were found in genes involved in metabolomic pathways such as nucleotide metabolism, leptin and adiponectin pathway, amino acid

metabolism and insulin signaling. The cytokine IL-4 pathway was regulated as well as the toll like receptor signaling and focal adhesion pathways (Table 8).

Tabel 8| Pathways identified by microarray analysis of sorted hepatic endothelial cells during graft-versus-host disease (GVHD). Selected pathways are sorted after relevance. In the first (grayish) column different pathways are listed. The red column shows numbers and names of up-regulated genes during GVHD in allogeneic bone marrow transplantation recipients. Accordingly, numbers and names of down-regulated genes during GVHD are displayed in the green column.

Pathway	#Up	Up-regulated genes	#Down	Down-redulated genes
IL-4 signaling pathway	**27**	*Il2rg, Il4, Ptpn11, Fes, Inpp5d, Ptpn6, Jak2, Ep300, Mapk14, Pik3r2, Cbl, Prkcz, Stat5a, Dok2, Irs2, Pik3cd, Grb2, Stat1, Cxcr4, Adrbk2, Shc1, Nfkb1, Bcl2l1, Socs1, Hmga1, Prkcd, Lck*	**29**	*Il4ra, Jak1, Irs1, Il13ra1, Crebbp, Tyk2, Stat6, Mapk3, Pawr, Pik3ca, Jak3, Socs3, Sos1, Src, Elk1, Ptk2, Fyn, Stam, Plcg1, Mapk11, Atf2, Socs5, Mapk1, Rasa1, Rela, Bad, Ets1, Akt1, Prkci*
Toll Like Receptor signaling	**8**	*Mal, Irak4, Myd88, Irak1, Fadd, Traf3, Tab2, Nfkb1*	**8**	*Tlr2, Tlr4, Tirap, Tlr3, Irf3, Tbk1, Traf6, Nfkb2*
Nucleotide metabolism	**14**	*Prps1, Prps2, Dhfr, Mthfd2, Adsl, Adss, Pola1, Pold1, Nme2, Sat1, Srm, Oaz1, Rrm1, Rrm2*	**4**	*Impdh1, Polb, Polg, Rrm2b*
Focal adhesion	**73**	*Tnc, Col5a3, Figf, Igf1, Pdgfb, Pgf, Itga2, Itga4, Itgae, Itgad, Itga2b, Itgal, Itgam, Itgb2, Itgb3, Itgax, Shc3, Itgb5, Zyx, Itgb7, Itgb8, Rap1a, Rap1b, Actn1, Shc1, Grb2, Vasp, Fn1, Col5a1, Fgr, Hck, Igf1r, Thbs1, Txk, Thbs3, Tesk2, Mapk6, Map2k2, Met, Map2k3, Pdgfra, Map2k1, Pdgfrb, Farp2, Flna, Tln1, Raf1, Mapk4, Capn1, Ppp1r12a, Pdpk1, Myl6, Mylk, Akt2, Diap1, Actg1, Vav1, Pik3cd, Rac1, Rac2, Pik3r2, Pik3cg, Pak1, Pik3r5, Pak3, Pak2, Pik3cb, Pak7, Pdgfc, Bcl2, Birc2, Birc3, Ccnd3*	**111**	*Thbs4, Tnr, Lamc3, Vtn, Tnn, Vwf, Lamc1, Tnxb, Egf, Col4a6, Hgf, Pdgfa, Pelo, Itga3, Itga5, Itga6, Itga9, Itga7, Itga10, Itga8, Itga11, Itgb1, Itgav, Itgb4, Sos1, Itgb6, Cav3, Ilk, Cav2, Dock1, Vcl, Col3a1, Fyn, Col4a1, Col4a2, Col4a4, Src, Col1a2, Chad, Comp, Col11a1, Col11a2, Ibsp, Col2a1, Lamb2, Lamc2, Col5a2, Reln, Col6a2, Spp1, Col1a1, Lama2, Flt1, Lama3, Lama4, Lama5, Ptk6, Srms, Thbs2, Lamb3, Map2k5, Lama1, Map2k6, Blk, Mapk12, Egfr, Mapk1, Erbb2, Kdr, Ptk2, Styk1, Arhgap5, Tnk2, Rhob, Tnk1, Araf, Braf, Pxn, Sepp1, Pip5k1c, Rhoa, Parvb, Akt1, Mylk2, Akt3, Rock1, Gsk3b, Rock2, Pten, Pik3ca, Pik3r1, Rac3, Pik3r4, Vegfc, Pak4, Bcar1, Crk, Pak6, Rapgef1, Elk1, Bad, Pdgfd, Vegfa, Vegfb, Mapk8, Mapk9, Jun, Ccnd1, Ccnd2, Cdc42, Mapk7*
Tryptophan metabolism	**20**	*Prmt1, Ddc, Acat1, Hsd17b10, Echs1, Ogdh, Haao, Kynu, Tdo2, Tph1, Wars, Aadat, Dhcr24, Afmid, Cyp1b1, Cyp2c55, Cyp4f14, Hadh, Aldh1a2, Aldh9a1*	**22**	*Ido1, Cyp2j6, Aanat, Mdm2, Maob, Gcdh, Acmsd, Cat, Aldh3a2, Cyp7b1, Aox1, Ubr5, Inmt, Cyp1a1, Cyp1a2, Cyp2e1, Cyp19a1, Cyp2f2, Aldh1a1, Aldh2, Ube3a, Rnf25*
Wnt signaling pathway and pluripotency	**33**	*Wnt7b, Wnt10b, Wnt3a, Fzd7, Prkcb, Prkcd, Ldlr, Fzd2, Racgap1, Myc, Prkca, Mmp7, Prkcz, Cd44, Dvl2, Sox2, Ppp2r4, Ppp2r5c, Ppp2r2c, Axin2, Ppp2r1a, Ppp2r2a, Pafah1b1, Ccnd3, Fosl1, Ctbp1, Zbtb33, Ep300, Ppp2r1b, Ppp2ca, Axin1, Nanog, Trp53*	**61**	*Wnt5b, Wnt1, Wnt7a, Wnt2, Wnt2b, Wnt10a, Wnt3, Fzd4, Wnt4, Fzd5, Wnt5a, Fzd6, Wnt6, Wnt11, Fzd8, Wnt9b, Wnt16, Prkch, Lrp5, Prkd1, Fzd1, Rhoa, Fzd3, Fzd9, Ccnd1, Prkce, Tcf3, Prkci, Map3k7, Prkcq, Lrp6, Dvl1, Ppard, Pou5f1, Dvl3, Ppp2r5e, Ppm1j, Csnk1e, Frat1, Gsk3b, Ppp2r2d, Ctnnb1, Mapk9, Mapk10, Fbxw2, Ccnd2, Jun, Lef1, Nlk, Apc, Ctnnd1, Plau, Ctbp2, Crebbp, Nkd1, Nkd2, Ppp2r2b, Ppp2cb, Nfya, Foxd3, Tcf4*
Leptin and adiponectin	**4**	*Lepr, Adipor2, Prkag1, Prkab1*	**2**	*Adipor1, Prkaa1*
Amino acid metabolism	**44**	*Gss, Eprs, Prodh, Ogdh, Suclg1, Fh1, Mdh2, Aco2, Acly, Asl, Srm, Rars, Cad, Sms, Pcx, Mdh1, Cs, Asns, Gpt, Auh, Sdhd, Pycr1, Ddc, Arg2, Adh5, Got2, Dlst, Dld, Pnmt, Fah, Iars, Mpst, Wars, Mars2, Tdo2, Pdha1, Tph1, Sds, Gsr, Hal, Hdc, Hnmt, Hibch, Pdhx*	**35**	*Gclc, Gls, Sdha, Idh1, Pck1, Pdk4, Aldh7a1, Got1, Mccc1, Acadm, Bcat1, Ehhadh, Hibadh, Hmgcs2, Tat, Oat, Maoa, Arg1, Adh7, Lars2, P4ha2, Tpo, Dbh, Aldh1a1, Th, Adh1, Adh4, Cbs, Vars2, Bhmt, Mut, Otc, Cth, Aoc3, Hmgcl*
Insulin signaling	**58**	*Irs2, Pik3cg, Pik3cd, Pik3cb, Pik3r2, Akt2, Arf6, Pik3c2g, Arf1, Pdpk1, Gsk3a, Shc1, Prkcz, Map2k2, Gys1, Map2k3, Grb2, Ptpn11, Mapk4, Raf1, Map2k1, Mapk6, Map2k4, Mapk13, Mapk14, Map3k9, Map4k1, Map3k5, Rps6ka1, Rps6ka5, Rps6ka6, Cblb, Rps6ka3, Cap1, Flot1, Flot2, Ppp1cc, Ptpn1, Eif4e, Cbl, Shc3, Lipe, Gys2, Egr1, Rrad, Prkca, Prkcd, Enpp1, Pfkl, Stxbp2, Socs1, Sgk3, Srf, Rac1, Rac2, Igf1r, Slc2a1, Slc2a4*	**92**	*Irs1, Irs4, Pik3ca, Pik3r1, Pik3c2a, Akt1, Pik3r3, Pik3r4, Pten, Pik3c3, Foxo1, Gsk3b, Pfkm, Prkci, Shc2, Sos1, Inpp4a, Sos2, Trib3, Gab1, Map2k6, Map3k1, Mapk1, Map2k5, Map3k10, Map3k2, Mapk8, Map3k3, Map3k4, Map3k8, Mapk3, Map2k7, Mapk9, Mapk11, Mapk10, Map4k4, Mink1, Map3k12, Mapk12, Map4k2, Map4k5, Map3k7, Map3k14, Map3k11, Mapk7, Map3k13, Map4k3, Rps6ka4, Map3k6, Rps6kb1, Cblc, Rps6ka2, Rapgef1, Rps6kb2, Irs3, Ptprf, Fos, Sorbs1, Jun, Rhoj, Grb10, Rhoq, Crk, Tsc1, Eif4ebp1, Rheb, Tsc2, Stxbp4, Vamp2, Snap25, Inppl1, Snap23, Ehd1, Prkcq, Ehd2, Prkch, Myo1c, Kif5b, Kif3a, Sgk1, Stx4a, Sgk2, Socs3, Tbc1d4, Prkaa1, Elk1, Prkaa2, Ikbkb, Grb14, Xbp1, Stxbp1, Insr*
Pentose phosphate pathway	**6**	*Pgls, Pgd, Rpia, Tkt, Taldo1, Rpe*	**0**	

Damage associated pathways are mainly classical pathways like complement activation-, apoptosis-, blood clotting-, oxidative damage- and IL-1 signaling pathways (Table 9). Furthermore, both the IL-6 signaling pathway and the pathways involved in the regulation of actin cytoskeleton were altered. Interaction analysis of the most interesting endothelium-specific genes was performed with string database. 46 of a total number of 67 genes showed possible direct interactions (Figure 29). Among this

set of genes, *Cdh1* and *Cdh13* (coding for cadherins), *Thbd* (coding for thrombomodulin), *Vegfc* (coding for vascular endothelial growth factor c), *Anpgt1* and *Angpt2* (coding for ANG1 and ANG2), *Icam4* and *Cxcr4* were differentially expressed between hepatic endothelial cells obtained from allo- and syn-BMT recipeints.

Tabel 9| Damage associated pathways identified by microarray analysis of sorted hepatic endothelial cells during graft-versus-host disease (GVHD). Selected pathways are sorted after relevance. In the first (grayish) column different pathways are listed. The red column shows numbers and names of up-regulated genes during GVHD in allogeneic bone marrow transplantation recipients. Accordingly, numbers and names of down-regulated genes during GVHD are displayed in the green column.

Pathway	#Up	Up-regulated genes	#Down	Down-regulated genes
IL-1 signaling pathway	**7**	*Il1b, Il1rn, Il1rap, Il1r2, Myd88, Irak1, Irak4*	**5**	*Il1r1, Il1a, Traf6, Sirpa, Irak2*
Blood clotting cascade	**7**	*F12, F10, F5, F7, Serpinb2, Serpine1, F8a*	**13**	*F11, F9, Vwf, F2, F13b, Serpinf2, Plau, Plat, Plg, Fgb, Fga, Fgg, F8*
Prostaglandin synthesis and regulation	**17**	*Ptgs2, Anxa3, Anxa2, Anxa1, S100a6, Anxa6, Hsd11b1, Anxa4, Ptgir, Prl, Ednra, Cyp11a1, Pla2g4a, Tbxas1, Ptger2, Ptger3, Ptger4*	**14**	*Ptgs1, Anxa5, Anxa8, Ednrb, Scgb1a1, Edn1, Ptgfr, Hpgd, Hsd11b2, S100a10, Ptgis, Ptgds, Ptgdr, Ptger1*
Oxidative damage	**20**	*Tnf, Tnfrsf1b, Traf1, Traf2, Mapk14, Casp3, Bcl2, Bak1, Casp9, Cycs, Traf3, Mapk13, Map3k9, Gadd45a, Pcna, C1qa, C1qb, C2, C3ar1, Nfkb1*	**15**	*Map3k1, Map2k6, Apaf1, Cyct, Bad, Mapk12, Bag4, Cdc42, Tnk2, Cdkn1c, Cdkn1b, Cdkn1a, Hc, Cr2, Traf6*
FAS pathway and stress induction of HSP regulation	**22**	*Daxx, Fasl, Mapkapk3, Gm10108, Tnf, Casp9, Mapkapk2, Bcl2, Casp3, Ripk2, Fadd, Casp7, Parp1, Arhgdib, Pak1, Pak2, Dffb, Rb1, Prkdc, Casp6, Lmnb1, Map2k4*	**14**	*Fas, Hspb1, Il1a, Apaf1, Casp8, Cflar, Faf1, Dffa, Map3k1, Map3k7, Lmna, Jun, Lmnb2, Mapk8*
Complement and coagulation cascades	**19**	*C1qb, C1qa, C2, C3, C6, Mbl1, Serping1, C4bp, C3ar1, F3, F7, F10, F5, Serpina5, Serpine1, Plaur, F12, Bdkrb1, C7*	**31**	*Daf2, Hc, C9, Masp1, Cd59a, Cfi, Masp2, Cr2, Cfh, F9, F8, F11, Vwf, F2, Fgb, Serpind1, Cpb2, Tfpi, F13b, F2r, Serpinc1, Proc, Pros1, Plat, Plau, Thbd, Plg, Klkb1, Kng1, Serpinf2, A2m*
Apoptosis	**48**	*Tnfsf10, Tradd, Tnf, Bak1, Tnfrsf1b, Traf1, Traf2, Bcl2l11, Map2k4, Hells, Fadd, Casp1, Birc3, Tnfrsf21, Birc2, Casp6, Nfkbib, Casp7, Nfkbie, Casp3, Birc5, Casp2, Irf1, Bcl2, Bcl2l1, Gzmb, Cdkn2a, Prf1, Pmaip1, Fasl, Bid, Igf1, Myc, Igf1r, Trp53, Nfkb1, Trp73, Casp9, Nfkbia, Dffb, Traf3, Irf4, Irf5, Irf7, Bbc3, Diablo, Mcl1, Cycs*	**34**	*Tnfrsf1a, Mdm2, Rela, Jun, Map3k1, Mapk10, Bad, Ripk1, Lta, Ikbkb, Xiap, Chuk, Irf2, Ikbkg, Irf3, Fas, Cradd, Cflar, Bcl2l2, Bax, Igf2, Trp63, Apaf1, Hrk, Bnip3l, Dffa, Casp4, Casp8, Tnfrsf25, Irf6, Bok, Pik3r1, Akt1, Cyct*
IL-6 signaling pathway	**52**	*Il6, Il6ra, Fes, Tec, Shc1, Btk, Grb2, Jak2, Stat3, Ptpn11, Vav1, Hdac1, Prkcd, Map2k4, Pik3r2, Hsp90aa1, Stat1, Mapk14, Cebpb, Nfkb1, Raf1, Casp3, Ppp2r1b, Ppp2r2a, Rac1, Ppp2r2c, Daxx, Ppp2r4, Ptk2b, Ppp2r5a, Gab2, Ep300, Erbb3, Rb1, Hck, Lyn, Map2k2, Casp9, Eif4e, Ppp2ca, Eif2a, Ppp2r1a, Bmx, Ppp2r5c, Ppp2r5d, Cd40, Fgr, Map2k1, Inpp5d, Stat5a, Stat5b, Mapkapk2*	**38**	*Il6st, Jak1, Tyk2, Sos1, Ar, Mapk1, Gab1, Jun, Nlk, Ncoa1, Crebbp, Ppp2r2b, Cdk9, Socs3, Map2k6, Fos, Plcg1, Erbb2, Map3k4, Akt1, Ppp2cb, Mapk8, Eif4ebp1, Ppp2r5b, Fyn, Ppp2r5e, Hspb1, Cdk5, Cdk5r1, Rps6ka2, Mapk3, Bad, Gsk3b, Foxo1, Ptk2, Pxn, Inppl1, Map3k7*
Regulation of actin cytoskeleton	**58**	*Fn1, Arhgef6, Csk, Vav1, Map2k1, Chrm1, Iqgap1, Arhgef1, Enah, Was, Arpc5, Rac1, Rac2, Cd14, Pdgfb, Fgf6, Fgf7, Fgf18, Fgfr4, Pdgfra, Pdgfrb, Pik3c2g, Pik3cb, Pik3cd, Pik3cg, Pik3r2, Raf1, Map2k2, Mapk4, Mapk6, Bdkrb1, Pak1, Pak2, Pak3, Pak7, Pfn1, Wasf1, Tmsb4x, Ezr, Pip4k2a, Msn, Pip5k1b, Pip4k2b, Pip4k2c, Actn1, Ppp1r12a, Mylk, Cfl1, Gsn, Pik3r5, Rassf7, Arhgef4, Cyfip2, Brk1, Actg1, Diap1, Vil1, Diap3*	**91**	*Egfr, Itga1, F2r, F2, Gna12, Sos1, Gna13, Bcar1, Crk, Ptk2, Mos, Mapk1, Gng12, Fgd1, Cdc42, Baiap2, Rhoa, Rock1, Rac3, Egf, Fgf1, Fgf2, Fgf3, Fgf4, Fgf5, Fgf9, Fgf20, Fgf11, Fgf22, Fgf12, Fgf17, Fgf23, Fgf8, Fgf13, Fgf10, Fgf21, Fgfr1, Fgfr3, Fgfr2, Sos2, Rras, Rras2, Kras, Pik3r4, Pik3c2a, Pik3c2b, Pik3c3, Pik3ca, Pik3r1, Pik3r3, Braf, Mapk3, Dock1, Chrm2, Chrm3, Bdkrb2, Chrm5, Rock2, Arhgef7, Apc, Apc2, Pak4, Pak6, Wasf2, Nckap1, Git1, Rdx, Slc9a1, Pip5k1a, Pip5k1c, Pip5kl1, Vcl, Limk1, Myl1, Myl3, Cfl2, Myh10, Mras, Nras, Ins1, Ins2, Fgf15, Fgf14, Fgf16, Pdgfa, Ssh3, Ssh2, Ssh1, Pxn, Chrm4, Abi2*
TNF-α, NF_kB signaling pathway	**94**	*Flna, Psmc3, Nfkb1, Cyld, Traip, Casp8ap2, Tnfrsf1b, Tnf, Prkcz, Ppp2ca, Casp7, Cdc34, Nfkbia, Traf2, Tradd, Psmd7, Psmd12, Psmd13, Tifa, Psmd1, Smarcc1, Cdc37, Smarca4, Hdac1, Hdac2, Kpna3, Psmb5, Psmc1, Stat1, Fadd, Psmc2, Bcl3, Ddx3x, Usp11, Smarcb1, Traf1, Cops3, Hdac6, Unc5cl, Ywhag, Pfdn2, Ywhab, Ywhae, Ywhaz, Tnfaip3, Tnip1, Akt2, Csnk2b, Traf3, Birc2, Birc3, Casp3, Cul1, G3bp2, Cd3eap, Nfkbib, Nkiras2, Polr1a, Polr1b, Polr1d, Polr2h, Polr1e, Polr1c, Nfkbie, Commd1, Mcm5, Mcm7, Ikbkap, Hsp90ab1, Hsp90aa1, Ptpn11, Fbl, Rpl4, Rps11, Traf5, Ikbke, Tank, Ube2i, Mark2, Rps6ka5, Nfkbiz, Usp2, Nsmaf, Gnb2l1, Casp2, Tnfrsf11a, Akap8, Ripk3, Ripk2, Pebp1, Nr2c2, Dap, Fancd2, Traf4*	**72**	*Traf6, Rel, Ikbkg, Tbk1, Eif4a3, Psmd6, Trpc4ap, Rnf216, Tnfrsf8, Hspb1, Tnfrsf1a, Rela, Prkaca, Map3k2, Capn3, Psmd3, Nfkb2, Relb, Kcnq1, Faf1, Papola, Pml, Iqgap2, Glg1, Gsk3b, Smarce1, Smarcc2, Pkn1, Kpna6, Pias3, Peg3, Cav1, Gtf2i, Txlna, Map3k3, Gab1, Ywhah, Tnip2, Chuk, Akt1, Src, Rnf25, Fbxw11, Csnk2a2, Ripk1, Casp8, Ptk2, Cflar, Btrc, Lrpprc, Mtif2, Nkiras1, Pdcd2, Gm10774, Ikbkb, Rasal2, Zfand5, Crebbp, Fkbp5, Map3k14, Ktn1, Azi2, Map3k1, Map3k8, Map2k5, Nlrp4e, Cradd, Actl6a, Ppp1r13l, Dpf2, Alpl, Bag4*

The purification process of the hepatic endothelial cells, however, was not ideal, because of contamination with T-cells, which are closely attached to endothelial cells and might be still persistent

after FACS sorting of cells. Gene pathways, which were differentially regulated but specific for immune cells, are displayed in the supplemental Table 1.

We could identify pathways that are regulated during endothelial damage in established GVHD. These pathways may be useful to develop and test endothelial modulating agents as therapeutic tools for GVHD.

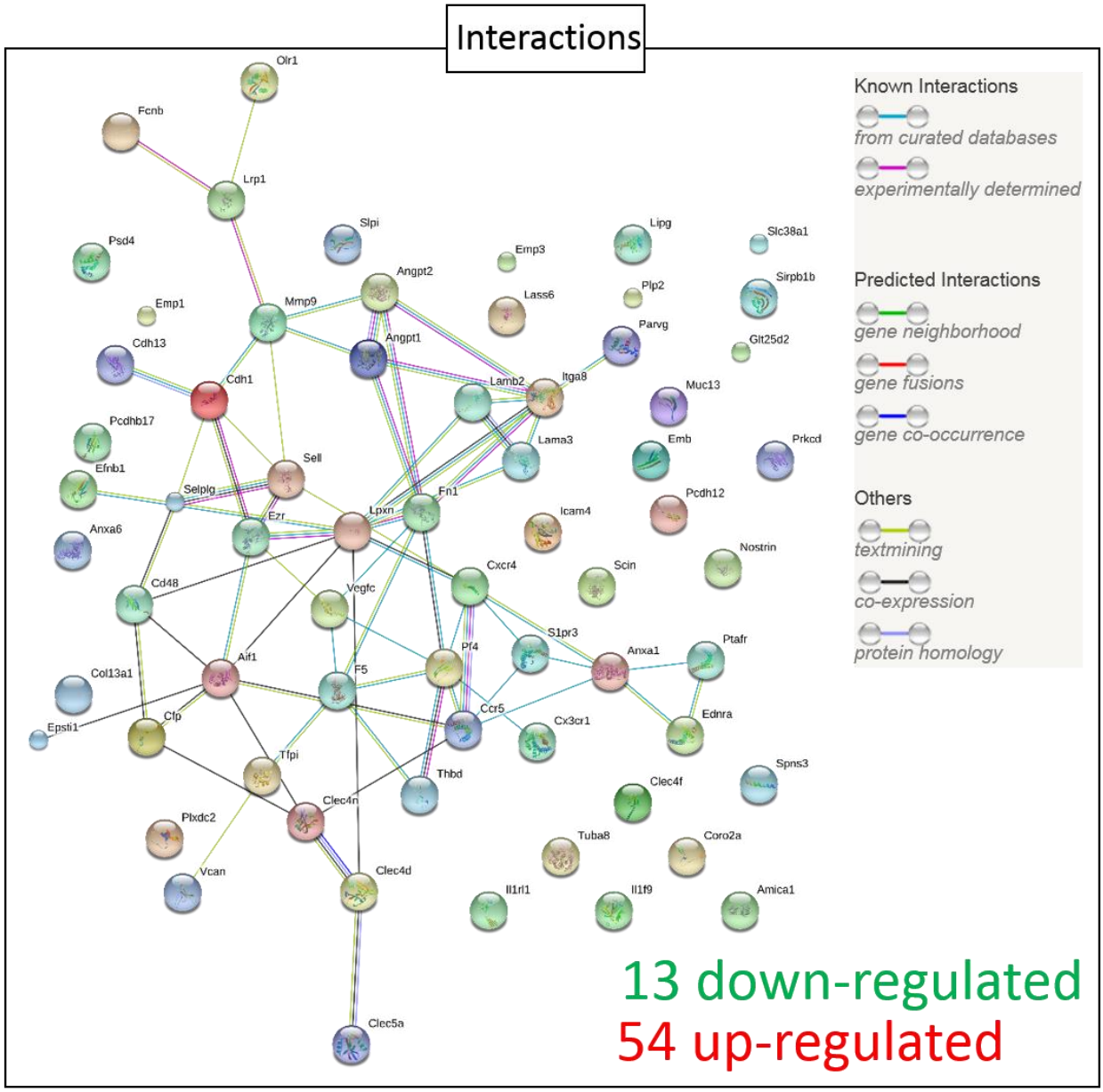

Figure 29| Interactive network of regulated genes. Network analysis of genes regulated in allogeneic bone marrow transplantation (BMT) recipients at day 15 after BMT in LP/J→B6 graft-versus-host disease model. Network analysis of selected, endothelium specific genes in hepatic endothelial cells revealed several interaction partners among the regulated genes. Analysis was performed with string database (https://string-db.org/).

3.11 ESTABLISHMENT OF A STEROID REFRACTORY GVHD MOUSE MODEL

To address the question whether endothelial damage is a pathologic condition during srGVHD, we established a srGVHD model. We were interested if endothelial biology is separating steroid non-responder (non-RS) from responder (RS). Normal GVHD models were used and treatment of allo-BMT recipients with different concentrations of Dexamethasone was started, in order to define the optimal dosage to get steroid non-RS and RS during GVHD.

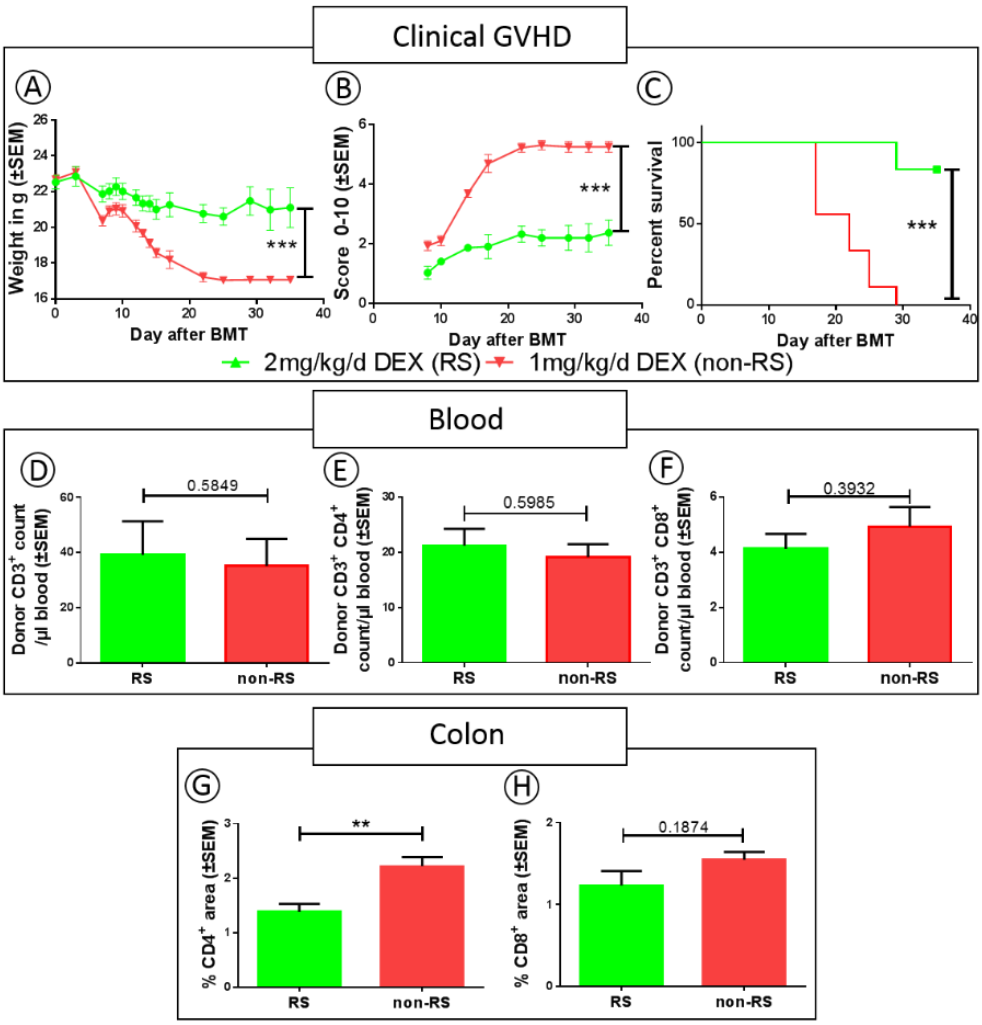

Figure 30| Murine model of steroid refractory graft-versus-host disease (srGVHD). A-C| Clinical parameters of Dexamethasone (DEX) treatment in B6→BDF GVHD model (n=10 animals per group). **A|** Weight loss of steroid responder (RS) and non-responder (non-RS) after allogeneic (allo) bone marrow transplantation (BMT). **B|** GVHD score of RS and non-RS after allo-BMT. **C|** Survival rate of RS and non-RS after allo-BMT. **D-F|** Quantification of donor T-cells of RS and non-RS in B6→Balb/C GVHD model (n=6 animals per group). **D|** Quantification of total donor T-cells ($CD3^+$) per µl blood in DEX-treated allo-BMT recipients. **E|** Quantification of total donor $CD4^+$ T-cells per µl blood in DEX-treated allo-BMT recipients. **F|** Quantification of total donor $CD8^+$ T-cells per µl blood in DEX-treated allo-BMT recipients. **G-H|** Quantification of T-cell infiltration in colonic mucousa 15 days after allo-BMT in B6→BDF GVHD model treated with DEX (n=5 animals per group). **G|** $CD4^+$ area in colonic mucosa from RS and non-RS. **H|** $CD8^+$ area in colonic mucosa from RS and non-RS. Significance was tested by student's *t*-test, survival was tested by Mantel-Cox log-rank test (***P* < .01; ****P* < .001). Error bars indicate mean ± standard error of the mean (SEM).

The appropriate dosage to mimic steroid non-RS was 1mg/kg/d Dexamethasone and the ideal dosage to mimic steroid RS was 2mg/kg/d Dexamethasone starting treatment at day 4 after BM. The weight

curve in Figure 30A shows significant differences between 2mg/kg/d Dexamethasone and 1mg/kg/d Dexamethasone treated allo-BMT recipients. In addition, GVHD score (Figure 30B) and survival rate (Figure 30C) were significantly different between both groups. In the peripheral blood, however, no difference in $CD3^+$ T-cell count (Figure 30D), or in T-cells subsets $CD3^+$ $CD4^+$ (Figure 30E) and $CD3^+$ $CD8^+$ (Figure 30F) were detected at day 15 after BMT. Infiltration of T-cell subset $CD4^+$ (Figure 30G) in colonic mucosa at day 15 after BMT was significantly increased in non-RS compared to RS. For $CD8^+$ cells a trend of higher infiltration was observed in non-RS compared to RS (Figure 30H). All BMT recipients responded to the high dosage of Dexamethasone, whereas the low dosage of Dexamethasone did not ameliorate GVHD. The same applied for another GVHD model (supplemental Figure 5).

In summary, we created an artificial model of srGVHD by an insufficient steroid treatment of GVHD.

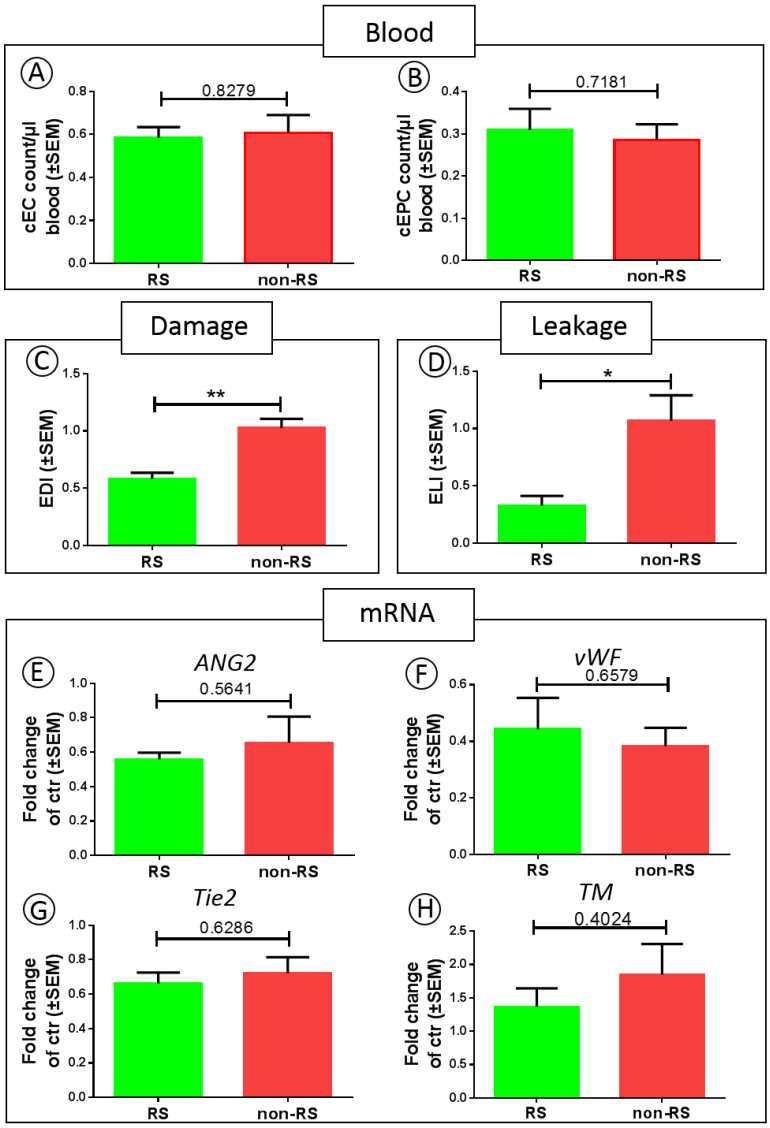

Figure 31| Involvement of endothelial damage and endothelial leakage in steroid refractory graft-versus-host disease (srGVHD). A-B| Quantification of circulating endothelial cells (cECs) and circulating endothelial progenitor cells (cEPCs) at day 15 after bone marrow transplantation (BMT) in steroid treated B6→Balb/C GVHD animals (n=6 animals per group). **A|** Quantification of cECs and **B|** of cEPCs per µl blood of responder (RS) and non responder (non-RS). **C|** Endothelial damage index (EDI) in colonic mucosa at day 15 after BMT of steroid treated B6→BDF GVHD animals (n=5 animals). **D|** Endothelial leakage index (ELI) in colonic mucosa at day 15 after BMT of steroid treated B6→BDF GVHD animals (n=5 animals). **E-H|** mRNA expression in whole organ lysates at day 15 after BMT in steroid-treated B6→BDF allo-BMT recipients (n=4 per group). Values are normalized to *Gapdh* mRNA expression and to the expression of untreated wild type control (ctr) of the studied gene. **E|** *Angiopoietin-2* (*ANG2*) mRNA expression, **F|** *von Willebrand factor* (*vWF*) mRNA expression, **G|** *Tyrosine kinase with immunoglobulin- and epidermal growth factor-like domains 2* (*Tie2*) mRNA expression and **H|** *thrombomodulin* (*TM*) mRNA expression in colon of steroid treated allo-BMT recipients. Significance was tested by student's *t*-test (**P* < .05; ***P* < .01). Error bars indicate mean ± standard error of the mean (SEM).

3.12 Endothelial damage in steroid refractory GVHD

To investigate the role of the endothelium during srGVHD, we analyzed endothelial damage markers in peripheral blood and in colon by mRNA expression and histology at day 15 after BMT from either

RS or non-RS group. In the blood, we quantified cECs as endothelial damage marker and circulating endothelial progenitor cells (cEPCs) as endothelial regeneration capacity marker. For mRNA expression, we used whole colon lysates from RS and non-RS allo-BMT recipients at day 15 after BMT. The amount of endothelial damage and leakage was assessed by histology. In the peripheral blood, we saw no differences between RS and non-RS concerning cECs and cEPCs. The endothelial damage index (EDI) and endothelial leakage index (ELI) in colon was significantly increased in the non-RS group (Figure 31C and D). mRNA expression of the endothelial damage markers *ANG2* (Figure 31E) and *TM* (Figure 31H) showed a slight increase in non-RS compared to RS, while *Tie2* (Figure 31G) and *vWF* (Figure 31F) were not differentially regulated.

These data show that endothelial damage and increased leakage may contribute to the progression of srGVHD.

3.13 ENDOTHELIAL ACTIVATION AND CO-STIMULATORY CAPACITY IN STEROID REFRACTORY GVHD

Besides endothelial damage, an up-regulation of activation-, adhesion- and co-stimulatory markers on endothelial cells from allo-BMT recipients was detectable. To address the question whether changes in activation and immunological capacity are occurring in endothelium during srGVHD, we measured colonic mRNA expression levels of endothelial activation and adhesion markers. Additionally, we analyzed hepatic endothelial cells from non-RS and RS by the use of flow cytometry for the total number of cells, their co-stimulatory capacity and adhesion molecule expression at day 15 after BMT. The percentage of endothelial cells in liver (Figure 32A) and the total number of endothelial cells (Figure 32B) per mg of hepatic tissue was significantly reduced in the non-RS group. The percentage of co-stimulatory molecules CD80 (Figure 32C) and CD86 (Figure 32D) of hepatic endothelial cells was the same in non-RS and RS. There was an almost significant reduction of the percentage of $ICAM1^+$ hepatic endothelial cells in non-RS (Figure 32E), while the expression level of ICAM1, quantified by mean fluorescence index (Figure 32F), showed the opposite trend in non-RS. The mRNA expression of *ICAM1* (Figure 32G) and of the endothelial activation marker *E-selectin* (Figure 32H) in whole colon lysates was not significantly down-regulated in non-RS compared to RS group at day 15 after BMT.

Based on the finding that endothelial damage is increased in srGVHD and endothelial cells show immune modulatory capacity, we hypothesize an important role of the endothelium during srGVHD.

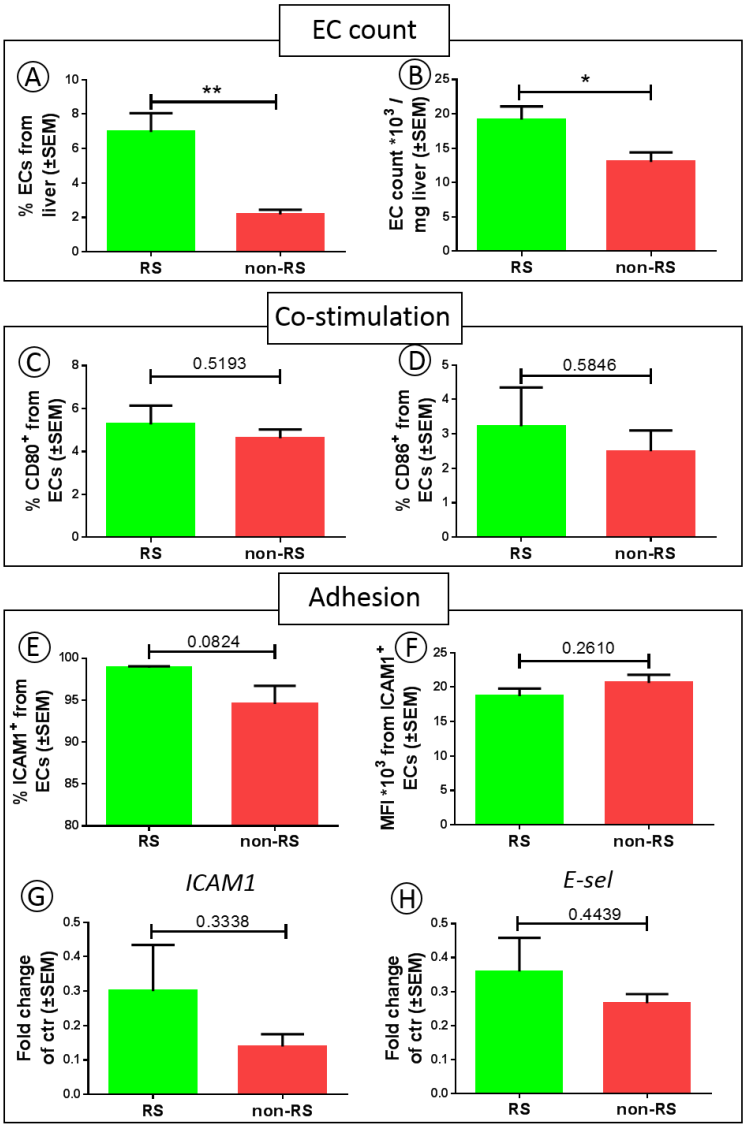

Figure 32| Co-stimulatory capacity and adhesion of endothelial cells in steroid refractory graft-versus-host disease (srGVHD). A-D| Quantification of hepatic endothelial cells at day 15 after allogeneic (allo) bone marrow transplantation (BMT) in steroid treated B6→Balb/C GVHD animals (n=6 animals per group). **A|** Percentage of hepatic endothelial cells from total cells of responder (RS) and non responder (non-RS). **B|** Total endothelial cell count per mg hepatic tissue. **C-D|** Co-stimulatory capacity of hepatic endothelial cells at day 15 after BMT in steroid treated B6→Balb/C GVHD animals (n=6 animals per group). **C|** Percentage of CD80 expression of hepatic endothelial cells. **D|** Percentage of CD86 expression of hepatic endothelial cells. **E-F|** Intracellular adhesion molecule 1 (ICAM1) quantification and expression intensity of hepatic endothelial cells at day 15 after BMT in steroid treated B6→Balb/C GVHD animals (n=6 animals per group). **E|** Quantification of ICAM1 expressing hepatic endothelial cells. **F|** Mean fluorescence intensity (MFI) of ICAM1 expression from hepatic endothelial cells. **G-H|** mRNA expression in whole organ lysates at day 15 after BMT in steroid treated B6→BDF allo-BMT recipients (n=4 per group). Values are normalized to *Gapdh* mRNA expression and the expression of untreated wild type control (ctr) of the studied gene. **G|** *E-selectin (E-sel)* mRNA expression and **I|** *ICAM1* mRNA expression in colon of steroid treated allo-BMT recipients. Significance was tested by student's *t*-test (*$P < .05$; **$P < .01$). Error bars indicate mean ± standard error of the mean (SEM).

4 DISCUSSION

4.1 ENDOTHELIAL DAMAGE DURING GVHD

We hypothesize that endothelial damage is involved in the pathobiology of GVHD and has functional consequences, which may influence treatment strategies to ameliorate GVHD while maintaining the GVT effect. Since characterization of the endothelium in inflammation associated to GVHD is sparse, we first had to prove that endothelial dysfunction is occurring during GVHD. We established different mouse models of GVHD and methods to describe endothelial dysfunction.

Many complications of allo-HSCT are associated with endothelial damage in the recipient[30]. As previously mentioned, the organism is prone to infection when barrier function of the endothelium is disturbed. In ES, the endothelial damage caused by the conditioning regime is supposed to promote inflammatory cytokine release and to contribute to the course of ES. TAM patients show increased serum levels of TM, ICAM1 and vWF[47,48]. In VOD, a complete destruction of the small hepatic vessels can occur[53]. In CS and DAH, little is known about the pathobiology. Endothelial damage by the conditioning regime is considered to contribute to these complications[31,58,61]. Additionally, recent studies suggest a contribution of endothelial damage in GVHD and srGVHD[87-89,175,187,188].

Endothelial damage was shown in various inflammatory diseases similar to GVHD. In patients with early rheumatoid arthritis and systemic lupus erythematosus, elevated endothelial damage has been detected[189,190]. These studies identified markers for endothelial damage such as vWF and cECs.

Our study shows that endothelial damage is increased in colon and duodenum of patients with GVHD. This finding is consistent with previously published studies, which show a higher amount of cECs and higher numbers of cEPCs during human GVHD. cECs are reflecting endothelial damage while cEPCs are reflecting endothelial regeneration. Furthermore, the numbers of cECs and cEPCs correlated with disease severity[191-194]. Previous studies showed that endothelial damage in intestine and skin biopsies was elevated during GVHD[172,195]. Other studies demonstrated that serum levels of endothelial stress markers like vWF, ANG2, ST2 and TM are elevated in GVHD and may serve as biomarkers for disease onset[188,196-198]. IL-6 and IL-8 are already in use as biomarkers[199,200]. Both can induce oxidative stress in endothelial cells[201,202] and contribute thereby to endothelial damage. Serum levels of soluble adhesion molecules, such as ICAM1 and E-selectin, are increased during GVHD[173]. In additon, single nucleotide polymorphisms in the genes of *TM* and *VEGF* have been shown to predict GVHD occurrence[174,203].

Several studies showed endothelial damage directly after conditioning[204,205] even before epithelial damage in the intestine[206]. We confirmed these findings by quantification of pericyte loss in chemotherapeutically treated animals. Pericyte loss has been well described as a marker of endothelial damage[207-210] but also immature vessels lack pericytes[211]. Caspase3 staining of endothelial cells in mouse microvasculature was not applicable to quantify endothelial damage. In other studies, terminal

deoxynucleotidyl transferase dUTP nick end labeling has been used to quantify endothelial damage mediated by allo-reactive T-cells. These studies, however, were performed in an artificial GVHD model without conditioning regime[212,213]. We show endothelial damage in chemotherapeutically conditioned GVHD mice by CTEM pictures of liver and colon. Endothelial damage was characterized by quantification of cECs in blood and by pericyte loss in target organs. We detected more severe endothelial damage during GVHD, a finding consistent with other studies of murine GVHD models, which showed endothelial lesions in the liver as well as elevated numbers of cECs and endothelial micro particles in mouse serum during GVHD[194,214-216].

As observed in tumor, perfusion and vascular connection to the circulation is critical in vessel regression. We addressed the question whether damaged vessels are still perfused and connected to the circulation by FITC-Lectin perfusion, a well-established approach in tumor studies[217]. During GVHD, no vessel regression is observable and vessels are perfused properly. Damaged endothelial cells may still be able to mediate vascular contraction and thereby modulate immune cell recruitment by controlling the vascular tone.

We speculated that endothelial damage might also affect vessel organization. We did not detect structural changes in terms of diameter, length, straightness and branch level. In other models like radiation induced thymus damage, however, straightness of vessels was reduced very early after the conditioning regime with TBI[218]. This difference may be caused by the radiation sensitivity of lymphatic organs, including the thymus, as described already in the 1960's[219]. Another explanation might be the different time course of structural vessel alterations, early after radiation, or in established GVHD.

4.2 Endothelial leakage during GVHD

In preclinical models of colitis, loss of endothelial barrier integrity potentiates inflammatory events[165,220]. As endothelial barrier integrity is one major obstacle for vascular permeability[165,207], we wanted to investigate and demonstrate consequences of endothelial damage occurring in GVHD. We speculated that endothelial damage is accompanied by increased endothelial leakage during GVHD. Therefore, we performed Evans blue assay and analyzed tight and intercellular adherence junction proteins in GVHD target organs liver and colon. During GVHD, the permeability for Evans blue dye is highly increased and the expression of tight junction protein ZO-1 and adherence junction protein VE-cadherin is significantly decreased in GVHD target organs in established GVHD. Leakage in GVHD non-target organs remains unaffected. ZO-1 is critical for recruitment of tight junction transmembrane proteins, such as claudins, and maintains barrier function of the epithelium and endothelium[133,221,222]. Studies, focusing on VE-cadherin, revealed that T-cell migration is enhanced by VE-cadherin[223,224]. Additionally, the promotion of VE-cadherin expression in tumor vasculature increases T-cell infiltration into the tumor[225]. This is the first time that increased endothelial leakage and loss of ZO-1 and VE-cadherin is related to GVHD. Studies using primary endothelial cells from

GVHD target organs may give a more detailed view on barrier integrity. Nevertheless, culturing of primary endothelial cells is problematic. We were not able to expand isolated hepatic endothelial cells. To overcome this problem, we are going to use $p19^{ARF-/-}$ mice, induce GVHD and isolate hepatic endothelial cells. The p19 mutation is destabilizing an activator of p53, which induces cell cycle arrest and apoptosis[226,227]. By using $p19^{ARF-/-}$ endothelial cells in *in vitro* assays, we hope to obtain further insight into the barrier function during GVHD. This approach, however, implies more problems such as the loss of the pro-inflammatory phenotype of the endothelial cells after culturing. The pro-inflammatory phenotype of endothelial cells is highly variable and may be altered by culturing conditions, like passaging, confluence and growth factors[228].

4.3 PHYSIOLOGICAL FUNCTIONS OF VESSELS IN GVHD

Besides the loss of endothelial cells and pericytes accompanied by increased vascular leakage, we became interested in the physiologic functions of the endothelium. In inflammatory bowel disease it was shown that physiologic alterations of mesenteric arteries could be induced by micro particles from the circulation of colitis patients[229]. We used the well-established method of myography to measure contraction and relaxation of mesenteric arteries[230]. Mesenteric arteries have been described as a potential target of the GVHD reaction[231], accompanied with increased blood pressure[231,232]. In our GVHD model, however, we found only small differences between syn- and allo-BMT recipients: an increase in the overall contraction capacity, whereas relaxation with ACh is reduced at lower concentrations, indicating high blood pressure. The mesenteric arteries are slightly affected by GVHD reaction, and physiological differences only appear at late observation points (day 28) in our GVHD model. The small extent of alterations compared to other studies can be explained by the different conditioning regime and GVHD model we used. Total body irradiation may have a greater impact on mesenteric arteries. In addition, the moderate GVHD course in our model may contribute to these weak effects on the mesenterium. We used a minor mismatch model, whereas a major mismatch model had been used in previous studies[231,232]. In human GVHD pathogenesis, physiological information is hard to obtain: the data are compromised by prophylactic treatment with drugs such as glucocorticoids and calcineurin inhibitors. Both are described to lead to increased blood pressure and alteration of physiologic functions[233,234].

4.4 ENDOTHELIAL ACTIVATION AND IMMUNE CELL CONTACT

In inflammatory bowel disease and rheumatoid arthritis, serum levels of soluble adhesion molecules, such as ICAM1, VCAM1 and E-selectin are elevated[235-238]. Histological assessment of colitis revealed increased E-selectin expression in colon biopsies of patients suffering from ulcerative colitis [239]. In these patients, an increased expression of MHC class II, ICAM1 and VCAM1 of endothelial cells was also observable[235,239,240]. A critical role of endothelial cells in inflammatory diseases is postulated, as they are described as semiprofessional APCs.

We speculated that adhesion molecule expression and antigen presentation is elevated during GVHD. We used CTEM to show direct immune cell-endothelial cell contact and mRNA expression analysis of adhesion molecules as well as flow cytometry analysis of co-stimulatory capacity and MHC expression. CTEM pictures of colon and liver show close contact of immune cells and the endothelium. mRNA expression of the adhesion molecules *ICAM1*, *VCAM1* and *P-selectin* is up-regulated and the co-stimulatory capacity as well as antigen presentation via MHC class II of hepatic endothelial cells is increased in GVHD, indicating endothelial cell activation and immune cell recruitment to the site of inflammation. These findings are consistent with previously published results: blockade of ICAM1 ameliorates organ transplantation complications[241]. Furthermore, P-selectin deficient recipient mice were shown to develop reduced GVHD[242]. Additionally, carcinoembryonic antigen related cell adhesion molecule 1, another kind of adhesion molecule, has functional relevance for GVHD and GVT response[243].

We also wanted to address the question, whether soluble factors in GVHD serum stimulate endothelial cells to promote endothelial cell activation. Serum of mice with GVHD does not induce endothelial cell activation *in vitro*. Antigen presentation by MCH class II, co-stimulatory capacity by CD80 and CD86 and ICAM1 expression is unaltered after incubation of MCECs with GVHD serum. This may speak for a need of direct immune cell-endothelial cell interaction to trigger endothelial activation. In contrast, human serum was shown to induce endothelial cell activation accompanied by increased expression of ICAM1 and VCAM1[244]. The lack of effect in our approach may be due to the minor role of cardiac endothelial cells in antigen-presenting function. Hepatic or colonic endothelial cells may react differently upon stimulation with serum from GVHD animals. In addition, human endothelial cells may be more prone to be activated than mouse endothelial cells. Beside the type of endothelial cells, alterations in cytokine concentrations from BMT-recipients may explain the different results. We used serum from BMT-recipients after established GVHD, whereas in the study from Mir et al.[244], serum from GVHD patients was collected directly after GVHD onset. Serum directly after GVHD onset has higher cytokine and chemokine concentrations than serum at later time points during GVHD[179].

4.5 Gene array data obtained from endothelial cells during GVHD

To identify possible endothelial pathways involved in GVHD, we performed a gene array from isolated hepatic endothelial cells. As shown, isolated endothelial cells obtained from syn-BMT and allo-BMT recipients clustered nicely. Pathways differentially regulated in endothelial cells during GVHD are related to metabolomic pathways such as nucleotide, amino acid, tryptophan and insulin pathways. Riesner et al.[152] had shown that metabolomic pathways of endothelial cells are also altered in the early phase of GVHD. Furthermore, IL-4 signaling, toll like receptor and cell pluripotency pathways were altered in established GVHD. IL-4 was shown to cause hyperpermeability of endothelial cells *in vitro*[245]. For toll like receptor signaling in endothelial cells a multitude of

consequences, for instance the release of pro-inflammatory cytokines and chemokines[246,247] as well as increased expression of adhesion molecules[248] and permeability factors[249] have been described. These alterations in gene expression of allo-BMT recipients further supports our data about the pro-inflammatory phenotype of endothelial cells and increased blood vessel leakage during GVHD.

Pathways related to endothelial damage included complement activation, oxidative damage, co-agulation and FAS signaling pathways, shedding light on possible treatment strategies to improve endothelial function during GVHD. Nevertheless, as shown in the appendix, we are not able to obtain a pure endothelial cell fraction. In the gene array data, up-regulation of TCR and B-cell receptor genes is also observable. Although we put a lot of effort into isolation of endothelial cells via FACS sorting with approximately 96% purity, immune cells seem to be strongly attached to endothelial cells. An additional enrichment step via CD31 magnetic bead labeling and magnetic cell isolation before FACS may be useful to reduce immune cell contamination of the endothelial cell fraction.

4.6 TREATMENT OF ENDOTHELIAL DYSFUNCTION TO AMELIORATE GVHD

In various inflammatory diseases, such as colitis and psoriasis, targeting adhesion molecule expression of endothelial cells by antibodies or natural compounds showed an amelioration of disease progression[250,251]. In preclinical models of peritonitis and rheumatoid arthritis the very elegant "sneaking ligand construct" (SLC) allowed to specifically inhibit NFκB in activated, E-selectin expressing endothelial cells. SLC treatment reduced T-cell migration during peritonitis and ameliorated the course of rheumatoid arthritis[252].

Data obtained on endothelial dysfunction in this study encouraged us to check, if endothelium-targeted agents are able to ameliorate GVHD. We used three different agents targeting different endothelial functions. Defibrotide was our first choice, since it is approved for the treatment of TAM. The precise mechanism of action has not yet been clarified, but Defibrotide has a series of effects on the endothelium involved in hemostasis. Defibrotide has been shown to increase the release of PGI2 and prostaglandin E2 (PGE2) and stimulates TM expression on endothelial cells as reviewed by Morabito et al.[184]. Furthermore, studies performed with endothelial cells *in vitro* showed decreased adhesion molecule expression, when cells were treated with Defibrotide[253]. The study from Eissner et al. also contains important findings in the transplantation setting: Defibrotide protects endothelial cells from the pro-apoptotic effect of chemotherapy[254,255]. Unexpectedly, the therapeutic effect of Defibrotide in mouse models of GVHD is not sufficient to ameliorate GVHD.

We next targeted the LOX1 pathway with the inhibitor ß-APN. LOX1 has been shown to catalyze elastin and collagen crosslinking, allowing the formation of a mature and functional extracellular matrix[185]. *In vitro* studies revealed a protective effect of LOX1 inhibition on retinal endothelial cells following high glucose exposure[256]. Under inflammatory conditions, LOX1 was up-regulated in oral tissue from rats[257]. Furthermore, tumor endothelial cells secrete LOX1 which promotes angiogenesis

and metastasis of tumors[258,259]. Additionally, LOX1 inhibition reduced arterial blood pressure[260]. Unexpectedly, in the GVHD mouse models applied in our study, inhibition of LOX1 by ß-APN could not ameliorate GVHD progression.

Another interesting drug targeting endothelial function is Plerixafor. Plerixafor in combination with G-CSF is applied in clinics, to mobilize hematopoietic stem cells[261]. Plerixafor functions as an antagonist of alpha chemokine receptor CXCR4 and as an allosteric agonist of CXCR7[186]. Studies revealed that the blockade of CXCR4 mobilized EPCs and improved wound healing in diabetic mice[262,263]. Additionally, re-endothelialization in a model of saccular cerebral aneurysm was accelerated after treatment with CXCR4 inhibitors[264]. Contrary to our expectations, the usage of CXCR4 antagonist Plerixafor in murine GVHD models was not sufficient to ameliorate the course of GVHD.

Although we tried substances aiming at different functions and pathways of endothelial cell function, amelioration of GVHD by targeting the endothelium was insufficient up to now. There can be a multitude of reasons for the therapeutic failure. First, endothelial damage might just present a bystander of GVHD without a functional role in the pathogenesis. This is an unlikely scenario, since endothelial damage is crucial in other inflammatory diseases. Furthermore, we detected substantial endothelial alterations in this study during GVHD. We believe that our negative data is provoked by the use of an insufficient treatment regime in the time-course of GVHD. In case of Defibrotide treatment, for instance, serum concentration of Defibrotide peaks two hours after injection. After three hours, Defibrotide cannot be detected any more in serum[265]. Although we used a higher dosage (700mg/kg) compared to clinical applications (ranging from 5 to 60mg/kg), the fast turnover rate of Defibrotide in serum may explain the lack of effect on endothelial cells during GVHD[266]. In rabbits injected with 200mg/kg of ß-APN, the serum concentration of ß-APN peaked at 100mg/l two hours after application, followed by a rapid decrease to 10mg/l[267]. We used 2mg/kg as treatment dosage, which may be below its inhibitory concentration. To overcome the rapid turnover of both drugs, a treatment of two times per day, or the usage of osmotic mini pumps enabling continuous supply will improve serum viability of the drugs and may thereby preserve endothelial function during GVHD. The effect of Plerixafor, however, is persistent and the number of hematopoietic stem cells as well as cEPCs, in the blood are increased for up to 18 hours after injection[261]. Although Plerixafor has been shown to promote re-endothelialization, the absence of endothelial CXRC4 in mice caused reduced re-endothelialization in atherosclerotic plaques[268]. *In vitro* Plerixafor could block endothelial progenitor cell function, indicating an important role of CXCR4 for endothelial cells[269]. A negative effect on endothelial cells by chronic CXCR4 blockade may be circumvented by a single injection, or by increased time intervals between injections.

As shown in recent studies using murine models of GVHD, different compounds such as statins and TM, ameliorated GVHD. The study by Zeiser et al. using Atorvastatin showed higher survival rates and reduced GVHD scores, mediated by reduced co-stimulation and antigen presentation of APCs[270].

A more recent study applied Simvastatin to ameliorate GVHD and found reduced serum levels of ANG2 and increased levels of ANG1 in treated GVHD mice, indicating a role of endothelial function in GVHD[271]. Ikezoe et al. investigated the effect of recombinant TM in murine GVHD models. TM treatment led to an increase of T_{reg}-cells and thereby reduced GVHD. The increased number of T_{reg}-cells may be crucial for the amelioration of symptoms in murine GVHD. The beneficial effect of TM is presumably mediated via direct interaction with endothelial cells[272].

Another study revealed the importance of inflammatory neovascularization in GVHD[162]. Leonhardt et al. identified α_v integrin and mircoRNA-100 as important factors modulating the endothelium during GVHD. Blockade of α_v integrin by Cilengitide resulted in better survival, while mircoRNA-100 antagonism resulted in higher mortality of GVHD. This study added evidence that targeting the endothelium in GVHD may be an appropriate way to reduce GVHD while maintaining the GVT reaction.

The capability of endothelial cells and endothelial progenitor cells to regenerate the endothelial monolayer came more into focus recently[273-276]. Different dosage and treatment schedules of tested compounds may be able to protect the endothelium during GVHD, but regeneration of the endothelium may be a more promising approach. To find out whether promoting the endothelial regeneration process could ameliorate GVHD, we would like to use $CD31^+$ BM cells in GVHD mouse models. Preliminary data showed that 10-20% of the bone marrow cells are $CD31^+$. We will transplant 0.5 to $1x10^7$ BM cells and thereby 0.1 to $0.2x10^7$ $CD31^+$ cells depending on the model. To prove an effect of injected $CD31^+$ BM cells, we are currently establishing a GVHD model, where we use lineage depleted, stem cell antigen 1 (sca-1) positive, proto-oncogene c-kit positive hematopoietic stem cells[277]. In this setting, $CD31^+$ cells in the transplant are absent, and the influence of injected $CD31^+$ BM on the course of GVHD is better assessable. The usage of $CD31^+$ cells from transgenic GFP mice would also allow tracking the injected cells and their incorporation into the vasculature.

4.7 Steroid refractory GVHD and endothelial function

Recent studies revealed evidence of endothelial damage during srGVHD. Elevated serum levels of sTM, ANG2, hepatocyte growth factor and IL8 were observed during srGVHD[88,175]. High levels of ANG2 and the loss of TM correlated with mortality rates of srGVHD patients[87,88]. The ANG1/ANG2 axis is critical for endothelial function and was related to vascular leakage and pericyte drop-out in a rat model of diabetes[278-280]. Furthermore, the activation status of T-cells in srGVHD patients was not elevated, indicating increased endothelial vulnerability without elevated immune response[88]. As srGVHD is one main obstacle in HSCT, and to date treatment options are not satisfactory, we wanted to establish a model for srGVHD and check for endothelial alterations. Treatment of murine GVHD models with corticosteroids has been previously performed. The work from Bouazzaouia et al. showed successful treatment of GVHD with steroids and addressed adhesion molecule mRNA-expression[281]. In our GVHD models, steroid treatment worked either for all animals or for none, depending on the

injected steroid dose. The time point (ranging from day 4 to day 10 after BMT) to start the treatment was not critical in our model. Analogously to the clinical situation, we defined "low dose steroid treatment group" with progressive GVHD as srGVHD and "high dose steroid treatment group" with ameliorated GVHD as steroid sensitive GVHD. This model is artificial, but displays the clinical situation in srGVHD, progressive GVHD despite of steroid treatment. In this model of srGVHD we investigated endothelial damage, leakage, adhesion molecules and co-stimulatory capacity of the endothelium. Endothelial damage (EDI) and leakage indicators (ELI) were increased in the colon of srGVHD animals. Those marker were used to describe damage and leakage in context of inflammation of RS and non-RS. EDI and ELI were not used in the analysis of syn- and allo-BMT tissues, since syn-BMT recipients show no inflammation in GVHD target-organs. In liver, the number of endothelial cells was decreased in srGVHD animals. mRNA levels indicating damage and activation of endothelial cells were not elevated during srGVHD. This finding was unexpected; it might be caused by a dilution effect, analyzing the complete tissue mRNA instead of mRNA of isolated endothelial cells. We also detected a trend of reduced ICAM1 expressing endothelial cells in liver during srGVHD. Reduced numbers of ICAM1 expressing hepatic endothelial cells may be explained by increased shedding of ICAM1 from endothelial monolayer during the ongoing inflammation in srGVHD. This may protect endothelial cells, as it has been shown *in vitro*, that tumor endothelial cells evade NK cell specific lysis by shedding of ICAM1[282]. In addition, sICAM1 levels are increased in sepsis and high levels of sICAM1 correlate with prolonged survival, suggesting a protective role of reduced ICAM1 surface expression[282]. The sICAM1 itself has also anti-inflammatory properties blocking T-cell and NK cell adhesion to endothelial cells[283,284]. At the same time, a tendency of increased intensity in ICAM1 surface expression of hepatic endothelial cells was observed. This may reflect a higher activation status of endothelial cells during srGVHD.

We are the first to describe endothelial alterations and endothelial dysfunction in murine srGVHD models. These findings further support the hypothesis that endothelial damage and activation are critical in disease progression of srGVHD.

4.8 OUTLOOK AND CLINICAL SIGNIFICANCE OF THE FINDINGS

As previously mentioned, successful treatment with compounds applied in this study, using adjusted treatment protocols might ameliorate GVHD. Endothelial cells would be an interesting therapeutic target in GVHD, as GVT reactions are supposed to be not affected. In addition, this approach evades additional immune suppression after GVHD onset. Thereby, targeting the endothelium in GVHD may decrease infection rates and minimize complications that arise of immune suppression in GVHD. Improving endothelial regeneration by a cell-mediated treatment, if successful in murine GVHD models, may be elegant in the setting of HSCT. Possible cross-reactions of immune suppressive compounds and compounds targeting the endothelium would be bypassed. Additionally, there may be fewer side effects due to injected endothelial cells derived from the BM and an increased specificity to

the endothelium[285]. Especially in srGVHD, the endothelium as a new target may be of clinical relevance.

This study shows increased endothelial damage and leakage during GVHD. The gene array revealed endothelial pathways, which are altered during GVHD. The pathways regulated during GVHD may contribute to the identification of clinical markers for GVHD onset and/or progression. In the detection of endothelial dysfunction in GVHD, the complement and oxidative stress pathways are of interest. They may increase the number of different biomarkers applicable in clinics to get an insight in endothelial dysfunction in human GVHD patients. Including additional markers might increase the sensitivity to recognize GVHD and srGVHD at earlier time points, thereby improving treatment and prognosis.

In this study, we focused on acute GVHD. Another inflammatory condition that can follow allo-HSCT is chronic GVHD (cGVHD), which is a multi-faceted immune response of allo-reactive T-cells to a variety of tissues in patients surviving early phases of allo-HSCT. The pathophysiology of cGVHD is not completely understood, yet[286]. Risk prediction of severe courses of cGVHD is important for optimized clinical management. Knowledge of risk factors for severe cGVHD will help to elucidate the underlying pathophysiology and allow to establish protocols to avoid this complication. Surprisingly, little is known about endothelial function as well as the interplay of endothelium and inflammation during cGVHD. It has been demonstrated in patient biopsies that rarefaction and destruction of blood vessels occur in skin during cGVHD[287], whereas a recent study showed increased vessel density during cGVHD[288]. In addition, up-regulation of adhesion molecules on endothelial cells during murine cGVHD has been demonstrated[289]. Thus, endothelial dysfunction may also contribute to the pathobiology of cGVHD. Preliminary data from established cGVHD mouse models are pointing to this direction.

4.9 SUMMARY

In summary, this study reveals endothelial leakage and alteration of physiological endothelial functions as features of endothelial dysfunction in GVHD. Furthermore, molecules indicating activation of endothelium were shown to be increased during GVHD. The expression of adhesion molecules, molecules involved in antigen presentation and co-stimulation, was increased on endothelial cells during established GVHD. These findings are schematically summarized in Figure 31.

In the context of GVHD, this study showed for the first time a loss of pericytes, elevated leakage and co-stimulatory capacity of endothelial cells during GVHD. Additionally, pathways involved in endothelial metabolomics and endothelial damage are revealed by gene array analysis of endothelial cells during GVHD.

For the first time, we established a model for srGVHD, revealing endothelial alterations and dysfunction in srGVHD. These findings further support the hypothesis that endothelial damage is critical for disease progression in srGVHD. Taken together, our results might lead to new therapeutic strategies for GVHD and srGVHD.

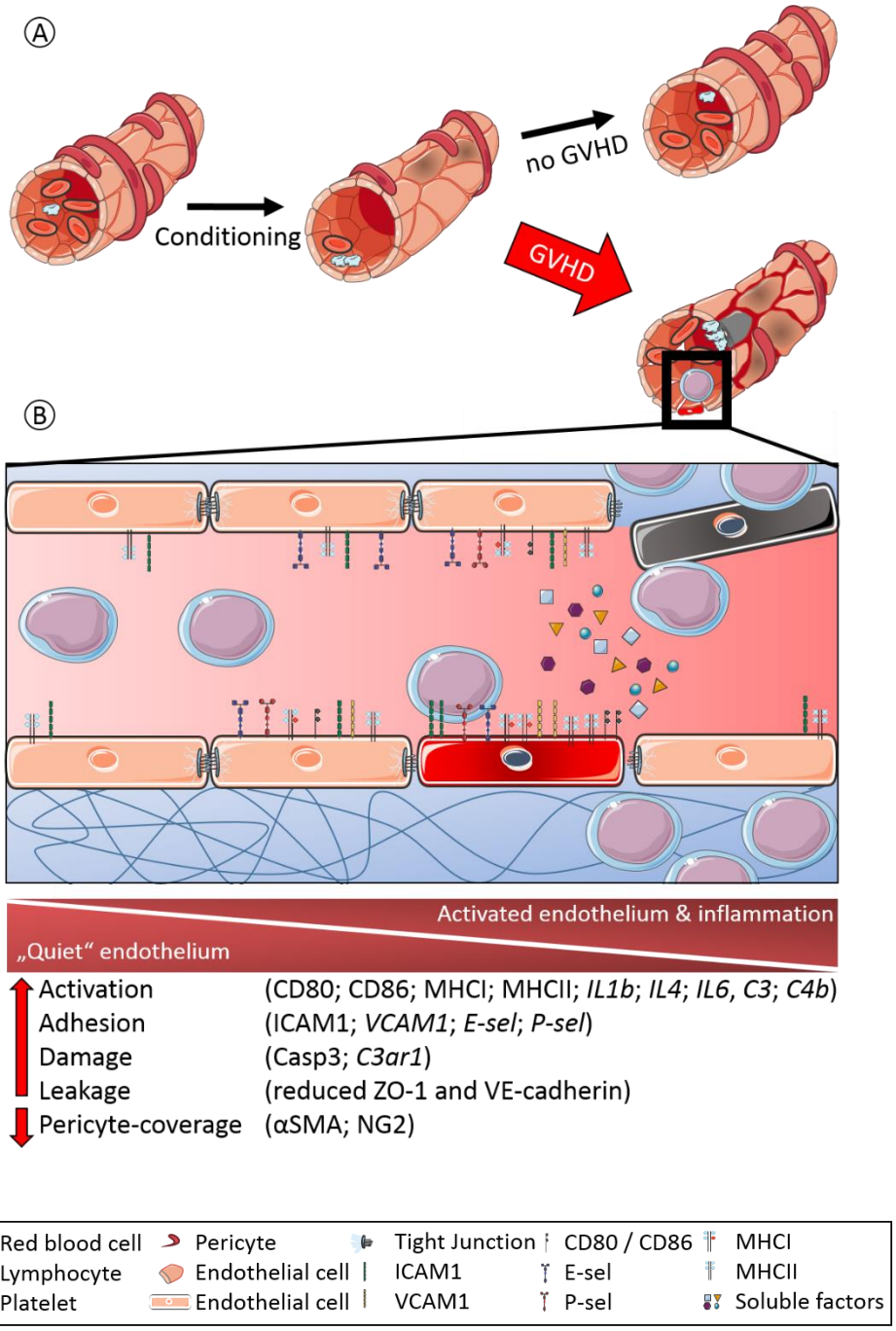

Figure 31| Overview of endothelial involvement in graft-versus-host disease (GVHD). A| During conditioning initial endothelial damage and activation of the endothelium is occurring. Without GVHD, the endothelium recovers. If GVHD reaction is initiated, the endothelium is damaged further and damage is persistent. **B|** Damaged endothelium is shown to be involved in the pathophysiology of GVHD. Different endothelial signs of dysfunction such as activation and increase in adhesion molecule expression are observable. In addition, endothelial pericyte-coverage is reduced during GVHD with the consequence of increased leakage. (ICAM1, intracellular adhesion molecule 1; VCAM1, vascular cell adhesion molecule 1; MHCI, major histocompatibility complex class I; MHCII, major histocompatibility complex class II; IL, interleukin; ZO-1, zonula occludens 1; VE-cadherin, vascular endothelial cadherin; E-sel, E-selectin; P-sel, P-selectin; Casp3, caspase 3; αSMA, alpha smooth muscle actin; NG2, neural/glial antigen 2; C3, complement component 3; C4b complement component 4b; C3ar1, complement C3a receptor 1). I created the illustration with templates from http://smart.servier.com/.

REFERENCES

1. Sureda A, Bader P, Cesaro S, et al. **Indications for allo- and auto-SCT for haematological diseases, solid tumours and immune disorders: current practice in Europe, 2015**. *Bone Marrow Transplantation*. 2015;50(8):1037-1056.
2. Singh AK, McGuirk JP. **Allogeneic Stem Cell Transplantation: A Historical and Scientific Overview**. *Cancer Res*. 2016;76(22):6445-6451.
3. Fowler DH. **Shared biology of GVHD and GVT effects: Potential methods of separation**. *Critical Reviews in Oncology Hematology*. 2006;57(3):225-244.
4. Brunet S, Urbano-Ispizua A, Ojeda E, et al. **Evidence of graft-versus-tumor (GVT) effect in 136 patients with advanced hematologic malignancies receiving unmanipulated peripheral blood stem cell allografts (allo-PSCT): The Spanish experience.** *Blood*. 1999;94(10):165a-165a.
5. Seggewiss R, Einsele H. **Immune reconstitution after allogeneic transplantation and expanding options for immunomodulation: an update**. *Blood*. 2010;115(19):3861-3868.
6. Passweg JR, Baldomero H, Bader P, et al. **Hematopoietic SCT in Europe 2013: recent trends in the use of alternative donors showing more haploidentical donors but fewer cord blood transplants**. *Bone Marrow Transplant*. 2015;50(4):476-482.
7. Gratwohl A, Pasquini MC, Aljurf M, et al. **One million haemopoietic stem-cell transplants: a retrospective observational study**. *Lancet Haematol*. 2015;2(3):e91-100.
8. Farge D, Labopin M, Tyndall A, et al. **Autologous hematopoietic stem cell transplantation for autoimmune diseases: an observational study on 12 years' experience from the European Group for Blood and Marrow Transplantation Working Party on Autoimmune Diseases**. *Haematologica*. 2010;95(2):284-292.
9. Niederwieser D, Baldomero H, Szer J, et al. **Hematopoietic stem cell transplantation activity worldwide in 2012 and a SWOT analysis of the Worldwide Network for Blood and Marrow Transplantation Group including the global survey**. *Bone Marrow Transplant*. 2016;51(6):778-785.
10. D'Souza A ZX. **Current Uses and Outcomes of Hematopoietic Cell Transplantation (HCT): CIBMTR Summary Slides, 2016.** *http://wwwcibmtrorg*. 2016.
11. Passweg JR, Baldomero H, Gratwohl A, et al. **The EBMT activity survey: 1990-2010**. *Bone Marrow Transplant*. 2012;47(7):906-923.
12. Thomas E, Buckner C, Rudolph R, et al. **Allogeneic marrow grafting for hematologic malignancy using HL-A matched donor-recipient sibling pairs**. *Blood*. 1971;38(3):267-287.
13. Hosomichi K, Shiina T, Tajima A, Inoue I. **The impact of next-generation sequencing technologies on HLA research**. *J Hum Genet*. 2015;60(11):665-673.
14. Liu J, Zhong JF, Zhang X, Zhang C. **Allogeneic CD19-CAR-T cell infusion after allogeneic hematopoietic stem cell transplantation in B cell malignancies**. *J Hematol Oncol*. 2017;10(1):35.
15. Boisset JC, Robin C. **On the origin of hematopoietic stem cells: progress and controversy**. *Stem Cell Res*. 2012;8(1):1-13.
16. Passweg JR, Baldomero H, Gratwohl A, et al. **The EBMT activity survey: 1990-2010**. *Bone Marrow Transplantation*. 2012;47(7):906-923.
17. Jacobsohn DA, Vogelsang GB. **Acute graft versus host disease**. *Orphanet J Rare Dis*. 2007;2:35.

18. Passweg JR, Baldomero H, Bader P, et al. **Hematopoietic stem cell transplantation in Europe 2014: more than 40 000 transplants annually**. *Bone Marrow Transplant*. 2016;51(6):786-792.
19. Morecki S, Yacovlev E, Gelfand Y, Vilensky A, Slavin S. **Allogeneic versus syngeneic killer splenocytes as effector cells for the induction of graft-versus-tumor effect**. *Biol Blood Marrow Transplant*. 2004;10(1):40-48.
20. Falkenburg JH, Warren EH. **Graft versus leukemia reactivity after allogeneic stem cell transplantation**. *Biol Blood Marrow Transplant*. 2011;17(1 Suppl):S33-38.
21. Bortin MM, Truitt RL, Rimm AA, Bach FH. **Graft-Versus-Leukemia Reactivity Induced by Alloimmunization without Augmentation of Graft Versus Host Reactivity**. *Nature*. 1979;281(5731):490-491.
22. Truitt RL, Johnson BD. **Principles of graft-vs.-leukemia reactivity**. *Biol Blood Marrow Transplant*. 1995;1(2):61-68.
23. Storb R, Gyurkocza B, Storer BE, et al. **Graft-Versus-Host Disease and Graft-Versus-Tumor Effects After Allogeneic Hematopoietic Cell Transplantation**. *Journal of Clinical Oncology*. 2013;31(12):1530-1538.
24. Guo M, Hu KX, Yu CL, et al. **Infusion of HLA-mismatched peripheral blood stem cells improves the outcome of chemotherapy for acute myeloid leukemia in elderly patients**. *Blood*. 2011;117(3):936-941.
25. Ramirez-Montagut T, Chow A, Kochman AA, et al. **IFN- and Fas Ligand Are Required for Graft-versus-Tumor Activity against Renal Cell Carcinoma in the Absence of Lethal Graft-versus-Host Disease**. *The Journal of Immunology*. 2007;179(3):1669-1680.
26. Tateishi K, Ohta M, Guleng B, et al. **TRAIL-induced cell death cooperates with IFN-gamma activation in the graft-versus-tumor effect against colon tumors**. *Int J Cancer*. 2006;118(9):2237-2246.
27. Areman EM, Mazumder A, Kotula PL, et al. **Hematopoietic potential of IL-2-cultured peripheral blood stem cells from breast cancer patients**. *Bone Marrow Transplant*. 1996;18(3):521-525.
28. Olson JA, Leveson-Gower DB, Gill S, Baker J, Beilhack A, Negrin RS. **NK cells mediate reduction of GVHD by inhibiting activated, alloreactive T cells while retaining GVT effects**. *Blood*. 2010;115(21):4293-4301.
29. Gill S, Olson JA, Negrin RS. **Natural killer cells in allogeneic transplantation: effect on engraftment, graft- versus-tumor, and graft-versus-host responses**. *Biol Blood Marrow Transplant*. 2009;15(7):765-776.
30. Carreras E, Diaz-Ricart M. **The role of the endothelium in the short-term complications of hematopoietic SCT**. *Bone Marrow Transplant*. 2011;46(12):1495-1502.
31. Palomo M, Diaz-Ricart M, Carbo C, et al. **Endothelial dysfunction after hematopoietic stem cell transplantation: role of the conditioning regimen and the type of transplantation**. *Biol Blood Marrow Transplant*. 2010;16(7):985-993.
32. Li HW, Sykes M. **Emerging concepts in haematopoietic cell transplantation**. *Nat Rev Immunol*. 2012;12(6):403-416.
33. Hebart H, Einsele H. **Clinical aspects of CMV infection after stem cell transplantation**. *Hum Immunol*. 2004;65(5):432-436.
34. Rovo A, Meyer-Monard S, Heim D, et al. **No evidence of plasticity in hair follicles of recipients after allogeneic hematopoietic stem cell transplantation**. *Exp Hematol*. 2005;33(8):909-911.
35. Einsele H, Bertz H, Beyer J, et al. **Infectious complications after allogeneic stem cell transplantation: epidemiology and interventional therapy strategies--**

guidelines of the Infectious Diseases Working Party (AGIHO) of the German Society of Hematology and Oncology (DGHO). *Ann Hematol*. 2003;82 Suppl 2:S175-185.
36. Cordonnier C, Mohty M, Faucher C, et al. **Safety of a weekly high dose of liposomal amphotericin B for prophylaxis of invasive fungal infection in immunocompromised patients: PROPHYSOME Study**. *Int J Antimicrob Agents*. 2008;31(2):135-141.
37. Lopes da Silva R, Costa F, Ferreira G, de Sousa AB. **Post-autologous hematopoietic SCT engraftment syndrome: a single center experience**. *Bone Marrow Transplant*. 2012;47(3):456-457.
38. Gorak E, Geller N, Srinivasan R, et al. **Engraftment syndrome after nonmyeloablative allogeneic hematopoietic stem cell transplantation: incidence and effects on survival**. *Biol Blood Marrow Transplant*. 2005;11(7):542-550.
39. Chang L, Frame D, Braun T, et al. **Engraftment syndrome after allogeneic hematopoietic cell transplantation predicts poor outcomes**. *Biol Blood Marrow Transplant*. 2014;20(9):1407-1417.
40. Cornell RF, Hari P, Drobyski WR. **Engraftment Syndrome after Autologous Stem Cell Transplantation: An Update Unifying the Definition and Management Approach**. *Biol Blood Marrow Transplant*. 2015;21(12):2061-2068.
41. Brownback KR, Simpson SQ, McGuirk JP, et al. **Pulmonary manifestations of the pre-engraftment syndrome after umbilical cord blood transplantation**. *Ann Hematol*. 2014;93(5):847-854.
42. Spitzer TR. **Engraftment syndrome: double-edged sword of hematopoietic cell transplants**. *Bone Marrow Transplant*. 2015;50(4):469-475.
43. Kaur P, Asea A. **Radiation-induced effects and the immune system in cancer**. *Front Oncol*. 2012;2:191.
44. Daly AS, Xenocostas A, Lipton JH. **Transplantation-associated thrombotic microangiopathy: twenty-two years later**. *Bone Marrow Transplant*. 2002;30(11):709-715.
45. Martinez MT, Bucher C, Stussi G, et al. **Transplant-associated microangiopathy (TAM) in recipients of allogeneic hematopoietic stem cell transplants**. *Bone Marrow Transplant*. 2005;36(11):993-1000.
46. Laurence J, Mitra D. **Apoptosis of microvascular endothelial cells in the pathophysiology of thrombotic thrombocytopenic purpura/sporadic hemolytic uremic syndrome**. *Semin Hematol*. 1997;34(2):98-105.
47. Zeigler ZR, Rosenfeld CS, Andrews DF, 3rd, et al. **Plasma von Willebrand Factor Antigen (vWF:AG) and thrombomodulin (TM) levels in Adult Thrombotic Thrombocytopenic Purpura/Hemolytic Uremic Syndromes (TTP/HUS) and bone marrow transplant-associated thrombotic microangiopathy (BMT-TM)**. *Am J Hematol*. 1996;53(4):213-220.
48. Jimenez JJ, Jy W, Mauro LM, Horstman LL, Ahn YS. **Elevated endothelial microparticles in thrombotic thrombocytopenic purpura: findings from brain and renal microvascular cell culture and patients with active disease**. *Br J Haematol*. 2001;112(1):81-90.
49. Carreras E, Diaz-Beya M, Rosinol L, Martinez C, Fernandez-Aviles F, Rovira M. **The incidence of veno-occlusive disease following allogeneic hematopoietic stem cell transplantation has diminished and the outcome improved over the last decade**. *Biol Blood Marrow Transplant*. 2011;17(11):1713-1720.

50. Czauderna P, Katski K, Kowalczyk J, et al. **Venoocclusive liver disease (VOD) as a complication of Wilms' tumour management in the series of consecutive 206 patients**. *Eur J Pediatr Surg*. 2000;10(5):300-303.
51. Brice K, Valerie B, Claire G, et al. **Risk-adjusted monitoring of veno-occlusive disease following Bayesian individualization of busulfan dosage for bone marrow transplantation in paediatrics**. *Pharmacoepidemiol Drug Saf*. 2008;17(2):135-143.
52. Mohty M, Malard F, Abecassis M, et al. **Sinusoidal obstruction syndrome/veno-occlusive disease: current situation and perspectives-a position statement from the European Society for Blood and Marrow Transplantation (EBMT)**. *Bone Marrow Transplant*. 2015;50(6):781-789.
53. Fan CQ, Crawford JM. **Sinusoidal obstruction syndrome (hepatic veno-occlusive disease)**. *J Clin Exp Hepatol*. 2014;4(4):332-346.
54. Lucchini G, Willasch AM, Daniel J, et al. **Epidemiology, risk factors, and prognosis of capillary leak syndrome in pediatric recipients of stem cell transplants: a retrospective single-center cohort study**. *Pediatr Transplant*. 2016;20(8):1132-1136.
55. Nurnberger W, Willers R, Burdach S, Gobel U. **Risk factors for capillary leakage syndrome after bone marrow transplantation**. *Ann Hematol*. 1997;74(5):221-224.
56. Funke I, Prummer O, Schrezenmeier H, et al. **Capillary leak syndrome associated with elevated IL-2 serum levels after allogeneic bone marrow transplantation**. *Ann Hematol*. 1994;68(1):49-52.
57. Rechner I, Brito-Babapulle F, Fielden J. **Systemic capillary leak syndrome after granulocyte colony-stimulating factor (G-CSF)**. *Hematol J*. 2003;4(1):54-56.
58. Assaly R, Olson D, Hammersley J, et al. **Initial evidence of endothelial cell apoptosis as a mechanism of systemic capillary leak syndrome**. *Chest*. 2001;120(4):1301-1308.
59. Park MS. **Diffuse alveolar hemorrhage**. *Tuberc Respir Dis (Seoul)*. 2013;74(4):151-162.
60. Ueda N, Chihara D, Kohno A, et al. **Predictive value of circulating angiopoietin-2 for endothelial damage-related complications in allogeneic hematopoietic stem cell transplantation**. *Biol Blood Marrow Transplant*. 2014;20(9):1335-1340.
61. Lara AR, Schwarz MI. **Diffuse alveolar hemorrhage**. *Chest*. 2010;137(5):1164-1171.
62. Flomenberg N, Baxter-Lowe LA, Confer D, et al. **Impact of HLA class I and class II high-resolution matching on outcomes of unrelated donor bone marrow transplantation: HLA-C mismatching is associated with a strong adverse effect on transplantation outcome**. *Blood*. 2004;104(7):1923-1930.
63. Ferrara JL, Levine JE, Reddy P, Holler E. **Graft-versus-host disease**. *Lancet*. 2009;373(9674):1550-1561.
64. Hahn T, McCarthy PL, Jr., Zhang MJ, et al. **Risk factors for acute graft-versus-host disease after human leukocyte antigen-identical sibling transplants for adults with leukemia**. *J Clin Oncol*. 2008;26(35):5728-5734.
65. Schroeder MA, DiPersio JF. **Mouse models of graft-versus-host disease: advances and limitations**. *Dis Model Mech*. 2011;4(3):318-333.
66. Boieri M, Shah P, Dressel R, Inngjerdingen M. **The Role of Animal Models in the Study of Hematopoietic Stem Cell Transplantation and GvHD: A Historical Overview**. *Front Immunol*. 2016;7:333.
67. Snell GD. **The Nobel Lectures in Immunology. Lecture for the Nobel Prize for Physiology or Medicine, 1980: Studies in histocompatibility**. *Scand J Immunol*. 1992;36(4):513-526.

68. Barth R, Counce S, Smith P, Snell GD. **Strong and weak histocompatibility gene differences in mice and their role in the rejection of homografts of tumors and skin**. *Ann Surg*. 1956;144(2):198-204.
69. DeFranco A, Locksley RM, Robertson M. Immunity: The Immune Response in Infectious and Inflammatory Disease: OUP Oxford; 2007.
70. Braud VM, Allan DS, McMichael AJ. **Functions of nonclassical MHC and non-MHC-encoded class I molecules**. *Curr Opin Immunol*. 1999;11(1):100-108.
71. Petersdorf EW, Kollman C, Hurley CK, et al. **Effect of HLA class II gene disparity on clinical outcome in unrelated donor hematopoietic cell transplantation for chronic myeloid leukemia: the US National Marrow Donor Program Experience**. *Blood*. 2001;98(10):2922-2929.
72. Petersdorf EW, Longton GM, Anasetti C, et al. **Association of HLA-C disparity with graft failure after marrow transplantation from unrelated donors**. *Blood*. 1997;89(5):1818-1823.
73. Kobayashi KS, van den Elsen PJ. **NLRC5: a key regulator of MHC class I-dependent immune responses**. *Nat Rev Immunol*. 2012;12(12):813-820.
74. Hewitt EW. **The MHC class I antigen presentation pathway: strategies for viral immune evasion**. *Immunology*. 2003;110(2):163-169.
75. van den Elsen PJ. **Expression regulation of major histocompatibility complex class I and class II encoding genes**. *Front Immunol*. 2011;2:48.
76. Natarajan K, Li H, Mariuzza RA, Margulies DH. **MHC class I molecules, structure and function**. *Rev Immunogenet*. 1999;1(1):32-46.
77. Blum JS, Wearsch PA, Cresswell P. **Pathways of antigen processing**. *Annu Rev Immunol*. 2013;31:443-473.
78. Roche PA, Furuta K. **The ins and outs of MHC class II-mediated antigen processing and presentation**. *Nat Rev Immunol*. 2015;15(4):203-216.
79. Reith W, LeibundGut-Landmann S, Waldburger JM. **Regulation of MHC class II gene expression by the class II transactivator**. *Nat Rev Immunol*. 2005;5(10):793-806.
80. Kambayashi T, Allenspach EJ, Chang JT, et al. **Inducible MHC class II expression by mast cells supports effector and regulatory T cell activation**. *J Immunol*. 2009;182(8):4686-4695.
81. Voskamp AL, Prickett SR, Mackay F, Rolland JM, O'Hehir RE. **MHC class II expression in human basophils: induction and lack of functional significance**. *PLoS One*. 2013;8(12):e81777.
82. Haverson K, Singha S, Stokes CR, Bailey M. **Professional and non-professional antigen-presenting cells in the porcine small intestine**. *Immunology*. 2000;101(4):492-500.
83. Mestas J, Hughes CCW. **Of Mice and Not Men: Differences between Mouse and Human Immunology**. *The Journal of Immunology*. 2004;172(5):2731-2738.
84. Ball LM, Egeler RM, Party EPW. **Acute GvHD: pathogenesis and classification**. *Bone Marrow Transplant*. 2008;41 Suppl 2:S58-64.
85. Cooke KR, Jannin A, Ho V. **The contribution of endothelial activation and injury to end-organ toxicity following allogeneic hematopoietic stem cell transplantation**. *Biol Blood Marrow Transplant*. 2008;14(1 Suppl 1):23-32.
86. Biedermann BC. **Vascular endothelium and graft-versus-host disease**. *Best Pract Res Clin Haematol*. 2008;21(2):129-138.
87. Andrulis M, Dietrich S, Longerich T, et al. **Loss of endothelial thrombomodulin predicts response to steroid therapy and survival in acute intestinal graft-versus-host disease**. *Haematologica*. 2012;97(11):1674-1677.

88. Luft T, Dietrich S, Falk C, et al. **Steroid-refractory GVHD: T-cell attack within a vulnerable endothelial system**. *Blood*. 2011;118(6):1685-1692.
89. Luft T, Benner A, Jodele S, et al. **EASIX in patients with acute graft-versus-host disease: a retrospective cohort analysis**. *Lancet Haematol*. 2017;4(9):e414-e423.
90. Manda K, Glasow A, Paape D, Hildebrandt G. **Effects of ionizing radiation on the immune system with special emphasis on the interaction of dendritic and T cells**. *Front Oncol*. 2012;2:102.
91. Servais S, Beguin Y, Delens L, et al. **Novel approaches for preventing acute graft-versus-host disease after allogeneic hematopoietic stem cell transplantation**. *Expert Opinion on Investigational Drugs*. 2016;25(8):957-972.
92. Zeiser R, Socie G, Blazar BR. **Pathogenesis of acute graft-versus-host disease: from intestinal microbiota alterations to donor T cell activation**. *Br J Haematol*. 2016;175(2):191-207.
93. Blazar BR, Murphy WJ, Abedi M. **Advances in graft-versus-host disease biology and therapy**. *Nat Rev Immunol*. 2012;12(6):443-458.
94. Shlomchik WD, Couzens MS, Tang CB, et al. **Prevention of graft versus host disease by inactivation of host antigen-presenting cells**. *Science*. 1999;285(5426):412-415.
95. Matte CC, Liu J, Cormier J, et al. **Donor APCs are required for maximal GVHD but not for GVL**. *Nat Med*. 2004;10(9):987-992.
96. Teshima T, Ordemann R, Reddy P, et al. **Acute graft-versus-host disease does not require alloantigen expression on host epithelium**. *Nat Med*. 2002;8(6):575-581.
97. Duffner UA, Maeda Y, Cooke KR, et al. **Host dendritic cells alone are sufficient to initiate acute graft-versus-host disease**. *J Immunol*. 2004;172(12):7393-7398.
98. Koyama M, Kuns RD, Olver SD, et al. **Recipient nonhematopoietic antigen-presenting cells are sufficient to induce lethal acute graft-versus-host disease**. *Nat Med*. 2011;18(1):135-142.
99. Tanaka J, Imamura M, Kasai M, et al. **The important balance between cytokines derived from type 1 and type 2 helper T cells in the control of graft-versus-host disease**. *Bone Marrow Transplant*. 1997;19(6):571-576.
100. Krenger W, Snyder KM, Byon JC, Falzarano G, Ferrara JL. **Polarized type 2 alloreactive CD4+ and CD8+ donor T cells fail to induce experimental acute graft-versus-host disease**. *J Immunol*. 1995;155(2):585-593.
101. Yi T, Zhao D, Lin CL, et al. **Absence of donor Th17 leads to augmented Th1 differentiation and exacerbated acute graft-versus-host disease**. *Blood*. 2008;112(5):2101-2110.
102. Kappel LW, Goldberg GL, King CG, et al. **IL-17 contributes to CD4-mediated graft-versus-host disease**. *Blood*. 2009;113(4):945-952.
103. Carlson MJ, West ML, Coghill JM, Panoskaltsis-Mortari A, Blazar BR, Serody JS. **In vitro-differentiated TH17 cells mediate lethal acute graft-versus-host disease with severe cutaneous and pulmonary pathologic manifestations**. *Blood*. 2009;113(6):1365-1374.
104. Yi T, Chen Y, Wang L, et al. **Reciprocal differentiation and tissue-specific pathogenesis of Th1, Th2, and Th17 cells in graft-versus-host disease**. *Blood*. 2009;114(14):3101-3112.
105. Coghill JM, Sarantopoulos S. **Effector CD4(+) T cells, the cytokines they generate, and GVHD: something old and something new**. 2011;117(12):3268-3276.
106. Garnett C, Apperley JF, Pavlů J. **Treatment and management of graft-versus-host disease: improving response and survival**. *Ther Adv Hematol*. 2013;4(6):366-378.

107. Eckstein LA, Van Quill KR, Bui SK, Uusitalo MS, O'Brien JM. **Cyclosporin a inhibits calcineurin/nuclear factor of activated T-cells signaling and induces apoptosis in retinoblastoma cells**. *Invest Ophthalmol Vis Sci*. 2005;46(3):782-790.
108. Schweitzer BI, Dicker AP, Bertino JR. **Dihydrofolate reductase as a therapeutic target**. *Faseb j*. 1990;4(8):2441-2452.
109. Levine JE, Paczesny S, Mineishi S, et al. **Etanercept plus methylprednisolone as initial therapy for acute graft-versus-host disease**. *Blood*. 2008;111(4):2470-2475.
110. Coutinho AE, Chapman KE. **The anti-inflammatory and immunosuppressive effects of glucocorticoids, recent developments and mechanistic insights**. *Mol Cell Endocrinol*. 2011;335(1):2-13.
111. Van Laethem F, Baus E, Smyth LA, et al. **Glucocorticoids Attenuate T Cell Receptor Signaling**. *J Exp Med*. 2001;193(7):803-814.
112. Cain DW, Cidlowski JA. **Immune regulation by glucocorticoids**. *Nat Rev Immunol*. 2017;17(4):233-247.
113. Matsumura-Kimoto Y, Inamoto Y, Tajima K, et al. **Association of Cumulative Steroid Dose with Risk of Infection after Treatment for Severe Acute Graft-versus-Host Disease**. *Biol Blood Marrow Transplant*. 2016;22(6):1102-1107.
114. Bouchlaka MN, Redelman D, Murphy WJ. **Immunotherapy following hematopoietic stem cell transplantation: potential for synergistic effects**. *Immunotherapy*. 2010;2(3):399-418.
115. Deeg HJ. **How I treat refractory acute GVHD**. *Blood*. 2007;109(10):4119-4126.
116. Furlong T, Martin P, Flowers MED, et al. **Therapy with mycophenolate mofetil for refractory acute and chronic graft-versus-host disease**. *Bone Marrow Transplant*. 2009;44(11):739-748.
117. Carpenter PA, Lowder J, Johnston L, et al. **A phase II multicenter study of visilizumab, humanized anti-CD3 antibody, to treat steroid-refractory acute graft-versus-host disease**. *Biol Blood Marrow Transplant*. 2005;11(6):465-471.
118. Gomez-Almaguer D, Ruiz-Arguelles GJ, del Carmen Tarin-Arzaga L, et al. **Alemtuzumab for the treatment of steroid-refractory acute graft-versus-host disease**. *Biol Blood Marrow Transplant*. 2008;14(1):10-15.
119. Jacobsohn DA, Hallick J, Anders V, McMillan S, Morris L, Vogelsang GB. **Infliximab for steroid-refractory acute GVHD: a case series**. *Am J Hematol*. 2003;74(2):119-124.
120. Rager A, Frey N, Goldstein SC, et al. **Inflammatory cytokine inhibition with combination daclizumab and infliximab for steroid-refractory acute GVHD**. *Bone Marrow Transplant*. 2011;46(3):430-435.
121. Drobyski WR, Pasquini M, Kovatovic K, et al. **Tocilizumab for the Treatment of Steroid Refractory Graft-versus-Host Disease**. *Biol Blood Marrow Transplant*. 2011;17(12):1862-1868.
122. Roddy JV, Haverkos BM, McBride A, et al. **Tocilizumab for steroid refractory acute graft-versus-host disease**. *Leuk Lymphoma*. 2016;57(1):81-85.
123. Westin JR, Saliba RM, De Lima M, et al. **Steroid-Refractory Acute GVHD: Predictors and Outcomes**. *Adv Hematol*. 2011;2011:601953.
124. Totoson P, Maguin-Gaté K, Nappey M, Wendling D, Demougeot C. **Endothelial Dysfunction in Rheumatoid Arthritis: Mechanistic Insights and Correlation with Circulating Markers of Systemic Inflammation**. *PLoS One*. 2016;11(1).
125. Piper MK, Raza K, Nuttall SL, et al. **Impaired endothelial function in systemic lupus erythematosus**. *Lupus*. 2007;16(2):84-88.
126. Kocaman O, Sahin T, Aygun C, Senturk O, Hulagu S. **Endothelial dysfunction in patients with ulcerative colitis**. *Inflamm Bowel Dis*. 2006;12(3):166-171.

127. Aird WC. **Phenotypic heterogeneity of the endothelium: I. Structure, function, and mechanisms**. *Circ Res*. 2007;100(2):158-173.
128. Lemichez E, Lecuit M, Nassif X, Bourdoulous S. **Breaking the wall: targeting of the endothelium by pathogenic bacteria**. *Nat Rev Microbiol*. 2010;8(2):93-104.
129. Hoeben A, Landuyt B, Highley MS, Wildiers H, Van Oosterom AT, De Bruijn EA. **Vascular endothelial growth factor and angiogenesis**. *Pharmacol Rev*. 2004;56(4):549-580.
130. Moon JJ, Matsumoto M, Patel S, Lee L, Guan JL, Li S. **Role of cell surface heparan sulfate proteoglycans in endothelial cell migration and mechanotransduction**. *J Cell Physiol*. 2005;203(1):166-176.
131. Ho G, Broze GJ, Jr., Schwartz AL. **Role of heparan sulfate proteoglycans in the uptake and degradation of tissue factor pathway inhibitor-coagulation factor Xa complexes**. *J Biol Chem*. 1997;272(27):16838-16844.
132. Kurihara N, Alfie ME, Sigmon DH, Rhaleb NE, Shesely EG, Carretero OA. **Role of nNOS in blood pressure regulation in eNOS null mutant mice**. *Hypertension*. 1998;32(5):856-861.
133. Tornavaca O, Chia M, Dufton N, et al. **ZO-1 controls endothelial adherens junctions, cell-cell tension, angiogenesis, and barrier formation**. *J Cell Biol*. 2015;208(6):821-838.
134. Garrett JP, Lowery AM, Adam AP, Kowalczyk AP, Vincent PA. **Regulation of endothelial barrier function by p120-catenin·VE-cadherin interaction**. *Mol Biol Cell*. 2017;28(1):85-97.
135. Rao RM, Yang L, Garcia-Cardena G, Luscinskas FW. **Endothelial-dependent mechanisms of leukocyte recruitment to the vascular wall**. *Circ Res*. 2007;101(3):234-247.
136. Pober JS, Sessa WC. **Evolving functions of endothelial cells in inflammation**. *Nat Rev Immunol*. 2007;7(10):803-815.
137. Hadi HAR, Suwaidi JA. **Endothelial dysfunction in diabetes mellitus**. *Vasc Health Risk Manag*. 2007;3(6):853-876.
138. Ley K, Laudanna C, Cybulsky MI, Nourshargh S. **Getting to the site of inflammation: the leukocyte adhesion cascade updated**. *Nat Rev Immunol*. 2007;7(9):678-689.
139. Vestweber D. **How leukocytes cross the vascular endothelium**. *Nat Rev Immunol*. 2015;15(11):692-704.
140. Lozanoska-Ochser B, Peakman M. **Level of major histocompatibility complex class I expression on endothelium in non-obese diabetic mice influences CD8 T cell adhesion and migration**. *Clin Exp Immunol*. 2009;157(1):119-127.
141. Turesson C. **Endothelial expression of MHC class II molecules in autoimmune disease**. *Curr Pharm Des*. 2004;10(2):129-143.
142. Omari KM, Dorovini-Zis K. **CD40 expressed by human brain endothelial cells regulates CD4+ T cell adhesion to endothelium**. *J Neuroimmunol*. 2003;134(1-2):166-178.
143. Mestas J, Crampton SP, Hori T, Hughes CC. **Endothelial cell co-stimulation through OX40 augments and prolongs T cell cytokine synthesis by stabilization of cytokine mRNA**. *Int Immunol*. 2005;17(6):737-747.
144. Klingenberg R, Autschbach F, Gleissner C, et al. **Endothelial inducible costimulator ligand expression is increased during human cardiac allograft rejection and regulates endothelial cell-dependent allo-activation of CD8+ T cells in vitro**. *Eur J Immunol*. 2005;35(6):1712-1721.

145. Aird WC. **Endothelial Cell Heterogeneity**. *Cold Spring Harb Perspect Med*. 2012;2(1).
146. Oelkrug C, Ramage JM. **Enhancement of T cell recruitment and infiltration into tumours**. *Clin Exp Immunol*. 2014;178(1):1-8.
147. Burton VJ, Butler LM, McGettrick HM, et al. **Delay of migrating leukocytes by the basement membrane deposited by endothelial cells in long-term culture**. *Exp Cell Res*. 2011;317(3-3):276-292.
148. Carman CV, Martinelli R. **T Lymphocyte-Endothelial Interactions: Emerging Understanding of Trafficking and Antigen-Specific Immunity**. *Front Immunol*. 2015;6:603.
149. Abrahimi P, Qin L, Chang WG, et al. **Blocking MHC class II on human endothelium mitigates acute rejection**. *JCI Insight*. 2016;1(1).
150. Rouhani SJ, Eccles JD, Tewalt EF, Engelhard VH. **Regulation of T-cell Tolerance by Lymphatic Endothelial Cells**. *J Clin Cell Immunol*. 2014;5.
151. Taflin C, Favier B, Baudhuin J, et al. **Human endothelial cells generate Th17 and regulatory T cells under inflammatory conditions**. *Proc Natl Acad Sci U S A*. 2011;108(7):2891-2896.
152. Riesner K, Shi Y, Jacobi A, et al. **Initiation of acute graft-versus-host disease by angiogenesis**. *Blood*. 2017;129(14):2021-2032.
153. Pezzella F, Pastorino U, Tagliabue E, et al. **Non-small-cell lung carcinoma tumor growth without morphological evidence of neo-angiogenesis**. *Am J Pathol*. 1997;151(5):1417-1423.
154. Paleolog EM. **Angiogenesis in rheumatoid arthritis**. *Arthritis Res*. 2002;4 Suppl 3:S81-90.
155. Alkim C, Alkim H, Koksal AR, Boga S, Sen I. **Angiogenesis in Inflammatory Bowel Disease**. *Int J Inflam*. 2015;2015.
156. Usui Y, Westenskow PD, Murinello S, et al. **Angiogenesis and Eye Disease**. *Annu Rev Vis Sci*. 2015;1:155-184.
157. Tas SW, Maracle CX, Balogh E, Szekanecz Z. **Targeting of proangiogenic signalling pathways in chronic inflammation**. *Nat Rev Rheumatol*. 2016;12(2):111-122.
158. Szade A, Grochot-Przeczek A, Florczyk U, Jozkowicz A, Dulak J. **Cellular and molecular mechanisms of inflammation-induced angiogenesis**. *IUBMB Life*. 2015;67(3):145-159.
159. Welti J, Loges S, Dimmeler S, Carmeliet P. **Recent molecular discoveries in angiogenesis and antiangiogenic therapies in cancer**. *J Clin Invest*. 2013;123(8):3190-3200.
160. Sidky YA, Auerbach R. **Lymphocyte-induced angiogenesis: a quantitative and sensitive assay of the graft-vs.-host reaction**. *J Exp Med*. 1975;141(5):1084-1100.
161. Penack O, Henke E, Suh D, et al. **Inhibition of neovascularization to simultaneously ameliorate graft-vs-host disease and decrease tumor growth**. *J Natl Cancer Inst*. 2010;102(12):894-908.
162. Leonhardt F, Grundmann S, Behe M, et al. **Inflammatory neovascularization during graft-versus-host disease is regulated by alphav integrin and miR-100**. *Blood*. 2013;121(17):3307-3318.
163. Penack O, Socie G, van den Brink MR. **The importance of neovascularization and its inhibition for allogeneic hematopoietic stem cell transplantation**. *Blood*. 2011;117(16):4181-4189.

164. Medinger M, Tichelli A, Bucher C, et al. **GVHD after allogeneic haematopoietic SCT for AML: angiogenesis, vascular endothelial growth factor and VEGF receptor expression in the BM**. *Bone Marrow Transplant*. 2013;48(5):715-721.
165. Tolstanova G, Deng X, French SW, et al. **Early endothelial damage and increased colonic vascular permeability in the development of experimental ulcerative colitis in rats and mice**. *Lab Invest*. 2012;92(1):9-21.
166. Alexander JS, Zivadinov R, Maghzi AH, Ganta VC, Harris MK, Minagar A. **Multiple sclerosis and cerebral endothelial dysfunction: Mechanisms**. *Pathophysiology*. 2011;18(1):3-12.
167. Thomas M, Felcht M, Kruse K, et al. **Angiopoietin-2 stimulation of endothelial cells induces alphavbeta3 integrin internalization and degradation**. *J Biol Chem*. 2010;285(31):23842-23849.
168. Rabelink TJ, de Boer HC, van Zonneveld AJ. **Endothelial activation and circulating markers of endothelial activation in kidney disease**. *Nat Rev Nephrol*. 2010;6(7):404-414.
169. Chintalgattu V, Rees ML, Culver JC, et al. **Coronary microvascular pericytes are the cellular target of sunitinib malate induced cardiotoxicity**. *Sci Transl Med*. 2013;5(187).
170. Tichelli A, Passweg J, Wojcik D, et al. **Late cardiovascular events after allogeneic hematopoietic stem cell transplantation: a retrospective multicenter study of the Late Effects Working Party of the European Group for Blood and Marrow Transplantation**. *Haematologica*. 2008;93(8):1203-1210.
171. Sviland L, Sale GE, Myerson D. **Endothelial changes in cutaneous graft-versus-host disease: a comparison between HLA matched and mismatched recipients of bone marrow transplantation**. *Bone Marrow Transplant*. 1991;7(1):35-38.
172. Dumler JS, Beschorner WE, Farmer ER, Di Gennaro KA, Saral R, Santos GW. **Endothelial-cell injury in cutaneous acute graft-versus-host disease**. *Am J Pathol*. 1989;135(6):1097-1103.
173. Matsuda Y, Hara J, Osugi Y, et al. **Serum levels of soluble adhesion molecules in stem cell transplantation-related complications**. *Bone Marrow Transplant*. 2001;27(9):977-982.
174. Rachakonda SP, Penack O, Dietrich S, et al. **Single-Nucleotide Polymorphisms Within the Thrombomodulin Gene (THBD) Predict Mortality in Patients With Graft-Versus-Host Disease**. *J Clin Oncol*. 2014;32(30):3421-3427.
175. Dietrich S, Falk CS, Benner A, et al. **Endothelial vulnerability and endothelial damage are associated with risk of graft-versus-host disease and response to steroid treatment**. *Biol Blood Marrow Transplant*. 2013;19(1):22-27.
176. Pihusch V, Rank A, Steber R, et al. **Endothelial cell-derived microparticles in allogeneic hematopoietic stem cell recipients**. *Transplantation*. 2006;81(10):1405-1409.
177. Marmont AM, Horowitz MM, Gale RP, et al. **T-cell depletion of HLA-identical transplants in leukemia**. *Blood*. 1991;78(8):2120-2130.
178. Miller HK, Braun TM, Stillwell T, et al. **Infectious Risk after Allogeneic Hematopoietic Cell Transplantation Complicated by Acute Graft-versus-Host Disease**. *Biology of Blood and Marrow Transplantation*;23(3):522-528.
179. Riesner K, Kalupa M, Shi Y, Elezkurtaj S, Penack O. **A preclinical acute GVHD mouse model based on chemotherapy conditioning and MHC-matched transplantation**. *Bone Marrow Transplant*. 2016;51(3):410-417.
180. Radu M, Chernoff J. **An in vivo assay to test blood vessel permeability**. *J Vis Exp*. 2013(73):e50062.

181. Brede C, Friedrich M, Jordan-Garrote AL, et al. **Mapping immune processes in intact tissues at cellular resolution**. *J Clin Invest*. 2012;122(12):4439-4446.
182. Bridges LE, Williams CL, Pointer MA, Awumey EM. **Mesenteric Artery Contraction and Relaxation Studies Using Automated Wire Myography**. *J Vis Exp*. 2011(55).
183. Dietrich A, Mederos YSM, Gollasch M, et al. **Increased vascular smooth muscle contractility in TRPC6-/- mice**. *Mol Cell Biol*. 2005;25(16):6980-6989.
184. Morabito F, Gentile M, Gay F, et al. **Insights into defibrotide: an updated review**. *Expert Opin Biol Ther*. 2009;9(6):763-772.
185. Kagan HM, Trackman PC. **Properties and function of lysyl oxidase**. *Am J Respir Cell Mol Biol*. 1991;5(3):206-210.
186. Kalatskaya I, Berchiche YA, Gravel S, Limberg BJ, Rosenbaum JS, Heveker N. **AMD3100 is a CXCR7 ligand with allosteric agonist properties**. *Mol Pharmacol*. 2009;75(5):1240-1247.
187. Dietrich S, Okun JG, Schmidt K, et al. **High pre-transplant serum nitrate levels predict risk of acute steroid-refractory graft-versus-host disease in the absence of statin therapy**. *Haematologica*. 2014;99(3):541-547.
188. Vander Lugt MT, Braun TM, Hanash S, et al. **ST2 as a marker for risk of therapy-resistant graft-versus-host disease and death**. *N Engl J Med*. 2013;369(6):529-539.
189. Rodriguez-Carrio J, Prado C, de Paz B, et al. **Circulating endothelial cells and their progenitors in systemic lupus erythematosus and early rheumatoid arthritis patients**. *Rheumatology (Oxford)*. 2012;51(10):1775-1784.
190. Foster W, Lip GY, Raza K, Carruthers D, Blann AD. **An observational study of endothelial function in early arthritis**. *Eur J Clin Invest*. 2012;42(5):510-516.
191. Almici C, Skert C, Bruno B, et al. **Circulating endothelial cell count: a reliable marker of endothelial damage in patients undergoing hematopoietic stem cell transplantation**. *Bone Marrow Transplant*. 2017.
192. Woywodt A, Scheer J, Hambach L, et al. **Circulating endothelial cells as a marker of endothelial damage in allogeneic hematopoietic stem cell transplantation**. *Blood*. 2004;103(9):3603-3605.
193. Medinger M, Heim D, Gerull S, et al. **Increase of endothelial progenitor cells in acute graft-versus-host disease after allogeneic haematopoietic stem cell transplantation for acute myeloid leukaemia**. *Leuk Res*. 2016;47:22-25.
194. Yan Z, Zeng L, Jia L, Xu S, Ding S. **Increased numbers of circulating ECs are associated with systemic GVHD**. *Int J Lab Hematol*. 2011;33(5):507-515.
195. Ertault-Daneshpouy M, Leboeuf C, Lemann M, et al. **Pericapillary hemorrhage as criterion of severe human digestive graft-versus-host disease**. *Blood*. 2004;103(12):4681-4684.
196. Tatekawa S, Kohno A, Ozeki K, et al. **A Novel Diagnostic and Prognostic Biomarker Panel for Endothelial Cell Damage-Related Complications in Allogeneic Transplantation**. *Biol Blood Marrow Transplant*. 2016;22(9):1573-1581.
197. Lindas R, Tvedt TH, Hatfield KJ, Reikvam H, Bruserud O. **Preconditioning serum levels of endothelial cell-derived molecules and the risk of posttransplant complications in patients treated with allogeneic stem cell transplantation**. *J Transplant*. 2014;2014:404096.
198. Biedermann BC, Tsakiris DA, Gregor M, Pober JS, Gratwohl A. **Combining altered levels of effector transcripts in circulating T cells with a marker of endothelial injury is specific for active graft-versus-host disease**. *Bone Marrow Transplant*. 2003;32(11):1077-1084.

199. Paczesny S, Krijanovski OI, Braun TM, et al. **A biomarker panel for acute graft-versus-host disease**. *Blood*. 2009;113(2):273-278.
200. Ferra C, de Sanjose S, Gallardo D, et al. **IL-6 and IL-8 levels in plasma during hematopoietic progenitor transplantation**. *Haematologica*. 1998;83(12):1082-1087.
201. Wassmann S, Stumpf M, Strehlow K, et al. **Interleukin-6 induces oxidative stress and endothelial dysfunction by overexpression of the angiotensin II type 1 receptor**. *Circ Res*. 2004;94(4):534-541.
202. Miyoshi T, Yamashita K, Arai T, Yamamoto K, Mizugishi K, Uchiyama T. **The role of endothelial interleukin-8/NADPH oxidase 1 axis in sepsis**. *Immunology*. 2010;131(3):331-339.
203. Kim DH, Lee NY, Lee MH, Sohn SK. **Vascular endothelial growth factor gene polymorphisms may predict the risk of acute graft-versus-host disease following allogeneic transplantation: preventive effect of vascular endothelial growth factor gene on acute graft-versus-host disease**. *Biol Blood Marrow Transplant*. 2008;14(12):1408-1416.
204. Zeng L, Yan Z, Ding S, Xu K, Wang L. **Endothelial injury, an intriguing effect of methotrexate and cyclophosphamide during hematopoietic stem cell transplantation in mice**. *Transplant Proc*. 2008;40(8):2670-2673.
205. Zeng L, Jia L, Xu S, Yan Z, Ding S, Xu K. **Vascular endothelium changes after conditioning in hematopoietic stem cell transplantation: role of cyclophosphamide and busulfan**. *Transplant Proc*. 2010;42(7):2720-2724.
206. Paris F, Fuks Z, Kang A, et al. **Endothelial apoptosis as the primary lesion initiating intestinal radiation damage in mice**. *Science*. 2001;293(5528):293-297.
207. Fuxe J, Tabruyn S, Colton K, et al. **Pericyte requirement for anti-leak action of angiopoietin-1 and vascular remodeling in sustained inflammation**. *Am J Pathol*. 2011;178(6):2897-2909.
208. Castellano G, Stasi A, Intini A, et al. **Endothelial dysfunction and renal fibrosis in endotoxemia-induced oliguric kidney injury: possible role of LPS-binding protein**. *Crit Care*. 2014;18(5):520.
209. Zhu X, Cao Y, Wei L, et al. **von Willebrand factor contributes to poor outcome in a mouse model of intracerebral haemorrhage**. *Sci Rep*. 2016;6:35901.
210. Simonavicius N, Ashenden M, van Weverwijk A, et al. **Pericytes promote selective vessel regression to regulate vascular patterning**. *Blood*. 2012;120(7):1516-1527.
211. Benjamin LE, Hemo I, Keshet E. **A plasticity window for blood vessel remodelling is defined by pericyte coverage of the preformed endothelial network and is regulated by PDGF-B and VEGF**. *Development*. 1998;125(9):1591-1598.
212. Janin A, Deschaumes C, Daneshpouy M, et al. **CD95 engagement induces disseminated endothelial cell apoptosis in vivo: immunopathologic implications**. *Blood*. 2002;99(8):2940-2947.
213. Deschaumes C, Verneuil L, Ertault-Daneshpouy M, et al. **CD95 ligand-dependant endothelial cell death initiates oral mucosa damage in a murine model of acute graft versus host disease**. *Lab Invest*. 2007;87(5):417-429.
214. Qiao J, Fu J, Fang T, et al. **Evaluation of the effects of preconditioning regimens on hepatic veno-occlusive disease in mice after hematopoietic stem cell transplantation**. *Exp Mol Pathol*. 2015;98(1):73-78.
215. Nie DM, Wu QL, Zheng P, et al. **Endothelial microparticles carrying hedgehog-interacting protein induce continuous endothelial damage in the pathogenesis of acute graft-versus-host disease**. *Am J Physiol Cell Physiol*. 2016;310(10):C821-835.

216. Zhang R, Wang X, Hong M, et al. **Endothelial microparticles delivering microRNA-155 into T lymphocytes are involved in the initiation of acute graft-versus-host disease following allogeneic hematopoietic stem cell transplantation**. *Oncotarget*. 2017;8(14):23360-23375.
217. Carretero R, Sektioglu IM, Garbi N, Salgado OC, Beckhove P, Hammerling GJ. **Eosinophils orchestrate cancer rejection by normalizing tumor vessels and enhancing infiltration of CD8(+) T cells**. *Nat Immunol*. 2015;16(6):609-617.
218. Wertheimer TV, E; Xiao, S ; Palikuqi, B ; Ottmuller, K ; Beilhack, A ; Butler, J ; Manley, N ; Rafii, S ; van den Brink, M ; Dudakov, J **Production of BMP4 by endothelial cells is crucial for endogenous thymic regeneration**. *EUROPEAN JOURNAL OF IMMUNOLOGY*. 2016;46:311-311.
219. Trowell OA. **The sensitivity of lymphocytes to ionising radiation**. *The Journal of Pathology and Bacteriology*. 1952;64(4):687-704.
220. Poritz LS, Garver KI, Green C, Fitzpatrick L, Ruggiero F, Koltun WA. **Loss of the tight junction protein ZO-1 in dextran sulfate sodium induced colitis**. *J Surg Res*. 2007;140(1):12-19.
221. Fanning AS, Little BP, Rahner C, Utepbergenov D, Walther Z, Anderson JM. **The unique-5 and -6 motifs of ZO-1 regulate tight junction strand localization and scaffolding properties**. *Mol Biol Cell*. 2007;18(3):721-731.
222. Umeda K, Ikenouchi J, Katahira-Tayama S, et al. **ZO-1 and ZO-2 independently determine where claudins are polymerized in tight-junction strand formation**. *Cell*. 2006;126(4):741-754.
223. Reyat JS, Chimen M, Noy PJ, Szyroka J, Rainger GE, Tomlinson MG. **ADAM10-Interacting Tetraspanins Tspan5 and Tspan17 Regulate VE-Cadherin Expression and Promote T Lymphocyte Transmigration**. *J Immunol*. 2017;199(2):666-676.
224. Vockel M, Vestweber D. **How T cells trigger the dissociation of the endothelial receptor phosphatase VE-PTP from VE-cadherin**. *Blood*. 2013;122(14):2512-2522.
225. Zhao Y, Ting KK, Li J, et al. **Targeting Vascular Endothelial-Cadherin in Tumor-Associated Blood Vessels Promotes T-cell-Mediated Immunotherapy**. *Cancer Res*. 2017;77(16):4434-4447.
226. Mikula M, Fuchs E, Huber H, Beug H, Schulte-Hermann R, Mikulits W. **Immortalized p19ARF null hepatocytes restore liver injury and generate hepatic progenitors after transplantation**. *Hepatology*. 2004;39(3):628-634.
227. Koudelkova P, Weber G, Mikulits W. **Liver Sinusoidal Endothelial Cells Escape Senescence by Loss of p19ARF**. *PLoS One*. 2015;10(11):e0142134.
228. Schor AM, Schor SL, Allen TD. **Effects of culture conditions on the proliferation, morphology and migration of bovine aortic endothelial cells**. *J Cell Sci*. 1983;62:267-285.
229. Leonetti D, Reimund JM, Tesse A, et al. **Circulating microparticles from Crohn's disease patients cause endothelial and vascular dysfunctions**. *PLoS One*. 2013;8(9):e73088.
230. Schleifenbaum J, Kassmann M, Szijarto IA, et al. **Stretch-activation of angiotensin II type 1a receptors contributes to the myogenic response of mouse mesenteric and renal arteries**. *Circ Res*. 2014;115(2):263-272.
231. Schmid PM, Bouazzaoui A, Doser K, et al. **Endothelial dysfunction and altered mechanical and structural properties of resistance arteries in a murine model of graft-versus-host disease**. *Biol Blood Marrow Transplant*. 2014;20(10):1493-1500.
232. Schmid PM, Bouazzaoui A, Schmid K, et al. **Vascular Alterations in a Murine Model of Acute Graft-Versus-Host Disease Are Associated With Decreased Serum**

Levels of Adiponectin and an Increased Activity and Vascular Expression of Indoleamine 2,3-Dioxygenase. *Cell Transplant*. 2016;25(11):2051-2062.
233. Sato A, Suzuki H, Nakazato Y, Shibata H, Inagami T, Saruta T. **Increased expression of vascular angiotensin II type 1A receptor gene in glucocorticoid-induced hypertension**. *J Hypertens*. 1994;12(5):511-516.
234. Hoorn EJ, Walsh SB, McCormick JA, et al. **The calcineurin inhibitor tacrolimus activates the renal sodium chloride cotransporter to cause hypertension**. *Nat Med*. 2011;17(10):1304-1309.
235. Jones SC, Banks RE, Haidar A, et al. **Adhesion molecules in inflammatory bowel disease**. *Gut*. 1995;36(5):724-730.
236. Navarro-Hernandez RE, Oregon-Romero E, Vazquez-Del Mercado M, Rangel-Villalobos H, Palafox-Sanchez CA, Munoz-Valle JF. **Expression of ICAM1 and VCAM1 serum levels in rheumatoid arthritis clinical activity. Association with genetic polymorphisms**. *Dis Markers*. 2009;26(3):119-126.
237. Goke M, Hoffmann JC, Evers J, Kruger H, Manns MP. **Elevated serum concentrations of soluble selectin and immunoglobulin type adhesion molecules in patients with inflammatory bowel disease**. *J Gastroenterol*. 1997;32(4):480-486.
238. Kuuliala A, Eberhardt K, Takala A, Kautiainen H, Repo H, Leirisalo-Repo M. **Circulating soluble E-selectin in early rheumatoid arthritis: a prospective five year study**. *Ann Rheum Dis*. 2002;61(3):242-246.
239. Bhatti M, Chapman P, Peters M, Haskard D, Hodgson H. **Visualising E-selectin in the detection and evaluation of**. *Gut*. 1998;43(1):40-47.
240. Matsumoto T, Kitano A, Nakamura S, et al. **Possible role of vascular endothelial cells in immune responses in colonic mucosa examined immunocytochemically in subjects with and without ulcerative colitis**. *Clin Exp Immunol*. 1989;78(3):424-430.
241. Isobe M, Yagita H, Okumura K, Ihara A. **Specific acceptance of cardiac allograft after treatment with antibodies to ICAM-1 and LFA-1**. *Science*. 1992;255(5048):1125-1127.
242. Lu SX, Kappel LW, Charbonneau-Allard AM, et al. **Ceacam1 separates graft-versus-host-disease from graft-versus-tumor activity after experimental allogeneic bone marrow transplantation**. *PLoS One*. 2011;6(7):e21611.
243. Lu SX, Holland AM, Na IK, et al. **Absence of P-selectin in recipients of allogeneic bone marrow transplantation ameliorates experimental graft-versus-host disease**. *J Immunol*. 2010;185(3):1912-1919.
244. Mir E, Palomo M, Rovira M, et al. **Endothelial damage is aggravated in acute GvHD and could predict its development**. *Bone Marrow Transplant*. 2017;52(9):1317-1325.
245. Skaria T, Burgener J, Bachli E, Schoedon G. **IL-4 Causes Hyperpermeability of Vascular Endothelial Cells through Wnt5A Signaling**. *PLoS One*. 2016;11(5):e0156002.
246. Park HS, Jung HY, Park EY, Kim J, Lee WJ, Bae YS. **Cutting edge: direct interaction of TLR4 with NAD(P)H oxidase 4 isozyme is essential for lipopolysaccharide-induced production of reactive oxygen species and activation of NF-kappa B**. *J Immunol*. 2004;173(6):3589-3593.
247. Lu Z, Li Y, Jin J, Zhang X, Lopes-Virella MF, Huang Y. **Toll-like receptor 4 activation in microvascular endothelial cells triggers a robust inflammatory response and cross talk with mononuclear cells via interleukin-6**. *Arterioscler Thromb Vasc Biol*. 2012;32(7):1696-1706.

248. Wilhelmsen K, Mesa KR, Prakash A, Xu F, Hellman J. **Activation of endothelial TLR2 by bacterial lipoprotein upregulates proteins specific for the neutrophil response**. *Innate Immun*. 2012;18(4):602-616.
249. Huang W, Liu Y, Li L, et al. **HMGB1 increases permeability of the endothelial cell monolayer via RAGE and Src family tyrosine kinase pathways**. *Inflammation*. 2012;35(1):350-362.
250. Mandalari G, Bisignano C, Genovese T, et al. **Natural almond skin reduced oxidative stress and inflammation in an experimental model of inflammatory bowel disease**. *Int Immunopharmacol*. 2011;11(8):915-924.
251. Friedrich M, Bock D, Philipp S, et al. **Pan-selectin antagonism improves psoriasis manifestation in mice and man**. *Arch Dermatol Res*. 2006;297(8):345-351.
252. Sehnert B, Burkhardt H, Wessels JT, et al. **NF-kappaB inhibitor targeted to activated endothelium demonstrates a critical role of endothelial NF-kappaB in immune-mediated diseases**. *Proc Natl Acad Sci U S A*. 2013;110(41):16556-16561.
253. Palomo M, Diaz-Ricart M, Rovira M, Escolar G, Carreras E. **Defibrotide prevents the activation of macrovascular and microvascular endothelia caused by soluble factors released to blood by autologous hematopoietic stem cell transplantation**. *Biol Blood Marrow Transplant*. 2011;17(4):497-506.
254. Koehl GE, Geissler EK, Iacobelli M, et al. **Defibrotide: an endothelium protecting and stabilizing drug, has an anti-angiogenic potential in vitro and in vivo**. *Cancer Biol Ther*. 2007;6(5):686-690.
255. Eissner G. **Fludarabine induces apoptosis, activation, and allogenicity in human endothelial and epithelial cells: protective effect of defibrotide**. *Blood*. 2002;100(1):334-340.
256. Kim D, Mecham RP, Trackman PC, Roy S. **Downregulation of Lysyl Oxidase Protects Retinal Endothelial Cells From High Glucose-Induced Apoptosis**. *Invest Ophthalmol Vis Sci*. 2017;58(5):2725-2731.
257. Trackman PC, Graham RJ, Bittner HK, Carnes DL, Gilles JA, Graves DT. **Inflammation-associated lysyl oxidase protein expression in vivo, and modulation by FGF-2 plus IGF-1**. *Histochem Cell Biol*. 1998;110(1):9-14.
258. Ribeiro AL, Kaid C, Silva PBG, Cortez BA, Okamoto OK. **Inhibition of Lysyl Oxidases Impairs Migration and Angiogenic Properties of Tumor-Associated Pericytes**. *Stem Cells Int*. 2017;2017:4972078.
259. Osawa T, Ohga N, Akiyama K, et al. **Lysyl oxidase secreted by tumour endothelial cells promotes angiogenesis and metastasis**. *Br J Cancer*. 2013;109(8):2237-2247.
260. Eberson LS, Sanchez PA, Majeed BA, Tawinwung S, Secomb TW, Larson DF. **Effect of lysyl oxidase inhibition on angiotensin II-induced arterial hypertension, remodeling, and stiffness**. *PLoS One*. 2015;10(4):e0124013.
261. Shi PA, Miller LK, Isola LM. **Prospective study of mobilization kinetics up to 18 hours after late-afternoon dosing of plerixafor**. *Transfusion*. 2014;54(5):1263-1268.
262. Nishimura Y, Ii M, Qin G, et al. **CXCR4 antagonist AMD3100 accelerates impaired wound healing in diabetic mice**. *J Invest Dermatol*. 2012;132(3 Pt 1):711-720.
263. Pitchford SC, Furze RC, Jones CP, Wengner AM, Rankin SM. **Differential mobilization of subsets of progenitor cells from the bone marrow**. *Cell Stem Cell*. 2009;4(1):62-72.
264. Li Z, Zhao R, Fang X, et al. **AMD3100 accelerates reendothelialization of neointima in rabbit saccular aneurysm after flow diverter treatment**. *World Neurosurg*. 2017.

265. Umemura K, Iwaki T, Kimura T, et al. **Pharmacokinetics and Safety of Defibrotide in Healthy Japanese Subjects**. *Clin Pharmacol Drug Dev*. 2016;5(6):548-551.
266. Fulgenzi A, Ferrero ME. **Defibrotide in the treatment of hepatic veno-occlusive disease**. *Hepat Med*. 2016;8:105-113.
267. Sevil MB, Anadon-Baselga MJ, Frejo MT, Llama E, Capo MA. **Pharmacokinetic analysis of beta-aminopropionitrile in rabbits**. *Vet Res*. 1996;27(2):117-123.
268. Noels H, Zhou B, Tilstam PV, et al. **Deficiency of endothelial CXCR4 reduces reendothelialization and enhances neointimal hyperplasia after vascular injury in atherosclerosis-prone mice**. *Arterioscler Thromb Vasc Biol*. 2014;34(6):1209-1220.
269. Yin Y, Huang L, Zhao X, et al. **AMD3100 mobilizes endothelial progenitor cells in mice, but inhibits its biological functions by blocking an autocrine/paracrine regulatory loop of stromal cell derived factor-1 in vitro**. *J Cardiovasc Pharmacol*. 2007;50(1):61-67.
270. Zeiser R, Youssef S, Baker J, Kambham N, Steinman L, Negrin RS. **Preemptive HMG-CoA reductase inhibition provides graft-versus-host disease protection by Th-2 polarization while sparing graft-versus-leukemia activity**. *Blood*. 2007;110(13):4588-4598.
271. Zheng P, Wu QL, Li BB, et al. **Simvastatin ameliorates graft-vs-host disease by regulating angiopoietin-1 and angiopoietin-2 in a murine model**. *Leuk Res*. 2017;55:49-54.
272. Ikezoe T, Yang J, Nishioka C, Yokoyama A. **Thrombomodulin alleviates murine GVHD in association with an increase in the proportion of regulatory T cells in the spleen**. *Bone Marrow Transplant*. 2015;50(1):113-120.
273. Edelberg JM, Tang L, Hattori K, Lyden D, Rafii S. **Young adult bone marrow-derived endothelial precursor cells restore aging-impaired cardiac angiogenic function**. *Circ Res*. 2002;90(10):E89-93.
274. Ding BS, Nolan DJ, Butler JM, et al. **Inductive angiocrine signals from sinusoidal endothelium are required for liver regeneration**. *Nature*. 2010;468(7321):310-315.
275. Griese DP, Ehsan A, Melo LG, et al. **Isolation and transplantation of autologous circulating endothelial cells into denuded vessels and prosthetic grafts: implications for cell-based vascular therapy**. *Circulation*. 2003;108(21):2710-2715.
276. Hooper AT, Butler JM, Nolan DJ, et al. **Engraftment and reconstitution of hematopoiesis is dependent on VEGFR2-mediated regeneration of sinusoidal endothelial cells**. *Cell Stem Cell*. 2009;4(3):263-274.
277. Na IK, Lu SX, Yim NL, et al. **The cytolytic molecules Fas ligand and TRAIL are required for murine thymic graft-versus-host disease**. *J Clin Invest*. 2010;120(1):343-356.
278. Hansen TM, Singh H, Tahir TA, Brindle NP. **Effects of angiopoietins-1 and -2 on the receptor tyrosine kinase Tie2 are differentially regulated at the endothelial cell surface**. *Cell Signal*. 2010;22(3):527-532.
279. Fiedler U, Reiss Y, Scharpfenecker M, et al. **Angiopoietin-2 sensitizes endothelial cells to TNF-alpha and has a crucial role in the induction of inflammation**. *Nat Med*. 2006;12(2):235-239.
280. Hammes HP, Lin J, Wagner P, et al. **Angiopoietin-2 causes pericyte dropout in the normal retina: evidence for involvement in diabetic retinopathy**. *Diabetes*. 2004;53(4):1104-1110.

281. Bouazzaoui A, Spacenko E, Mueller G, et al. **Steroid treatment alters adhesion molecule and chemokine expression in experimental acute graft-vs.-host disease of the intestinal tract**. *Exp Hematol*. 2011;39(2):238-249 e231.
282. Fiore E, Fusco C, Romero P, Stamenkovic I. **Matrix metalloproteinase 9 (MMP-9/gelatinase B) proteolytically cleaves ICAM-1 and participates in tumor cell resistance to natural killer cell-mediated cytotoxicity**. *Oncogene*. 2002;21(34):5213-5223.
283. Spark JI, Scott DJ, Chetter IC, Guillou PJ, Kester RC. **Does soluble intercellular adhesion molecule-1 (ICAM-1) affect neutrophil activation and adhesion following ischaemia-reperfusion?** *Eur J Vasc Endovasc Surg*. 1999;17(2):115-120.
284. Rieckmann P, Michel U, Albrecht M, Bruck W, Wockel L, Felgenhauer K. **Soluble forms of intercellular adhesion molecule-1 (ICAM-1) block lymphocyte attachment to cerebral endothelial cells**. *J Neuroimmunol*. 1995;60(1-2):9-15.
285. Rafii S, Butler JM, Ding BS. **Angiocrine functions of organ-specific endothelial cells**. *Nature*. 2016;529(7586):316-325.
286. MacDonald KP, Hill GR, Blazar BR. **Chronic graft-versus-host disease: biological insights from preclinical and clinical studies**. *Blood*. 2017;129(1):13-21.
287. Biedermann BC, Sahner S, Gregor M, et al. **Endothelial injury mediated by cytotoxic T lymphocytes and loss of microvessels in chronic graft versus host disease**. *Lancet*. 2002;359(9323):2078-2083.
288. Fleming JN, Shulman HM, Nash RA, et al. **Cutaneous chronic graft-versus-host disease does not have the abnormal endothelial phenotype or vascular rarefaction characteristic of systemic sclerosis**. *PLoS One*. 2009;4(7):e6203.
289. Schiltz PM, Giorno RC, Claman HN. **Increased ICAM-1 expression in the early stages of murine chronic graft-versus-host disease**. *Clin Immunol Immunopathol*. 1994;71(2):136-141.

APPENDIX

SUPPLEMENTARY METHODS

Detailed description of the LSFM setup

The illumination arm of this microscope consists of a multi-line laser, which provides all excitation wavelengths (491, 642, and 730nm) with a fiber coupled laser combiner (BFI OPTiLAS GmbH, Germany). An objective lens (A10/0.25 Hund, Germany) provides a beam diameter of roughly 3mm and all laser lines are joined via a dichroic beam splitter (DCLP 660, AHF Analysentechnik, Germany). A galvanometer scanner (6210H, Cambridge Technology, USA) elongates the resulting laser beam with a frequency of 600Hz before being focused by a theta lens (VISIR f. TCS-MR II, Leica, Germany) to create a virtual light sheet. The focused beam is relayed with a tube lens and an objective lens (EC Plan-Neofluar 5x/0.16 M27, Zeiss, Germany) to the sample. In the detection arm, a HCX APO L20x/0.95 IMM Objective (Leica, Germany) is mounted on a translation stage perpendicular to the light sheet. The fluorescence emission is spectrally filtered using a motorized filter wheel (MAC 6000 Filter Wheel Emission TV 60 C 1.0x (D)) with a MAC 6000 Controller (Zeiss, Germany) equipped with filters according to the fluorescence labels. The specimen is mounted on a customized metal holder for translation (Newport, Germany) and rotation (Standa, Lithuania). A customized cover glass chamber allows imaging of the cleared sample. Images are taken by an infinity-corrected tube lens and detected by a sCMOS camera (Andro, UK). The electronic module is mainly controlled by a personal computer equipped with data acquisition cards.

SUPPLEMENTARY FIGURES

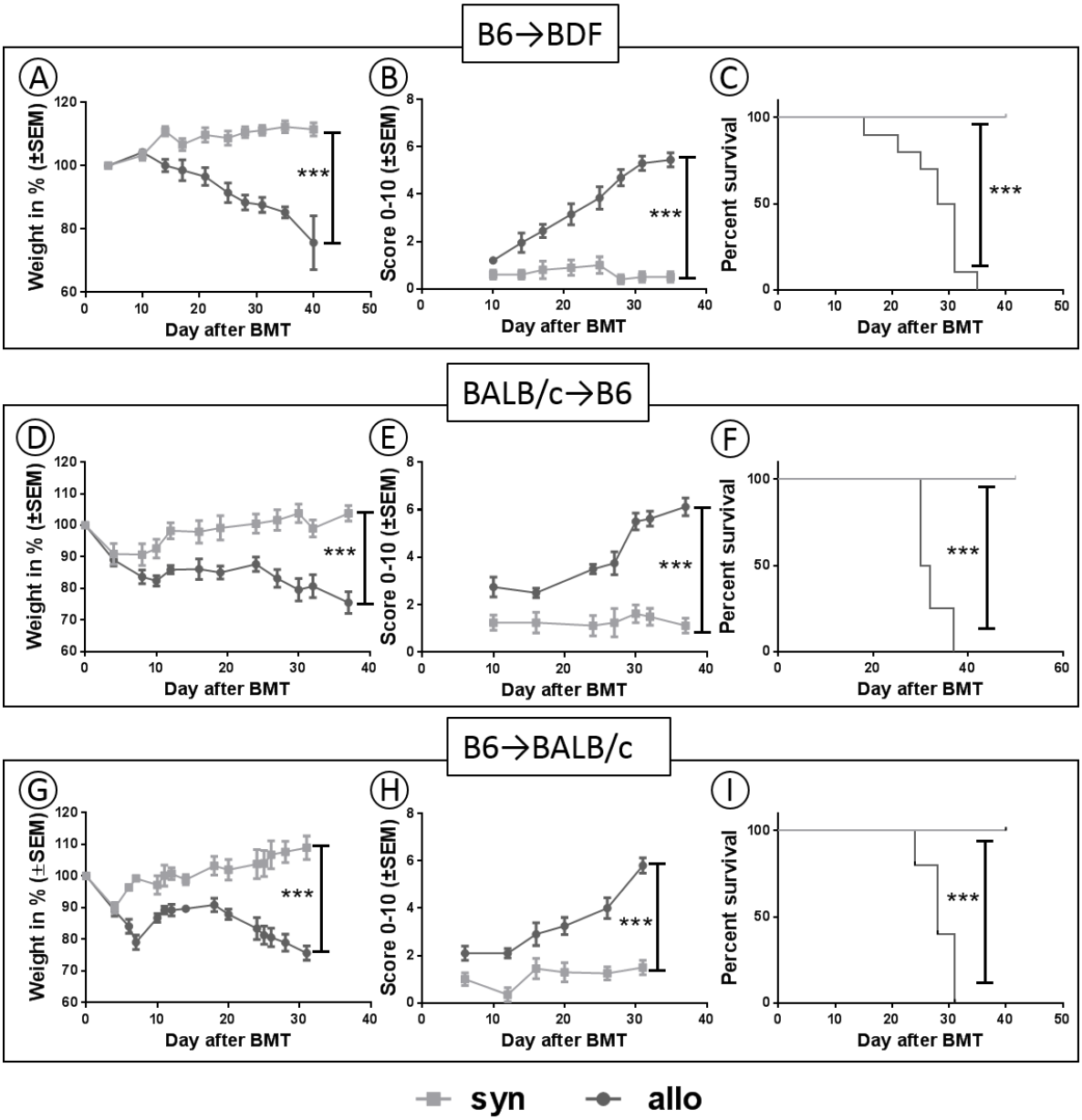

Supplemental Figure 1| Establishing different murine graft-versus-host disease (GVHD) models. A-C| Establishing of a chemotherapeutic based major mismatch GVHD model B6→BDF (n=10 for allogeneic (allo) versus n=5 for syngeneic (syn) bone marrow transplantation (BMT) recipients). **A|** Weight loss in percent, **B|** GVHD score and **C|** survival of allo- and syn-BMT recipients after BMT. **D-F|** Establishing of a radiation based major mismatch GVHD model BALB/c→B6 (n=5 per group). **D|** Weight loss in percent, **E|** GVHD score and **F|** survival of allo- and syn-BMT recipients. **G-I|** Establishing of a radiation based major mismatch GVHD model B6→BALB/c (n=5 per group). **G|** Weight loss in percent, **H|** GVHD score and **I|** survival of allo- and syn-BMT recipients. Significance was checked by student's *t*-test (***$P < .001$). Error bars indicate mean ± standard error of the mean (SEM).

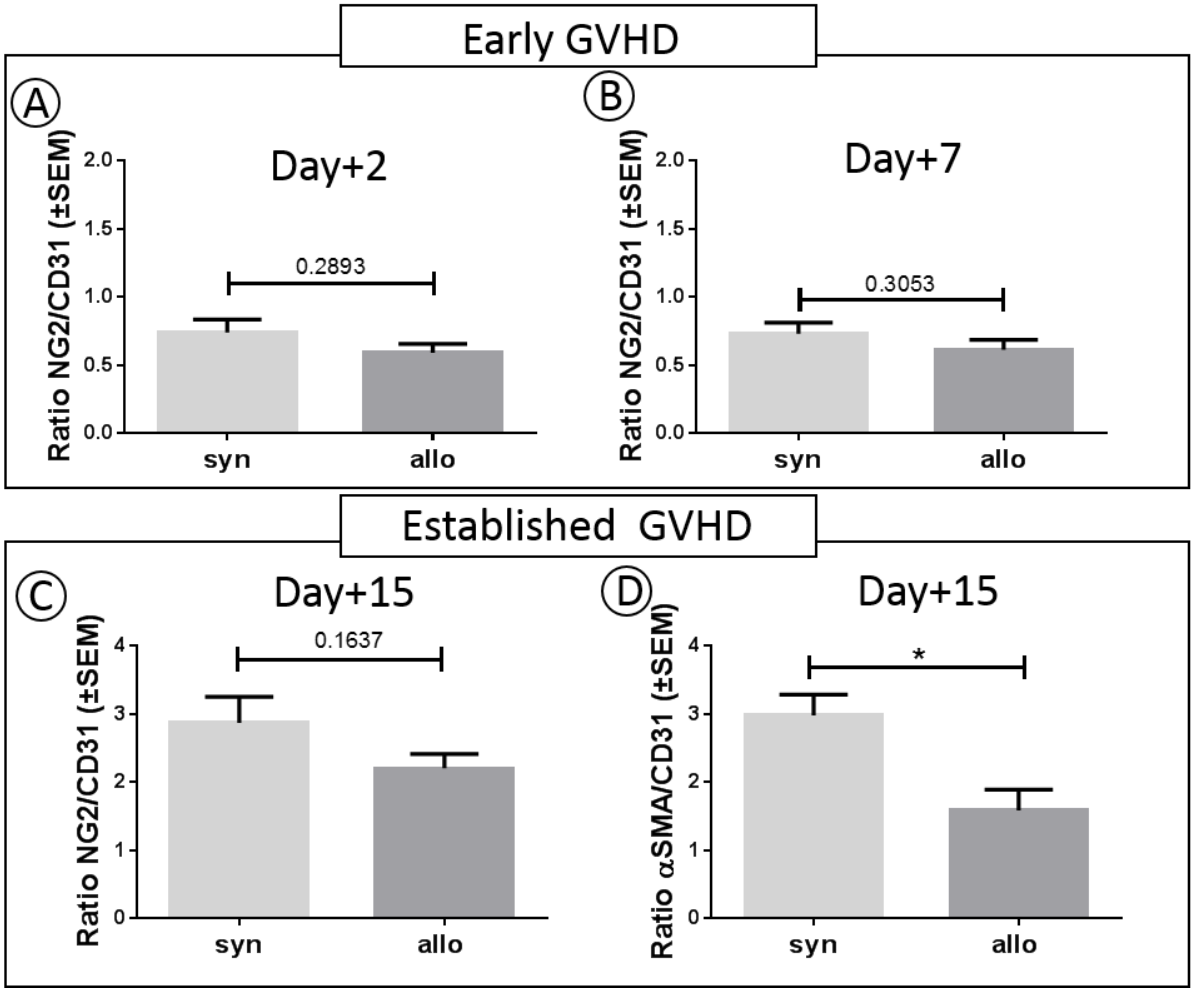

Supplemental Figure 2| Quantification of pericyte-coverage as marker of endothelial damage during early graft-versus-host disease (GVHD) and at established GVHD in another mouse model of GVHD. A-B| Quantification in colonic mucosa at indicated time points after bone marrow transplantation (BMT) in LP/J→B6 GVHD model **A|** Ratio of pericyte marker neural/glial antigen 2 (NG2) and endothelial cell marker CD31 in colonic mucosa at day 2 after BMT in syngeneic (syn) versus allogeneic (allo) BMT recipients. **B|** Ratio of pericyte marker NG2 and endothelial cell marker CD31 in colonic mucosa at day 7 after BMT in syn- vs allo-BMT recipients. **C-D|** Quantification in colonic mucosa at day 15 after BMT in B6→Balb/c GVHD model **C|** Ratio of pericyte marker NG2 and endothelial marker CD31 in colonic mucosa of allo- and syn- BMT recipients. **D|** Ratio of pericyte marker alpha smooth muscle actin (αSMA) and endothelial marker CD31 in colon of allo- and syn-BMT recipient. Ratios of NG2/CD31 or αSMA/CD31 were tested for significance by student's *t*-test (**P* < .05; n=5 animals per group). Error bars indicate mean ± standard error of the mean (SEM).

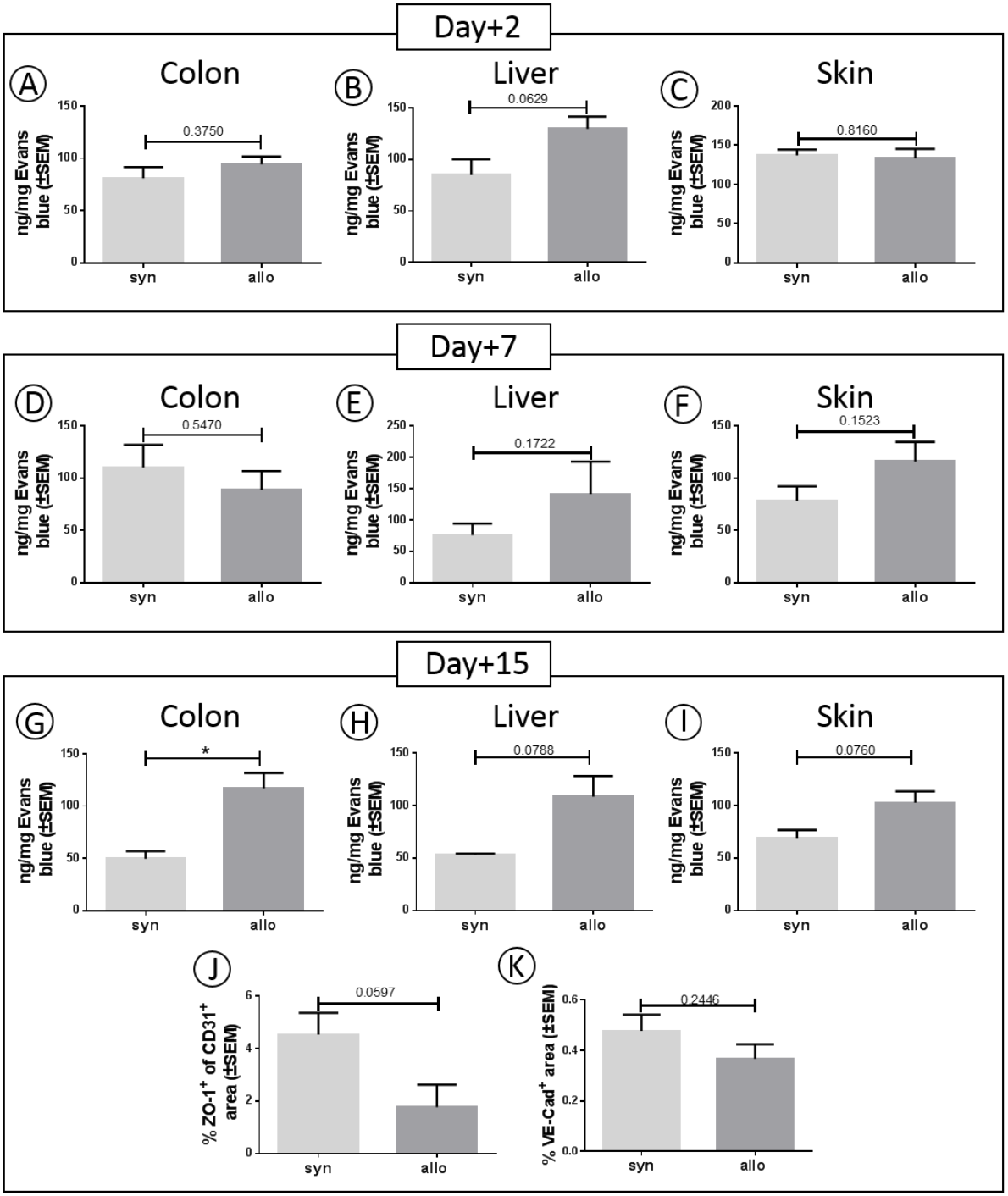

Supplemental Figure 3| Assessment of endothelial leakage during early graft-versus-host disease (GVHD) and in late GVHD in a different GVHD model. A-F| Measurement of Evans blue extravasation during indicated time points after bone marrow transplantation (BMT) in B6→BDF GVHD model. **A|** Evans blue extravasation in colon **B|** liver and **C|** skin of allogeneic (allo) and syngeneic (syn) BMT recipients at day 2 after BMT. **D|** Evans blue extravasation in colon **E|** liver and **F|** skin of allo- and syn-BMT recipients at day 2 after BMT. **G-K|** Measurement of Evans blue extravasation at day 15 after BMT in B6→Balb/c GVHD model. **G|** Evans blue extravasation in colon **H|** liver and **I|** skin of allo- and syn-BMT recipients at day 15 after BMT. **J|** Zonula occludes 1 (ZO-1) expression of $CD31^+$ cells in colonic mucosa of syn- and allo-BMT recipients. **K|** Vascular endothelial cadherin **(**VE-cad) expression in colonic mucosa of syn- and allo-BMT recipients. Significance was tested by student's *t*-test (**P* < .05; n=5-6 animals per group). Error bars indicate mean ± standard error of the mean (SEM).

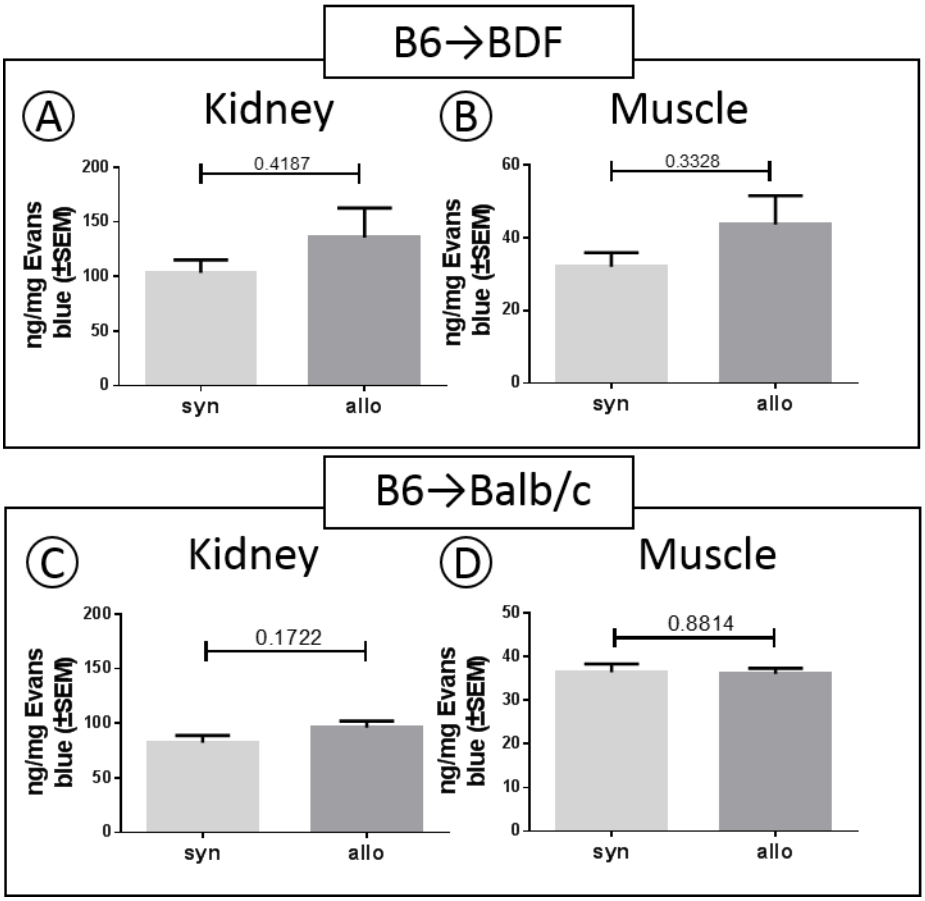

Supplemental Figure 4| Assessment of endothelial leakage during graft-versus-host disease (GVHD) in non-target organs. A-B| Measurement of extravasation of Evans blue at day 15 after bone marrow transplantation (BMT) in B6→BDF GVHD model. **A|** Evans blue extravasation in kidney and **B|** in muscle tissue of allogeneic (allo) and syngeneic (syn) BMT recipients. **C-D|** Measurement of Evans blue extravasation at day 15 after BMT in B6→Balb/c GVHD model. **C|** Evans blue extravasation in kidney and **D|** in muscle tissue of allo- and syn-BMT recipients. Significance was tested by student's *t*-test (n=5-6 animals per group). Error bars indicate mean ± standard error of the mean (SEM).

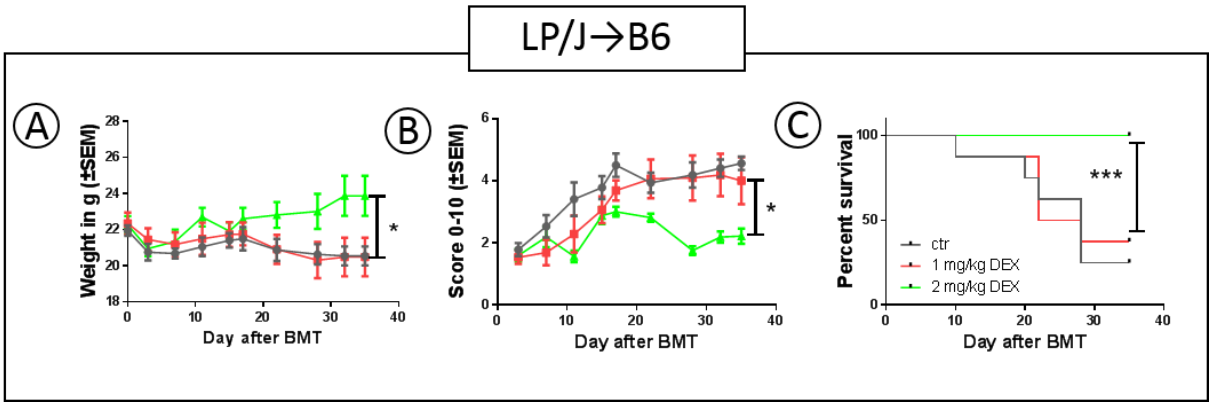

Supplemental Figure 5| Establishing steroid refractory graft-versus-host disease (GVHD) model. A-C| Clinical parameters of GVHD in LP/J→B6 GVHD model with different dosages of Dexamethasone (DEX) and PBS treated control (ctr) animals (n=10 animals per group). **A|** Weight loss of DEX treated and ctr animals after allogeneic (allo) bone marrow transplantation (BMT). **B|** GVHD score of DEX treated and ctr animals after allo-BMT. **C|** Survival of DEX treated and ctr animals after allo-BMT. Significance between the 1mg/kg DEX group and the 2mg/kg DEX group in score and weight was tested by student's *t*-test, survival was tested by Mantel-Cox log-rank test (**P* < .05; ****P* < .001). Error bars indicate mean ± standard error of the mean (SEM).

SUPPLEMENTARY TABLES

Supplemental Table 1| Contamination of purified endothelial cells with immune cells. Gene array data revealed up-regulated genes, which are specific for different immune cell compartments. In the first (grayish) column different pathways are listed. The red column shows numbers and names of up-regulated genes during GVHD in allogeneic bone marrow transplantation recipients. Accordingly, numbers and names of down-regulated genes during GVHD are displayed in the green column.

Pathway	#Up	Up-regulated genes	#Down	Down-regulated genes
T-cell receptor signaling pathway	**75**	*Cd3g, Cd3d, Cd3e, Cd5, Ptpn6, Sla, Syk, Cbl, Pik3r2, Trat1, Lax1, Gab2, Shc1, Vav1, Fyb, Map2k1, Sit1, Ptpn11, Map2k2, Stat1, Stat5a, Bcl10, Pak1, Skap1, Skap2, Dbnl, Ptpn22, Cblb, Cd4, Cd8a, Sh3bp2, Stat5b, Cd2, Rap1a, Lyn, Rac2, Cd247, Zap70, Lck, Map4k1, Tubb5, Fcrl5, Sla2, Card11, Wipf1, Nfam1, Def6, Was, Grap2, Lcp2, Arhgdib, Dtx1, Pstpip1, Lat, Grb2, Txk, Khdrbs1, Unc119, Tuba4a, Itk, Arhgef6, Vasp, Evl, Ptprc, Sh2d2a, Pag1, Cebpb, Ppp3cb, Cabin1, Nfatc2, Dock2, Ripk2, Acp1, Ptk2b, Ptprj*	**53**	*Nck1, Pik3r1, Prkcq, Dusp3, Ptpn12, Mapk1, Prkd2, Map3k1, Ptprh, Mapk3, Vav3, Vav2, Mapk7, Jak3, Sh2d3c, Sos2, Abl1, Rasa1, Crkl, Ctnnb1, Shb, Src, Ptk2, Akt1, Fyn, Muc1, Grap, Crk, Nedd9, Rapgef1, Sos1, Plcg1, Pxn, Arhgef7, Dnm2, Dlg1, Creb1, Crebbp, Git2, Wasf2, Abi1, Rasgrp2, Cd2ap, Homer3, Itpr1, Jun, Fos, Cish, Lime1, Sh2b3, Stk39, Hdac7, Braf*
B-cell receptor signaling pathway	**89**	*Cd79b, Blnk, Lyn, Hcls1, Syk, Actr2, Map4k1, Actr3, Cd5, Arpc1b, Ptpn6, Was, Arpc2, Plcg2, Arpc3, Pik3ap1, Arpc4, Arpc5, Cbl, Grb2, Shc1, Ptk2b, Vav1, Ptpn11, Cd22, Casp9, Casp7, Pik3r2, Cblb, Sh3bp2, Btk, Lck, Itk, Hck, Tec, Bank1, Lcp2, Pdpk1, Stap1, Dok1, Gsk3a, Ptpn18, Pip4k2a, Gab2, Pip5k1b, Pip4k2b, Rb1, Pip4k2c, Rps6ka1, Cdk6, Prkcd, Prkcb, Lat2, Cd72, Inpp5d, Dapp1, Dok3, Csk, Mapk14, Card11, Bcl6, Bcl10, Mapkapk2, Cdk2, Ccnd3, Ccne1, Nfkbia, Ccna2, Nfatc2, Gm10108, Nfatc3, Raf1, Map2k1, Ppp3cb, Map2k2, Stat3, Ptprc, Ppp3r1, Pdk2, Nfatc1, Cdk7, Cd79a, Stat1, Zap70, Bcl2l11, Mapk4, Sla2, Bcl2, Pik3cg*	**65**	*Blk, Fyn, Ptk2, Plcg1, Cd81, Mapk1, Sos1, Nedd9, Nck1, Cr2, Cd19, Pik3r1, Elk1, Vav2, Prkd1, Bcar1, Crkl, Crk, Rapgef1, Itpr2, Akt1, Rap2a, Pip5k1a, Fcgr2b, Jun, Atf2, Pip5k1c, Cdk4, Mapk3, Ctnnb1, Rasa1, Rela, Rel, Creb1, Foxo1, Plekha2, Lime1, Mapk8, Map3k7, Ikbkg, Gsk3b, Ccnd2, Ikbkb, Chuk, Atp2b4, Hdac7, Ppp3ca, Sh2b2, Dusp4, Gtf2i, Dusp6, Plekha1, Hnrnpk, Rasgrp3, Braf, Bax, Prkcq, Gab1, Prkce, Itpr1, Hdac5, Rhoa, Chst15, Cmtm3, Sos2*

IMAGEJ/FIJI MACROS

Macro: Analyze double staining (CLDS)

```
dir1 = getDirectory("Choose Source Directory Dapi ");
dir2 = getDirectory("Choose Source Directory FITC ");
dir3 = getDirectory("Choose Source Directory Cy3");
dir4 = getDirectory("Choose Source Directory for Analyse");
list = getFileList(dir1);
list2 = getFileList(dir2);
list3 = getFileList(dir3)
for (i=0; i<list.length; i++){ showProgress(i+1, list.length); open(dir1+list[i]);
		title1 = "Area Analyse";
		msg1 = "Please select \"Area\" tool to\nadjust the Area, then click \"OK\".";
waitForUser(title1, msg1);
run("Add to Manager ");
roiManager("Sort");
roiManager("Select", 0);
roiManager("Rename", "Area of interest" +list[i]);
close();
}
roiManager("Sort");
roiManager("Save", dir4+"ROI.zip");
run("Set Measurements...", "area mean standard min area_fraction limit display redirect=None decimal=3");
list2 = getFileList(dir2);
for (i=0; i<list2.length; i++){
 showProgress(i+1, list2.length);
 open(dir2+list2[i]);
run("32-bit");
roiManager("Select", 0);
//run("Threshold...");
		title1 = "Set Threshold";
		msg1 = "Please select \"Threshold\" tool to\nadjust the Threshould, then click \"OK\"
waitForUser(title1, msg1);
roiManager("Select", 0);
run("Measure");
saveAs("jpeg", dir4+"Analyse "+list2[i]);
roiManager("Select", 0);
roiManager("Delete");
```

```
close();
}
list3 = getFileList(dir3);
for (i=0; i<list3.length; i++){
 showProgress(i+1, list3.length);
 open(dir3+list3[i]);
run("32-bit");
roiManager("Open", dir4+"ROI.zip");
roiManager("Select", 0);
//run("Threshold...");
                title1 = "Set Threshold";
                msg1 = "Please select \"Threshold\" tool to\nadjust the Threshould, then click \"OK\".";
waitForUser(title1, msg1);
roiManager("Select", 0);
run("Measure");
roiManager("Select", 0);
roiManager("Delete");
saveAs("jpeg", dir4+"Analyse "+list3[i]);
close();
}
saveAs("Measurements", dir4+"Analyse.txt");
close();
```

Macro: Analyze single staining in colon and liver (CLSS)

```
dir1 = getDirectory("Choose Source Directory Dapi ");
dir2 = getDirectory("Choose Source Directory FITC ");
dir3 = getDirectory("Choose Destination Directory");
list = getFileList(dir1);
list2 = getFileList(dir2);
for (i=0; i<list.length; i++){
 showProgress(i+1, list.length);
 open(dir1+list[i]);
                title1 = "Area Analyse";
                msg1 = "Please select \"Area\" tool to\nadjust the Area, then click \"OK\".";
waitForUser(title1, msg1);
run("Add to Manager ");
roiManager("Sort");
roiManager("Select", 0);
roiManager("Rename", "Mucosa" +list2[i]);
close();
}
roiManager("Sort");
roiManager("Save", dir3+"ROI.zip");
run("Set Measurements...", "area mean standard min area_fraction limit display redirect=None decimal=3");
list2 = getFileList(dir2);
for (i=0; i<list2.length; i++){
 showProgress(i+1, list2.length);
 open(dir2+list2[i]);
run("32-bit");
roiManager("Select", 0);
//run("Threshold...");
                title1 = "Set Threshold";
                msg1 = "Please select \"Threshold\" tool to\nadjust the Threshould, then click \"OK\".";
waitForUser(title1, msg1);
roiManager("Select", 0);
run("Measure");
roiManager("Select", 0);
roiManager("Delete");
saveAs("jpeg", dir3+"Analyse "+list2[i]);
close();
```

```
}
saveAs("Measurements", dir3+"Analyse.txt");
close();
```

Macro: Analyze ZO-1 from endothelium (CLZE)

```
dir1 = getDirectory("Choose Source Directory CD31 ");
dir2 = getDirectory("Choose Source Directory ZO1 ");
dir4 = getDirectory("Choose Source Directory for Analyse");
list = getFileList(dir1);
list2 = getFileList(dir2);
for (i=0; i<list.length; i++){
 showProgress(i+1, list.length);
 open(dir1+list[i]);
run("8-bit");
		title1 = "Set Threshold";
		msg1 = "Please select \"Threshold\" tool to\nadjust the Threshold, then click \"OK\".";
waitForUser(title1, msg1);
run("Convert to Mask");
//run("Threshold...");
setAutoThreshold();
run("Analyze Particles...", "size=0-Infinity circularity=0.00-1.00 show=Nothing include add");
roiManager("Save", dir4+list[i]+"Roi.zip");
roiManager("Delete");
close();
}
for (i=0; i<list2.length; i++){
 showProgress(i+1, list2.length);
 open(dir2+list2[i]);
run("8-bit");
		title1 = "Set Threshold";
		msg1 = "Please select \"Threshold\" tool to\nadjust the Threshold, then click \"OK\".";
waitForUser(title1, msg1);
roiManager("Open", dir4+list[i]+"Roi.zip");
roiManager("Measure");
run("Summarize");
saveAs("Measurements", dir4+list[i]+"Analyse.txt");
run("Clear Results");
roiManager("Delete");
close();
}
```

PUBLICATION LIST

Publications

Mengwasser J, Babes L, **Cordes S**, Mertlitz S, Riesner K, Shi Y, McGearey A, Kalupa M, Reinheckel T, Penack O. **Cathepsin E Deficiency Ameliorates Graft-versus-Host Disease and Modifies Dendritic Cell Motility.** *Front Immunol*. 2017 Mar 1;8:203.

Impact factor: 5,849

Riesner K, Shi Y, Jacobi A, Kraeter M, Kalupa M, McGearey A, Mertlitz S, **Cordes S**, Schrezenmeier JF, Mengwasser J, Westphal S, Perez-Hernandez D, Schmitt C, Dittmar G, Guck J, Penack O. **Initiation of acute graft-versus-host disease by angiogenesis.** *Blood.* 2017 Apr 6;129(14):2021-2032.

Impact factor: 10,891

Mertlitz S, Shi Y, Kalupa M, Grötzinger C, Mengwasser J, Riesner K, **Cordes S**, Elezkurtaj S, Penack O. **Lymphangiogenesis is a feature of acute GVHD, and VEGFR-3 inhibition protects against experimental GVHD.** *Blood.* 2017 Mar 30;129(13):1865-1875.

Impact factor: 10,891

Meyer Zu Horste G*, **Cordes S***, Pfaff J, Mathys C, Mausberg AK, Bendszus M, Pham M, Hartung HP, Kieseier BC. **Predicting the Response to Intravenous Immunoglobulins in an Animal Model of Chronic Neuritis.** PLoS One. 2016 Oct 6;11(10):e0164099.
*=contributed equally to this work **Impact factor: 3,394**

Nogai A, Shi Y, Pérez-Hernandez D, **Cordes S**, Mengwasser J, Mertlitz S, Riesner K, Kalupa M, Erdmann JH, Ziebig R, Dittmar G, Penack O. **Organ siderosis and hemophagocytosis during acute graft-versus-host disease.** *Haematologica*. 2016 Aug;101(8):e344-6.

Impact factor: 6,372

Meyer zu Hörste G, **Cordes S**, Mausberg AK, Zozulya AL, Wessig C, Sparwasser T, Mathys C, Wiendl H, Hartung HP, Kieseier BC. **FoxP3+ regulatory T cells determine disease severity in rodent models of inflammatory neuropathies.** PLoS One. 2014 Oct 6;9(10):e108756.

Impact factor: 3,394

Meyer zu Horste G, Mausberg AK, **Cordes S**, El-Haddad H, Partke HJ, Leussink VI, Roden M, Martin S, Steinman L, Hartung HP, Kieseier BC. **Thymic epithelium determines a spontaneous chronic neuritis in Icam1(tm1Jcgr)NOD mice.** J Immunol. 2014 Sep 15;193(6):2678-90.

Impact factor: 5,185

Manuscript with results obtained in this thesis is in preparation:

Endothelial Dysfunction and its contribution to GVHD and srGVHD

Abstracts, Poster & Talks

Mausberg, A. K. ;Heininger, M. K. ;zu Horste, G. M. ;**Cordes, S**. ;Kleinschnitz, C. ;Kieseier, B. C. ;Stettner, M. **Can NK cells help discriminate IVIG treatment response in patients with CIPD?** 2017

Heininger, M. K. ;zu Horste, G. M. ;**Cordes, S**. ;Warnke, C. ;Stettner, M. ;Mausberg, A. K. ;Kieseier, B. C. **Effect of intravenous immunoglobulins on natural killer cells in peripheral blood of patients with chronic inflammatory demyelinating polyneuropathy.** 2016

Riesner, K. ;Shi, Y. ;Kalupa, M. ;McGearey, A. ;Mengwasser, J. ;Mertlitz, S. ;**Cordes, S**. ;Perez-Hernandez, D. ;Dittmar, G. ;Penack, O. **Angiogenesis in acute GVHD**. 2016

Mengwasser, J. ;Shi, Y. ;**Cordes, S.** ;Riesner, K. ;Mertlitz, S. ;McGearey, A. Kalupa, M. ;Penack, O. **The role of Cathepsin E in GVHD**. 2016

Mertlitz, S. ;Shi, Y. ;Kalupa, M. ;Mengwasser, J. ;Riesner, K. ;**Cordes, S**. ;Penack, O. **The role of lymphangiogenesis and its inhibition during GVHD**. 2016

Nogai, A. ;Shi, Y. ;**Cordes, S**. ;Riesner, K. ;Mertlitz, S. ;Mengwasser, J. ;Perez-Hernandez, D. ;Erdmann, J. H. ;Ziebig, R. ;Dittmar, G. ;Penack, O. **Organsiderosis and Hemophagocytosis during acute GVHD.** 2016

Shi, Y. ;Perez-Hernandez, D. ;Mengwasser, J. ;**Cordes, S.** ;Riesner, K. ;McGearey, A. ;Mertlitz, S. ;Kalupa, M. ;Dittmar, G. ;Penack, O. **Common Protein Changes in Target Organs during Acute Graft-Versus-Host Disease**. 2015

Heininger, M. K. ;Horste, G. M. Z. ;**Cordes, S**. ;Stettner, M. ;Mausberg, A. K. ;Kieseier, B. C. **Effect of intravenous immunoglobulins on natural killer cells.** 2014

Riesner, K. ;**Cordes, S.** ;Mengwasser, J. ;Shi, Y. ;Westphal, S. ;Penack, O. **Neovascularization precedes leukocyte infiltration and target organ damage during acute GVHD and experimental colitis.** 2014

Shi, Y. ;Perez-Hernandez, D. ;**Cordes, S.** ;Mengwasser, J. ;Dittmar, G. ;Penack, O. **Proteomic peptide profiling in the liver during acute Graft-versus-Host Disease.** 2014

Riesner, K. ;Kalupa, M. ;**Cordes, S**. ;Elezkurtaj, S. ;Grossmann, K. ;Rudloff, S. ;Shi, Y. ;Westphal, S. ;Wilke, A. ;Mengwasser, J. ;Penack, O. **Close To Clinics: Acute Gvhd In a Novel Chemotherapy Based Minor Mismatch Transplantation Model.** 2013

Horste, G. M. Z. ;**Cordes, S**. ;Mausberg, A. ;Hartung, H. ;Kieseier, B. **Regulatory T Cells Determine Disease Severity in Experimental Autoimmune Neuropathies.** 2012

Horste, G. M. Z. ;Mausberg, A. ;**Cordes, S**. ;Hartung, H. P. ;Kieseier, B. **Spontaneous demyelinating autoimmune neuropathy in ICAM-1 deficient NOD mice.** 2012

SELBSTÄNDIGKEITSERKLÄRUNG

Hiermit erkläre ich, dass ich diese Arbeit selbständig verfasst habe und keine anderen als die angegebenen Quellen und Hilfsmittel in Anspruch genommen habe. Ich versichere, dass diese Arbeit in dieser oder anderer Form keiner anderen Prüfungsbehörde vorgelegt wurde.

Berlin, den 27.11.17 Steffen Cordes